Sara Filipa Silva Pestana

Degree in Biomedical Science

Screening for asymmetrically expressed genes in the left-right organizer of the zebrafish embryo

A thesis submitted in fulfillment of the requirements for the degree of the Masters in Molecular Genetics and Biomedicine

Supervisor: Susana Santos Lopes, PhD, CEDOC-FCM

Jury:

President: Dr. Ilda Maria Barros dos Santos Gomes Sanches, PhD

Arguer: Dr. Raquel de Amaro Lourenço, PhD

FACULDADE DE CIÊNCIAS E TECNOLOGIA
UNIVERSIDADE NOVA DE LISBOA

September, 2016

Sara Filipa Silva Pestana

Degree in Biomedical Science

Screening for asymmetrically expressed genes in the left-right organizer of the zebrafish embryo

A thesis submitted in fulfillment of the requirements for the degree of the Masters in Molecular Genetics and Biomedicine

September, 2016

Screening for asymmetrically expressed genes in the left-right organizer of the zebrafish embryo

ACKNOWLEDGMENTS

I would like to start by thanking to Susana Lopes, my supervisor, for the opportunity she gave me by accepting me in Cilia Regulation and Disease Lab, for all the support and mentor throughout this year, for her help when I needed.

I also want to thank to Mónica, Bárbara and Pedro for all the things they taught me, all the advices and reviews given that helped me to build this project. I am honestly thankful for Raquel's patience to teach me and for the great support showed to me since the beginning. This thesis was only possible due to your help. I am privileged for having worked with you all.

A special thanks to Inês and Marta, for being on my side throughout these last five years and for all good moments. I also want to thanks to Sara, Tânia and Neuza for their friendship over the years and for all the support.

I want to thanks to Gonçalo for his unconditional support and for his motivating sayings.

A special thanks to Maria for help me and motivate me in these lasts weeks.

And for the most important people, I want to thank to my parents for the unconditional love and support. Without them nothing of this would be possible.

ABSTRACT

The left-right axis is established during early development in four steps. First the asymmetry is broken through the cilia movement within the left-right organizer (LRO) generating a leftward fluid flow. Second, the flow, or what it transports, is sensed by some organizer cells that produce an asymmetric signal. Such signal triggers a genetic cascade that transmits the asymmetric information from the organizer to the lateral plate mesoderm. Ultimately, leading to an organ-specific morphogenesis with visceral organs being placed in the correct side of the body plan.

Two hypotheses try to explain how the fluid flow is sensed. The Chemosensation model proposes that a morphogen accumulates on the left side of the LRO where it is perceived by ciliated cells. To test this model we studied several taste sensing-related genes. We focused on *gnaia*, a gene encoding a G protein alpha subunit, highly expressed in the zebrafish LRO. However, we could not draw definitive conclusions, as *gnaia* knockdown did not produce major left-right defects.

The second hypothesis, the 'two cilia model' is based on mechanosensation and predicts that two cilia populations have different functions in the LRO: the motile cilia generate the directional flow and the immotile cilia sense it through the Pkd1l1-Pkd2 complex. To test this hypothesis we looked for the expression patterns of possible downstream targets of Pkd2, screening for left-right asymmetries. However, we were not able to find new asymmetric genes, confirming that, so far, *dand5* is still the only asymmetrically expressed gene in the LRO.

The two-cilia model also raised the question of what makes these two cilia populations different. In order to try to understand if the difference between motile and immotile cilia was structural, we looked for the localization of Dnal1, a crucial dynein component of outer dynein arms. Results showed mCherry-Dnal1 is expressed in both cilia types, suggesting that LRO cilia may be structural identical.

Key words: Left-right asymmetry, cilia, Chemosensation Model, Two-cilia Hypothesis, Pkd2, expression pattern studies.

RESUMO

O eixo esquerda-direita do plano corporal é estabelecido durante o desenvolvimento embrionário em quatro passos principais, coordenados pelo organizador esquerda-direita. O primeiro evento de quebra de Simetria consiste num fluxo direcional, sendo mais forte no lado esquerdo do organizador, gerado por cílios móveis. O fluido, ou o que nele é transportado, é posteriormente detetado pelas células do organizador, produzindo um sinal assimétrico que é transmitido ao longo da placa de mesoderme lateral através da ativação de uma cascada de genes assimétrica. Por último, esta informação assimétrica leva ao posicionamento correto dos órgãos viscerais ao longo do plano esquerda-direita do corpo.

Existem dois modelos que tentam explicar como é que o fluido é detetado pelo organizador esquerda-direita. O modelo Quimiosensor propõem que um morfogénio seja acumulado no lado esquerdo do organizador e detetado pelos cílios do mesmo lado. Para testar este modelo, diferentes genes relacionados com a percepção de sabores químicos foram estudados, sendo que o gene *gnaia*, que codifica uma proteína G subunidade alfa, encontra-se ativo nas células do organizador. No entanto, a redução dos níveis desta proteína Gnaia por injeção de um morfolino bloqueador da tradução deste gene, não mostraram defeitos significativos no posicionamento dos órgãos internos.

O segundo modelo, 'two cilia model' também chamado de Mecanosensor, prevê que as duas populações de cílios existentes no organizador esquerda-direita desempenham funções distintas: os cílios móveis geram o fluxo direcional do fluido que, por sua vez é detetado pelos cílios imóveis. Neste projeto avaliámos os padrões de expressão de possíveis efetores do canal de cálcio, Pkd2, sendo que o objetivo seria encontrar novos genes assimétricos com um papel relevante do estabelecimento do eixo esquerda-direita. No entanto, nenhuma assimetria foi detetada, sugerindo que *dand5* seja o único gene assimétrico no organizador.

O modelo dos dois cílios assume a existência de duas populações de cílios no organizador. Para tentar perceber a diferença entre cílios móveis e imóveis, usámos um componente da maquinaria ciliar necessária para a mobilidade do cílio, a dineina *dnal1*, fundido com um marcador de fluorescência para questionar se estava presente em ambas as populações ou só na móvel. A mCherry-Dnal1 foi observada nos dois tipos de cílios, o que indicia que ambos podem apresentar a mesma constituição estrutural.

Palavras-chave: Assimetria esquerda-direita, cílios, Modelo da Sensação química, Modelo dos dois Cílios, Pkd2, estudo dos padrões de expressão

TABLE OF CONTENTS

LIST OF FIGURES

LIST OF TABLES

1. INTRODUCTION

1.1. Left-Right Axis

The formation of the Left–Right (LR) body axis throughout the development of vertebrate embryos has been an interesting and enigmatic subject of developmental biology for many years.

Although most vertebrate animals are bilaterally symmetric on the outside, they exhibit highly conserved LR asymmetries on the inside, mainly visceral organs regarding their position and morphology. Each thoracic and abdominal structure is located to one side or the other of the longitudinal midline, for instances the heart as well as stomach and spleen are positioned on the left side while the liver and gall bladder are on the right side. This arrangement, named *situs solitus,* corresponds to the normal anatomic left-right relation of the asymmetric viscera and such orientations are essential for their functions. According to epidemiological studies, *situs* anomalies are rare with an overall frequency estimated at 1 in 10 000 human births (Lin *et al*. 2014) which may result in significant morbidity and mortality. Reversal of visceral organ position can be either total or partial (Figure1.1). The complete reversal of all organs position, termed as *situs inversus,* can be isolated or may occur in combination with other abnormalities (Lamver *et al*. 2016). Whereas *heterotaxia* refers to the displacement of some organs but not all of them and represents the worst case scenario causing serious health problems due to the abnormal arrangement of the abdominal-thoracic organ-vessels in relation to each other (Shapiro *et al*. 2015).

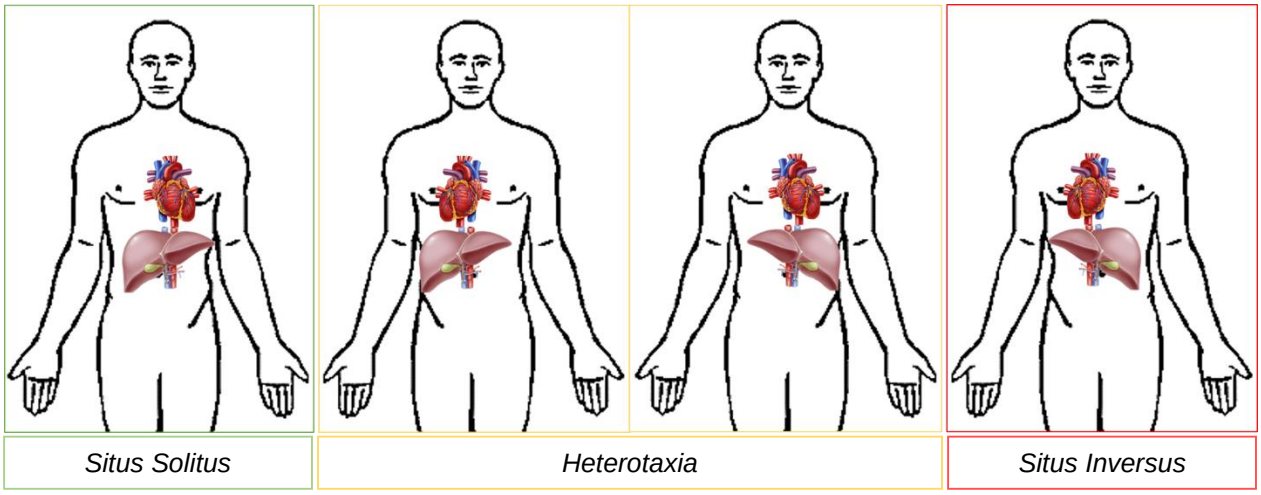

Figure 1.1: Organ situs.
Schematic representation of the heart and liver position. In a *situs solitus* situation the heart is positioned on the left side of the chest, while the liver is located on the right side. *Situs inversus* is the complete mirror-imaged of *situs solitus*. *Heterotaxia* involves any laterality defects in the thoracic-abdominal internal organs with respect to the LR body axis.

During early embryogenesis, the temporally synchronized establishment of tissues that delineates the orientation and polarity along the three body axes – anteroposterior (AP), dorsoventral (DV) and left-right (LR) axes - coordinates the patterning of the body plan in vertebrates. The AP and DV axis are first patterned by Wnt and BMP (Bone Morphogenetic Protein family) gradients. And then the LR axis is established and oriented orthogonally to the pre-existing DV and AP axes (Niehrs 2004).

Although the mechanisms underlying AP and DV breaking symmetry have been studied exhaustively with the advent of molecular genetics, the initial steps of LR asymmetry patterning were, until a few decades, completely unknown. Through recent molecular and genetic studies, several discoveries have led to uncover mechanisms responsible for the generation of LR asymmetry patterning as well as genes with LR asymmetric expression, which propagate and translate the LR information into asymmetric organogenesis during development. These mechanisms are largely conserved among vertebrates, although some diversity has been identified.

In the 1970s, Afzelius had identified cilia defects in Kartagener Syndrome patients, with respiratory difficulties, resulting from immotile cilia in the trachea, male infertility stemmed from sperm tail immotility, and frequently with *situs inversus.* This evidence suggested for the first time a link between visceral LR asymmetry establishment and cilia motility within an embryonic tissue (Afzelius 1976). Furthermore, Supp and colleagues later showed that *inversus viscerum* (*iv*) mouse, which result in LR complete inversion of fifty percent of homozygote embryos, carry a missense mutation on the ciliary axonemal dynein heavy-chain gene, *left-right dynein* (*ldr*) (Supp *et al*. 1997; Okada *et al*. 1999). A targeted mutation in left-right dynein gene showed similar phenotypes to *iv* mutants, confirming that *lrd* is required for normal LR development and also that *lrd* mutations leads to paralyzed cilia as a result of defective axonemal dynein motors (Supp *et al*. 1999). In addition, approximately half of live-born Kif3a or Kif3b null mutant mice showed LR laterality defects, resembling the phenotype of Kartagener Syndrome patients. These mutants were deficient in genes encoding two kinesin proteins, which normally form a motor protein complex ATP-dependent that track along microtubules, being involved in the trafficking of several cargoes within the cell and in ciliogenesis through intraflagellar transport. Thus in kif3 mutants, assembly of motile cilia is impaired (Nonaka *et al*. 1998; Takeda *et al*. 1999).

Such evidence that cilia-beating movement is involved in LR breaking asymmetry drew attention to this organelle, which has emerged as a key organelle in several physiological and developmental processes (Singla and Reiter 2006). Investigators have now identified a staggering correlation between human genetic diseases and dysfunctional ciliogenesis or cilia function.

1.2. Cilia

Eukaryotic cilia and flagella are hair-like specialized cellular compartments. From protists to mammals, cilia project from the surface of almost all cell types, serving as “antennae” to sense extracellular signals. They are highly conserved across evolution, both in structure as function, but cilia and flagella vary in number per cell, length, tilt and in the beat patterns that they generate. Either through mechanosensation or chemosensation, cilia act as an interface between the cell and the extracellular environment, which is essential for survival, organism development and homeostasis (Fisch and Dupuis-Williams 2011). These

organelles have been associated with several cell functions as cellular motility, signal transduction, regulation of intracellular calcium levels, Wnt and Hedgehog signaling pathways (Fliegauf *et al*. 2007).

Cilia have a complex ultrastructure with compartmentalization of molecular components that combine in functional modules, such as a basal body, transition zone, axoneme, ciliary membrane and the ciliary tip, comprising more than 650 proteins (Ishikawa and Marshall 2011).

Depending on the cell type from which cilia protrude, ciliogenesis can lead to the formation of two different structures within the axoneme. The typical conformation is mentioned as “9+2”, since the nine doublet microtubules, organized in a circle, surround a central pair of singlet microtubules covered by the cell membrane. While another group of cilia have a “9+0” microtubule structure, meaning that they do not have a central pair of microtubules. At the ultrastructure level, each doublet microtubule itself consists of two conjoined tubulins, α and β tubulin heterodimers, making a total of 13 protofilaments of α tubulin and 10 protofilaments of β tubulin. The tubulin can undergo several post-translational modifications, as acetylation, glutamylation and glycylation, which have implications on ciliary assembly and motility (Ishikawa and Marshall 2011). And like the cytoplasmic microtubules, doublet microtubules polymerize with the plus end growing towards the ciliary tip.

1.2.1. Types of Cilia

Although all cilia types share the basic structural units, the specialization of cilia within a certain cell type to perform a specific function has resulted in significant variations of structure and regulation. Conventionally, depending on cilia axonemal structure, function and ability to move, cilia are categorized into two classes: primary and motile cilia.

Primary cilia are single and typically short organelles that protrude from almost vertebrate cell types between cell division, including stem, epithelial, endothelial connective-tissue, muscle cells and neurons. The majority of these type of cilia has a “9+0” microtubule conformation (Figure 1.2). Since primary cilia are immotile, the lack of ability to move was associated with the absence of the central pair microtubules. However, studies discovered non-motile with the typical conformation of “9+2” microtubules structure, in vestibular cilia of the auditory organ (Sobkowicz *et al*. 1995). Therefore, primary cilia are unable to move due to the lack of dyneins arms, which comprise the molecular motor proteins that power the cilia-beating movement, along with other interconnecting multiprotein complexes (Kobayashi and Takeda 2012)

Cilia are functionally distinct from the cytoplasm, acting as a cellular sensory structure. Besides the ciliary membrane being highly enriched for receptors and ion channels, high concentrations of transporter proteins and signaling effectors were found in the cilium and basal body, which allows the cilium to organize signaling in a highly ordered and concentrated microenvironment (Hilgendorf *et al*. 2016).

Signaling in the cilium coordinates key processes during development and in tissue homeostasis, including cell migration, differentiation and/or re-entry into the cell cycle, specification of the plane of cell division, and apoptosis. Primary cilia are specialized morphologically and molecularly in order to participate in numerous biological process ranging from mechanosensation (by bending of the cilium) and chemosensation (detection of a specific ligands, growth factors, hormones or morphogens) to the transduction of essential signaling cascades, including Hedgehog and Wnt signaling and Planar Cell Polarity pathways. Furthermore, cilia also respond to light, sound waves, temperature, osmolarity or gravity (Singla and Reiter 2006). This impact of primary cilia in signaling has been highlighted by its defective function on specific organ diseases and developmental disorders, commonly referred to as ciliopathies.

Motile cilia are usually longer and they can be found as a single cilium per cell (motile monocilia) or as many cilia at high density at the surface of the cells (multiple motile cilia) moving in a coordinated bending motion. To drive wave-like movement, motile cilia have a number of multiprotein complexes that interconnect the different components, within the microtubule core, including radial spokes, nexin links, central sheath and dynein arms. The two dynein arm classes, outer dyneins (ODA) and inner dyneins (IDA), encoded by different genes show distinct motor and ATPase properties that together generate the force necessary for rhythmic movement of the axonemes. Dynein arms are attached to the microtubules while the other components, mainly the central sheath apparatus and radial spokes, form a signal-transduction scaffold between the central pair microtubule and the dynein arms (Ibañez-Tallon *et al*. 2003).

Most of motile cilia have a “9+2” conformation (Figure 1.2), with a central pair of microtubules within the axonemes, and are present in epithelial cells in the respiratory tract and oviducts, sperm and ependymal cells lining the brain ventricles (Vincensini *et al*. 2011). Thus, cilia motility is required in a synchronized wave like fashion for the generation of fluid flow over epithelia to promote the clearance of mucus in the airways and the passage of cerebrospinal fluid within the brain and spinal cord. However, motile cilia showing a “9+0” microtubule structure were observed within the embryonic mouse node to create a leftward fluid flow that is essential for LR determination (Nonaka *et al*. 1998). Although motile cilia had been associated only with fluid and cell movement, recent studies throughout the diverse groups of organisms from protists to humans showed that these cilia also have sensory properties (Bloodgood 2010). Motile cilia express specialized receptors that are capable to detect and consequently respond to specific signals in the cell environment through changes in the cilia beat frequency. For instances, sensory proteins have been identified in motile cilia detecting shear stress, osmotic force, fluid flow, bitter taste and sex hormones (reviewed in Jain *et al*. 2012).

Thus, the simplistic classification of cilia as motile and immotile, according to their microtubule conformation, seems increasingly unsuitable as the number of exceptions rise. So far four cilia types have been identified and all of them have been associated with human disease, favoring the distinction of cilia into four subtypes (Figure 1.2): motile “9+2” cilia (such as respiratory and ependymal cilia); motile “9+0” cilia (embryonic nodal cilia); immotile “9+2” cilia (kinocilium of vestibular cells); and immotile “9+0” cilia (renal monocilia and photoreceptor-connecting cilia).

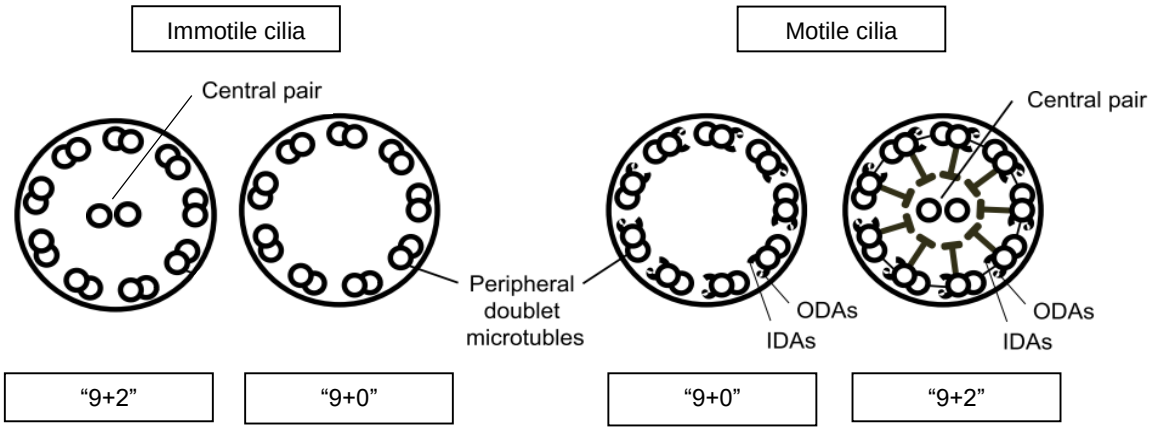

Figure 1.2: Cilia structures in vertebrates.
A schematic representation of “9+2” and “9+0” axoneme cross-sections is shown. Both immotile and motile cilia can have either microtubule conformation, depending on their function within the cell type where they protrude. “9+0” structure comprise nine peripheral doublet microtubules whereas “9+2” conformation have an additional central pair of singlet microtubules. In addition, motility requires axoneme-associated dynein arms to generate the sliding of microtubules and thus motion. ODAs outer dynein arms. IDAs inner dynein arms. Adapted from Kobayashi and Takeda, 2012.

1.2.2. Ciliogenesis

Ciliogenesis is tightly coordinated with cell cycle progression and differentiation (Avasthi and Marshall 2012). During interphase, centrioles move to the plasma membrane and from a plasma membrane-associated foundation where the basal bodies are formed, docked onto actin-rich cortex and fused with the membrane (Ishikawa and Marshall 2011). Basal bodies position and their orientation dictates the alignment of the resulting cilia, creating an anchor and a template for the nucleation of the axoneme. After that, nine triplets of microtubules begin to form beneath an extension of membrane until the transition zone wherein nine axonemal doublets microtubules project radially around a central pair of singlet of microtubules, giving rise to the ciliary axoneme (Figure 1.3) (Mitchell 2007).

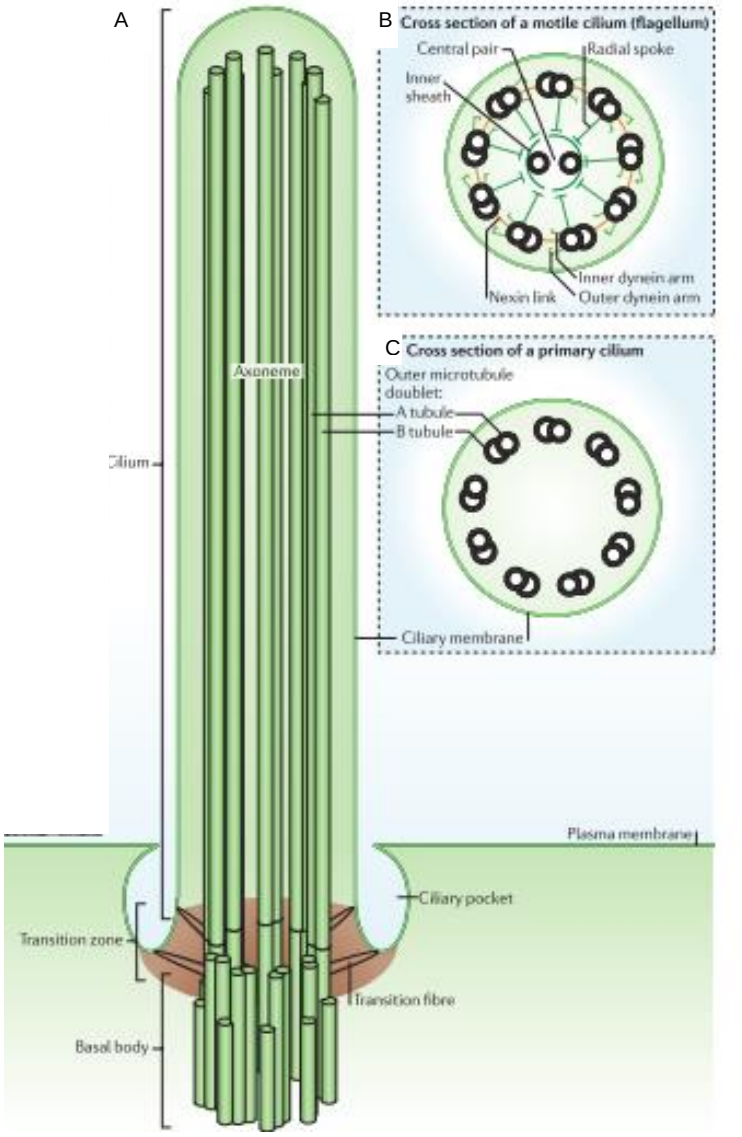

Figure 1.3: Cilia architecture.
Schematic diagram of a cilium: the cilium (green) is produced once per cell and extends from the basal body, forming the transition zone, the axoneme and the ciliary tip (A). Cross-section diagrams of a typical motile cilium (which is identical to a flagellum) (B) and a non-motile primary cilium (C). Adapted from Ishikawa and Marshall, 2011.

Since ribosomes are missing from the cilium, all proteins are synthesized in the cytoplasm and carried across the ciliary compartment and along the length of the axoneme by a bidirectional intraflagellar transport (IFT) (Vincensini *et al*. 2011). Proteins loaded onto the IFT particles are trafficked along the polarized microtubules, between the doubles and the membrane, from the basal body to the ciliary tip (anterograde movement) and in the opposite direction (retrograde movement). In the anterograde movement of cargo proteins, IFT is powered by heterotrimeric motor kinesin of the kinesin-2 family, whereas the retrograde movement is catalyzed by dyneins of the cytoplasmic dynein 2 family (Figure 1.4). It has been suggested that the transition zone acts as docking site for IFT particles and their motors, as well as it regulates the trafficking of proteins into and out of the cilium (Fisch and Dupuis-Williams 2011).

Apart from the diverse functions of cilia, in response to cell cycle progression, cell differentiation or cellular stress, cilia can be shortened or reabsorbed, where the disassembled ciliary components return to the cell body for recycling or degradation.

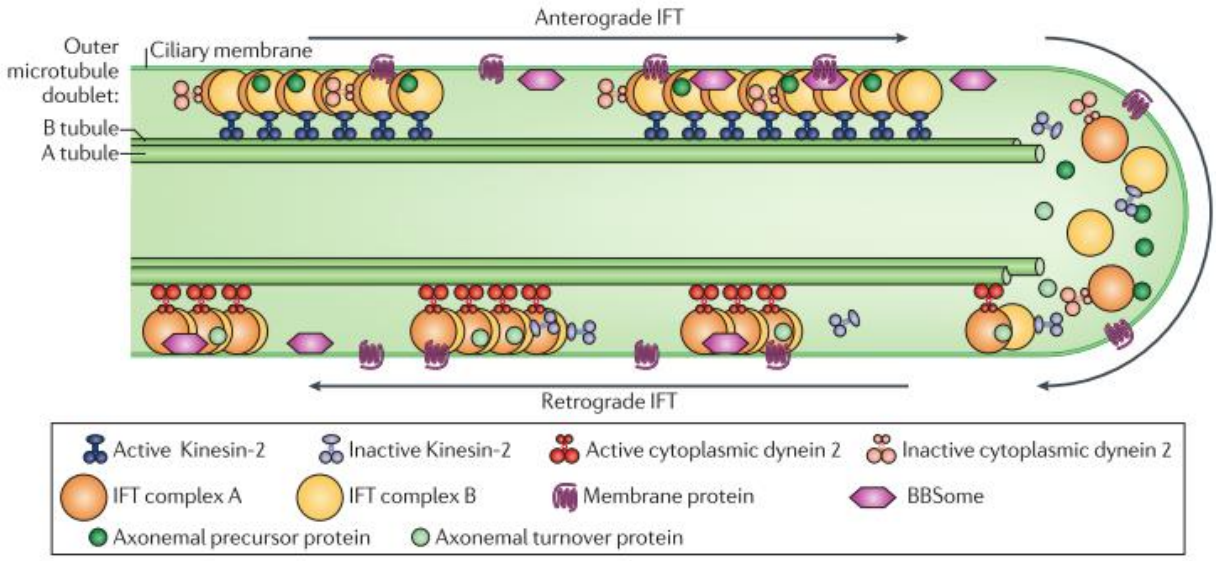

Figure 1.4: Intraflagellar transport machinery.
The canonical anterograde intraflagellar transport (IFT) motor, heterotrimeric Kinesin-2, transports IFT complexes A and B, axonemal proteins and cytoplasmic dynein 2 (previously known as cytoplasmic dynein 1b) to the tip of cilium. During this anterograde motion, Kinesin-2 is active and the retrograde motor, cytoplasmic dynein 2, is somehow kept inactive to allow smooth processive anterograde movement. At the tip of cilium, anterograde IFT trains release axonemal proteins and rearrange their conformation for retrograde IFT. Cytoplasmic dynein 2 is activated and transports retrograde IFT trains to the cell body. Figure and legend from Ishikawa and Marshall 2011.

1.2.3. Dynein-mediated motility

As previously mentioned, cilia have an intrinsic structure within their axoneme, that contains all the components necessary to generate and propagate waveforms. Although the path by which signals are propagated through the axonemal superstructure is complex and not yet well understood, ultimately cilia movement is powered by the molecular motors present in dynein arms.

Dyneins are highly complex macromolecular systems containing more than 20 different protein subunits, which are preassembled in the cytoplasm to generate fully assembly-competent dynein particles. An example of an assembly factor being *ccdc151* which is a coiled coil domain containing 151 gene (Jerber *et al*. 2014). During the cilium growth, axonemal dyneins are transported from the cytoplasm into the ciliary shaft, by specific adaptors to attach the different arms to the IFT machinery (Kobayashi and Takeda 2012). These dynein arms are large protein complexes formed by the combined assembly of heavy (HC of 400-500 kDa), intermediate (IC of 45–110 kDa) and light (LC of 8–55 kDa) chains. Once assembled, these multiproteins are permanently attached to the α tubulin of one doublet microtubule and transiently interact with the β tubulin of an adjacent doublet in an adenosine triphosphate (ATP)-dependent manner.

Thus dynein arms convert the chemical energy, released by the ATPase activity of heavy chain molecules, into mechanical work through the sliding movement of doublet microtubules, to produce the beating of the cilium. The intermediate and light chain components allow the motors to be regulated by external factors, such as calcium levels, phosphorylation status and the mechanical state or local curvature of the motors themselves (King 2016).

Dynein arm function is dependent on the integrity of many dynein components. Studies using *Chlamydomonas* have reported so far 30-40 different axonemal dyneins. These dyneins combine to form two significantly different dynein arms, in subunit structure content and arrangement within the axoneme (reviewed in Kamiya 2002). Nevertheless, both rows of dynein arms are capable of generating motive force. The outer dynein arms (ODA) are positioned proximally to the cilia membrane, being responsible for increase cilia-generated propulsive force output (cilia beat frequency), while the inner dynein arms (IDA) are proximal to the central pair and they are required the proper control necessary to generate and propagate specific ciliary waveforms (Brokaw and Kamiya 1987, Kamiya *et al*. 1991). In *Chlamydomonas*, the IDA and ODA are spaced as specific liner repeats of 96 nm and 24 nm, respectively, along the axis of each doublet microtubule (Goodenough and Heuser 1985).

One of the most highly conserved component of axonemal ODA is DNAL1, which stands for axonemal dynein light chain 1, known as LC1 in *Chlamydomonas*. New insights on this protein came from analysis of Chlamydomonas *oda2-t* mutants, that express a truncated form of γ-HC, one of the three heavy chain motors. In this mutant, LC1 is not present, unlike the other components (Liu *et al*. 2008). Like LC1, DNAL1 physically interacts with DNAH5, the human orthologue of the *Chlamydomonas* ODA γ-HC (Horváth *et al*. 2005). And when dnal1 is mutated leads to the absence of ODAs within the cilia causing PCD (Mazor *et al*. 2011). PCD patients with dnal1 mutations present *situs inversus,* showing that DNAL1 is also important within the cilia that generates the flow necessary for the LR determination. In addition, LC1/DNAL1 also binds to the α tubulin in a ternary complex, thus connecting the motor γ-HC/DNAH5 to the doublet microtubules making dnal1 an important player in motility mechanics (Mazor *et al*. 2011)(Figure 1.5).

For an axoneme to propagate bending waves, microtubule sliding must be strictly controlled spatially and temporally. In other words, the activity of various dynein components must be regulated according to the phase of wave propagation, in order to the dyneins on one side of the axoneme bend the cilium in one direction of the beat cycle, and the dyneins on the opposite side contribute to bending in the opposite direction. LC1/DNAL1 bound to the α tubulin is thought to be required for the modulation of this dynein motors activity in cilia, through a conformational switch in response to alterations in axonemal curvature (King and Patel-King 2012). Dynein activity is also regulated by the nexin-dynein regulatory complex (N-DRC), where the nexin links are responsible for the connections between each adjacent doublet microtubule, while the DRC is in close contact with inner dynein arms (Lindemann and Lesich 2010). Furthermore, the radial spokes, which are T-shaped projections, link the doublet microtubules to the

central pair to determine bend direction, shape (motion pattern) and speed in response to specific chemical inputs (Smith and Yang 2004)(Figure 1.5).

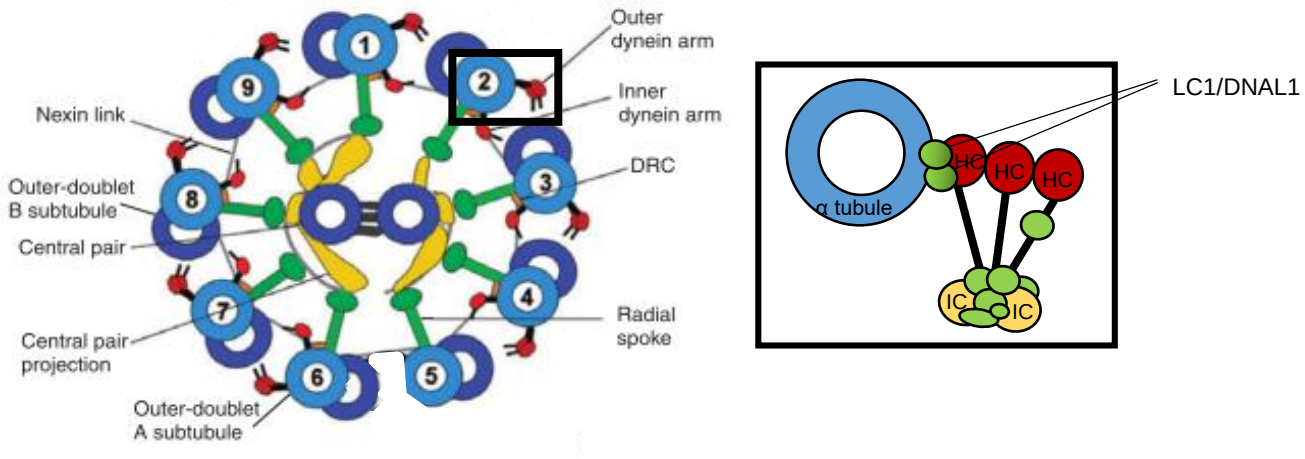

Figure 1.5: Schematic diagram of the motile ciliary and flagellar axoneme.
The cross-section illustrates the "9+2" conformation have nine doublet microtubules linked to two outer and inner dynein arms, the dynein regulatory complex (DRC) and the radial spokes, that connect it to the central pair apparatus (central pair projection plus central pair microtubule). Nexin link connect the adjacent doublet microtubules. The expanded view of the ODA schematically depicts several light (in green), intermediate (IC, in yellow) and heavy (HC, in red) chains, where two LC1/DNAL1 proteins link the heavy chain to the α tubule (in blue). Adapted from Kobayashi and Takeda 2012.

The sliding of the doublet microtubules relative to one another constitutes the basic movement-inducing interaction in the cilium structure. Dynein-generated forces cause this sliding, which is consequently converted to axonemal bending by the restraining influence of the basal bodies that anchor the axonemal microtubules to the cell.

Although much has been learned about dyneins in terms of their composition and location, there remain many outstanding questions concerning how they are assembled, transported and located at precise sites within the cilium. In addition, the dynamics of the dynein motor itself need to be better understood.

1.2.4. Ciliopathies

Ciliated cells are present in almost all organs throughout the human body, with a nearly ubiquitous appearance among the vertebrates. Adding to the fact that cilia exert innumerous functions during development, tissue morphogenesis and homeostasis, it is not surprising that cilia defects lead to an inadequate function of these tissues. Consistently, cilia dysgenesis and dysfunction have been associated to many different human disorders, generally named as ciliopathies. These cilia-related diseases can either involve single organs or can occur as multisystemic disorders with phenotypically variable and

overlapping disease manifestations. Consequently, these diseases have been associated with developmental defects affecting the central nervous system and the skeleton, reproductive system dysfunction, chronic airway diseases, cystic disorders of the kidney, liver and pancreas, defects in vision, smell and hearing and even in oncogenesis (Fliegauf *et al*. 2007).

Regarding the immotile cilia, defects appear to underlie a broad range of phenotypes, probably due to their nearly ubiquitous presence and their emerging role in signal transduction. Some major ciliopathies include Polycystic Kidney Disease (PKD), Bardet−Biedl Syndrome (BBS), Joubert Syndrome, Oral-Facial-Digital Syndrome, Alström Syndrome or Meckel Gruber Syndrome (Fliegauf *et al*. 2007, Hildebrandt *et al*. 2011) .

PKD or Autosomal Dominant PKD (ADPKD) is the most common potentially lethal disease in Europe, affecting 1 person in 1000. The disease hallmark is the development of hundreds of microscopic fluid-filled cysts in the kidney, which grow exponentially and continuously causing loss of normal renal tissue. ADPKD is caused by loss of function mutations in either Pkd1 or Pkd2, which encode the proteins polycystic kidney disease-1 and polycystic kidney disease-2, respectively. These two proteins interact with each other forming a complex localized in the cilia of the renal epithelial cells (Qian *et al*. 1997, Nauli *et al*. 2003) which is thought to be required to sense the fluid flow inside renal tubules. The mechanical stimulation of Pkd2, a calcium channel, leads to the influx of extracellular calcium, probably to regulate cell growth and differentiation. Recently, Kim and colleagues (2016) suggested that Pkd1/Pkd2 complex actively respond to non-canonical wnt ligands during kidney development, where Pkd1 is likely to function as a co-receptor. Consequently in ADPKD, the defective wnt-induced Pkd1/Pkd2-mediated calcium signaling would adversely affect multiple processes, contributing to cyst initiation/formation (S. Kim *et al*. 2016). Since polycystins are widely expressed, wnt/Ca^{2+} signaling is thought to mediate responses in other tissues rather than only in the kidney. Such assumption is supported by the wider phenotypic spectrum caused by Pkd1 and Pkd2 mutations compared with the phenotypic spectrum of ADPKD patients.

In contrast to the disorders of immotile cilia, the consequences of motile cilia dysfunction have four major manifestations in mammals resulting from the role of motile cilia in physiological processes: early embryonic death due to failure of embryonic turning, respiratory dysfunction, reproductive sterility, and hydrocephalus (Badano *et al*. 2006) being the Primary Ciliary Dyskinesia (PCD) the most prominent ciliopathy. PCD is a rare respiratory disease, usually with an autosomal recessive inheritance. It is characterized by respiratory tract infections and inflammation, sinusitis and bronchiectasis, due to impaired mucociliary clearance, resulting from motility defects in respiratory cilia, and to male infertility due to the lack of sperm motility. Almost 50% of all PCD patients also display organ laterality defects, as *situs inversus,* thereby defining the Kartagener syndrome (Afzelius 1976). The diagnosis of PCD is based on the identification of functional and ultrastructural abnormalities, and 80% of cases concern mutations in dynein arms (Papon *et al*. 2010), more recurrently in ODA. Depending on the ultrastructural defect, the

phenotypic movement of cilia can vary: when both ODA and IDA are affected, the majority of cilia are immotile; while IDA defects cause abnormal cilia beating pattern with reduced beating amplitude. Also anomalies in the radial spokes can lead to abnormal cilia beating (Chilvers *et al*. 2003). PCD is a group of heterogeneous disorders and so far more than 30 genes have been implicated as causative of these disease, which is predicted to explain roughly 70% of PCD cases (Horani *et al*., 2016).

1.3. Left-right organizer

In 1976, after the movement of cilia in a, yet to discover, embryonic epithelial tissue was linked to LR asymmetry (Afzelius 1976), several studies suggested that the node in mouse embryos was indeed the structure responsible for the LR axis formation, being designated as left-right organizer (LRO). Motile monocilia were observed on the ventral surface of the node in early developed embryonic mice (Sulik *et al*. 1994, Bellomo *et al*. 1996) and the gene encoding the left-right dynein, *lrd*, was found to be specifically expressed at the node, providing randomized *situs* when mutated (Supp *et al*. 1997). Ultimately, node ablation disrupted LR positioning at early organogenesis of the mouse embryos (Davidson *et al*. 1999).

The node is a quiescent structure located at the anterior tip of the primitive streak in mouse embryos, flanked by endoderm and the lateral plate mesoderm (LPM). The cup-shaped ventral node contributes to the formation of the notochordal plate and the floor plate (Sulik *et al*. 1994). Ultrastructural studies have shown that monocilia present on the ventral side of the node rotate in a counterclockwise direction, suggesting that a fluid flow is necessary for establishing LR asymmetry (Nonaka *et al*. 1998, Okada *et al*. 1999). Nonaka and co-workers demonstrated a leftward flow of embryonic fluid, which they called nodal flow, as the earliest LR asymmetric event in mouse development. Furthermore, they provided strong elegant arguments for the pivotal role of mechanical nodal flow in the patterning of LR asymmetries, through a culture system in which embryos grow under artificial constant flow (Nonaka *et al*. 2002). Applying a rapid rightward flow in WT embryos, which should develop a normal organ situs, resulted in reverse direction of observed nodal flow and consequently most of the embryos exhibited complete reversal of *nodal* and *pitx2* (LR markers of the LPM that precede organ *situs*). In opposition, when an externally leftward flow was applied in mutant embryos, which would normally lead to inverted LR orientation, it was sufficient to completely rescue the phenotype. For instances, the randomized LR patterning exhibited by the impairment of motile cilia in *iv* mutants was restored when the embryos were cultured under an external artificial leftward flow (Nonaka *et al*. 2002).

Such evidence, indicates that cilia within the cells of the node do not break the LR asymmetry by themselves rather they rotate in order to generate the directional leftward fluid flow essential for proper LR determination (McGrath and Brueckner 2003).

In zebrafish, the left-right organizer homologue of the mouse node is the Kupffer's Vesicle (KV). Thus, the KV is a ciliated organ of asymmetry in the zebrafish embryo that initiates LR development of the brain, heart and gut (Essner *et al*. 2005), and it is conserved among teleost fishes.

Cilia within the zebrafish KV arise from a group of approximately two-dozen of dorsal surface epithelial cells, known as dorsal forerunner cells (DFCs). These cells migrate at the leading edge of the embryonic shield throughout gastrulation and, ultimately DFCs cluster and undergo a mesenchymal-to-epithelial transition to differentiate into KV cells. Epithelial KV cells form a monolayer ellipsoid vesicle with fluid filled lumen at the tail region. During early somite stages, the KV rapidly expands as each cell forms and elongates a single cilium from their apical surface facing the lumen (Matsui and Bessho 2012).

Consistently with being analogous to node cells, KV cells express the left-right dynein-related 1 gene (*lrdr1*), the mouse homologue of the *lrd* gene. When *lrdr1* is knocked down, the motile cilia-driven fluid flow is impaired, which consequently alters LR development (Essner *et al*. 2005, Kramer-Zucker *et al*. 2005). Although the mouse and zebrafish LRO architectures are different, the net fluid flow in zebrafish KV is analogous to the nodal flow in the mouse, producing a leftward counterclockwise movement essential for LR patterning (Okabe *et al*. 2008). In addition, two populations of cilia, one motile and other immotile, were observed recently within the KV-lining cells (Sampaio *et al*. 2014) in agreement to McGrath and colleagues previous report in the mouse node (McGrath *et al*. 2003). Nevertheless, cilia within these two organizers have different conformations. Mouse node motile cilia are widely distributed through the ventral node and have a "9+0" structure, which generate an almost perfect circular motion by stiff cilia. As for the motile cilia within KV cells, they show both a bending and rotational motion, and present a "9+2" microtubule conformation. The fish cilia make a cluster on the anterior dorsal roof, in order to produce the directional flow. The presence of immotile cilia in the zebrafish KV supports the hypothesis that they may function as sensors of flow, as described for crown cell cilia of the mouse node (Yoshiba *et al*. 2012).

1.4. Two left-right models

The leftward fluid flow is the first LR asymmetric event and once it is settled leads to the second step which is sensing the flow. Two models have been proposed to explain how cells recognize the flow and translate the physical left-sided information into gene expression. Each model is based on different cilia properties, such as chemosensation and mechanosensation.

1.4.1. Morphogen model

The "morphogen model" was first proposed by Nonaka and colleagues (Nonaka *et al*. 1998). Based on the observation of a motile cilia-driven leftward fluid flow in the node, they suggested that a putative secreted factor was being transported by the nodal flow towards the left side (Figure 1.6). Such morphogen could

be the determinant for both sides, where the left side determinant activated the expression of the left side-specific genetic pathway, while the right sided determinant inhibits its expression. Thus the nodal flow would maintain a concentration gradient of the morphogen along the LR axis in the node (Okada *et al*. 1999, Okada *et al*. 2005). Tanaka and colleagues' work added important evidence to this model with regard to the identity of the putative morphogen. The authors observed flowing material composed by a lipid core and an outer membrane, which they called nodal vesicular parcels (NVPs). NVPs were described as being released from dynamic protruding cilia into the flow and then broken by crashing into cilia or cells, thereby releasing their contents in proximity to the left wall of the node. Tanaka and co-workers have shown that NPVs carry Sonic Hedgehoc (Shh) and Retinoic acid (RA), which are known to act synergistically. NVPs release was dependent on fibroblast growth factor (FGF) signaling (Tanaka *et al*. 2005). However, Cartwright and colleagues took these observations into account, modeled the movement of NVPs and showed that the flow could indeed cause them to accumulate on the left side of the node, for proper symmetry breaking. However, they argued that due to properties of the nodal flow there could not be any impact process involved in the NVPs rupture by cilia nor by the node wall. Instead, they predicted that a yet undiscovered biochemical mechanism that actively ruptures NVPs must exist, presumably chemical in nature (Cartwright *et al*. 2007).

Despite these interesting insights, several observations argue against this morphogen hypothesis. Although critical diffusivity indicates only proteins with mass higher than 20 kDa (kilo Dalton) can be directional transported, supporting the Shh and RA as morphogens, genetic analysis of mutants does not provide convincing support of their roles as nodal flow morphogens (Vermot *et al*. 2005, Zhang *et al*. 2001).

1.4.1.1. Revisiting the Chemosensation

In airways epithelial cells, Shah and colleagues (2009) discovered that not only taste receptors were expressed but also the main downstream effectors of the taste sensing pathway. Different Tas2 receptors were expressed throughout the ciliary membrane, while the G protein α-gustducin and the channel TRPM5 were localized within the cilia. As for phospholipase Cβ2, its expression was detected below cilia in the apical portion of the cell (Figure 1.7). The authors showed that bitter compounds induced both a transient, dose-dependent increase in intracellular calcium in ciliated cells as well as an increase in ciliary beat frequency. The response is thought to provide protection for the airway epithelium from noxious compounds and products of bacterial infection by speeding up the process of mucociliary clearance (Shah *et al*. 2009).

In spermatozoa, Meyer and co-workers (2012) detected the Tas1 receptors and the G protein α-gustducin. These proteins were localized not only in the convex side of the sperm head but also in the sperm flagellum, where it is thought to sense the diverse environmental chemical cues during the sperm passage through the female genital tract (Meyer *et al*. 2012).

Such evidence reinforce the idea that motile cilia, highly enriched with receptors and channels, are capable to sense, interpret and transmit external environment information through chemical signals, supporting the chemosensory hypothesis of the morphogen model.

The taste 1 and 2 receptors are part of the G protein-mediated system which is relatively complex comprising a receptor, a heterotrimeric G protein and an effector, which can be regulate independently by accessory proteins, soluble mediators or on the transcriptional level (Wettschureck and Offermanns 2005). G protein-coupled receptors (GPCRs) are seven transmembrane receptors that actively respond to several signals, including light, odor, chemokines, hormones, growth factors and neurotransmitters, thus affecting numerous cellular processes. Heterotrimeric G proteins function as molecular switches that activate intracellular signaling cascades in response to the stimulation of GPCRs, having a central role in cell biology. Heterotrimeric G proteins are divided in three subunits: alpha (α), beta (β) and gamma (γ), where the α-subunit controls the switching function through its own ability to cycle between an inactive GDP-bound conformation and an active GTP-bound conformation that modulates the activity of downstream effectors. Additionally, α-subunits can be distinguished into four families according to their structural and functional properties: Gs,Gi/Go, Gq/G11, and G12/G13, and βγ subunits form a functional unit to regulate ion channels, particular isoforms of adenylyl cyclase (AC), phospholipase C (PLC) and phophoinositide-3-kinase (PI3K). Therefore, heterotrimeric G proteins modulate cyclic AMP (adenosine monophosphate) through the enzymes adenylyl cyclase and phosphodiesterase (PDE) and lead to an increased calcium release from intracellular stores, via phosphoinositide-3-kinase enzyme (Oldham and Hamm 2008). Several components of the G protein mediated signaling are present in primary cilia, which have been associated with many sensory functions and also with ciliary defects (Hilgendorf *et al*. 2016).

In taste bud cells, these taste receptors namely Tas2r and Tas1r, detect bitter, umami and sweet ligands and transmit such information to nerves for food evaluation. The elicited response can vary from innate behavioral actions as aversion to attraction to food sources (Hoon *et al*. 1999, Adler *et al*. 2000, Ishimaru *et al*. 2005). Moreover, taste signaling is mediated specifically by G-protein alpha (α) subunit gustducin (McLaughlin *et al*. 1992) and its partners beta and gamma (βγ) subunits (Huang *et al*. 1999). Upon activation, these GPCRs activate phospholipase Cβ2 (Rössler *et al*. 1998) signaling pathway, triggering calcium release from endoplasmic reticulum in order to stimuli the transient receptor potential cation channel subfamily M member 5 (TRPM5). Opening of TRPM5 channels leads to sodium influx and depolarization of the taste receptor cell, which is necessary for ATP release, as a transmitter to activate afferent gustatory fibers (Zhang *et al*. 2007) (Figure 1.7). On the other hand, G protein α-gustducin activates a phosphodiesterase enzyme to decrease intracellular levels of cyclic AMP (adenosine monophosphate). Although the precise targets of cAMP have not been identified yet, it is thought that low levels of cAMP keep the phosphorylation levels of upstream effectors low as well as prevent chronic adaption to bitter taste stimuli (Clapp *et al*. 2008). Besides G protein α-gustducin, a G14 α-subunit was found to mediate residual partial responses that are sufficient for animal survival and reproduction (Wong *et al*. 1996).

Tas1 and Tas2 receptors and phospholipase Cβ2 orthologues have been found also in fish taste bud cells sharing a significant homology to each mammalian cognate taste receptor families (Ishimaru *et al*. 2005). Although the diversity of taste cells varies among species, the presence of the main components of taste sensing suggests a common mechanism of taste reception and an intracellular signal transduction pathway, at least at the level of effector molecules, among vertebrates (Matsumoto *et al*. 2013). Consistently, fish species respond to water-soluble chemical compounds and avoid a diet highly enriched with bitter components, where Tas2r are involved in avoidance feeding behaviors. However, phylogeny studies revealed a major exception concerning the G protein protein α-gustducin specialized gene for taste signaling in mammalians. No orthologue was found in several teleost and amphibian genomes, which could be due to the acquisition of gustducin gene by the land-living vertebrates or to the loss of it during evolution of teleost lineage (Oka and Korsching 2011). Nonetheless, two other G protein α subunits, gnaia and gna14, were discovered to be expressed in zebrafish taste-related tissues (Ohmoto *et al*. 2011). *gnaia* is a member of Gi α subunit class, which function as inhibitors of different adenylyl cyclases, and *gna14* is a member of Gq/G11 class, orthologue of the mammalian equivalent G14 α-subunit, that is thought to act as activator of phospholipase C isoforms. The outcome of these two G proteins is reduced cAMP levels, similar to the effect of G protein α-gustducin in mammalians, suggesting similar roles within taste sensing pathway.

Shah and Meyer's findings (Shah *et al*. 2009, Meyer *et al*. 2012) suggest an unexplored possibility for taste sensing-related signaling in LR patterning, through the Chemosensation Model.

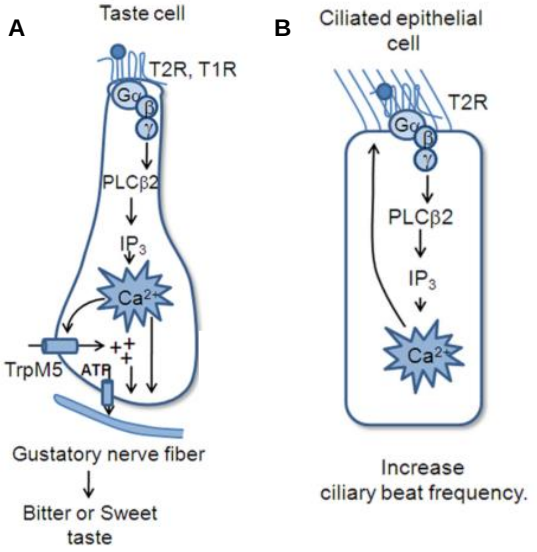

Figure 1.7: Diagrammatic illustration of differences in GPCR signaling effectors in the different cell types.

In both cases taste GPCRs activate the downstream PLC signal effectors, but the effects of increased calcium differ among the taste cells (A) and the ciliated epithelial cells (B). Adapted from Kinnamon 2012.

1.4.2. Two-cilia model

The second model was proposed by McGrath and colleagues (2003) upon the observation of two different populations of cilia in the mouse node, therefore they named it as the two-cilia model (Figure 1.6). The

authors reported that nodal cells in the center of the node had cilia expressing the left-right dynein (Lrd), the mouse orthologue of human DNAH11 (dynein axonemal heavy chain 11), whereas cilia of the surrounding horseshoe-shape ring cells were negative for the motor protein. Since left-right dynein is important for cilia movement, its presence or absence was interpreted as cilia capable or not to rotate. Hence, this model predicts that motile cilia in the center of the node generate the leftward fluid flow and the immotile cilia located at the node periphery are able to sensing it (McGrath *et al*. 2003, Tabin and Vogan 2003). This implies that a mechanosensor must be present in the ciliary membrane and that it undergoes a distortion in response to the external fluid shear stress, which can lead to the opening or closing of the conductive pathway through the channel. The force was envisaged to be applied either through cytoskeletal and extracellular matrix elements attached to the channel, or through membrane tension by the lipid bilayer itself (Sukharev and Corey 2004).

1.4.2.1. Evidence for Mechanosensation

Pennekamp and colleagues (2002) reported distinct LR laterality defects in Pkd2 null mouse embryos (Pennekamp *et al*. 2002). These homozygous mutants fail to produce the polycystic kidney disease 2 (Pkd2), a calcium channel that if mutated in humans causes autosomal dominant polycystic kidney disease (ADPKD). Moreover, McGrath and colleagues also reported that all nodal cilia expressed Pkd2, suggesting that it could have a sensory role in the negative lrd cilia population (McGrath *et al*. 2003).

An important cue to the mechanosensory model came from the finding that polycystic kidney disease 1 (Pkd1) and Pkd2 were expressed in primary cilia in kidney tubule cells, forming a complex that detects fluid flow and transduces it into an increase of intracellular calcium (Nauli *et al*. 2003). Nauli and colleagues proposed that Pkd1 functions as a mechanosensor that detects the bending of cilia induced by fluid flow, leading to conformational changes that in turn would open the Pkd2 channel. Pkd2, as a calcium channel, would then give rise to an influx of calcium that ultimately would alter gene expression, growth, differentiation and apoptosis.

Although Pkd1 is not expressed in the node and consequently is not necessary for the establishment of LR signaling, Pkd1l1 was found to be the functional partner of Pkd2 in mouse and medaka left-right organizers (Field *et al*. 2011, Kamura *et al*. 2011). In mouse node, Pkd1l1-Pkd2 complex is present in both motile and immotile cilia, where Pkd2 rescue specifically in crown cells (negative for lrd) restored the expression of left-sided genes Nodal and Pitx2 (Yoshiba *et al*. 2012). In medaka Kupffer's Vesicle, which is the fish homologue of the mouse node, all cilia contain the *lrd* motor protein and the Pkd1l1-Pkd2 sensor channel complex. Thus, Kamura and colleagues reconsidered the two-cilia model, arguing that in medaka generators and sensors of nodal flow are not segregated and motile KV cilia have both functions (Kamura *et al*. 2011).

In zebrafish, left-right patterning defects were also observed using Pkd2 morphants and mutants (Bisgrove *et al*. 2005, Schottenfeld *et al*. 2007). Motile and immotile cilia have also been found in the zebrafish KV (Sampaio *et al*. 2014) and Pkd2 is present in all zebrafish KV cilia along the axoneme and the basal body (Roxo-Rosa *et al*. 2015) reinforcing the idea that Pkd2 plays an important and conserved role in LR patterning among species. So far, no Pkd2 partner has been identified in the zebrafish KV.

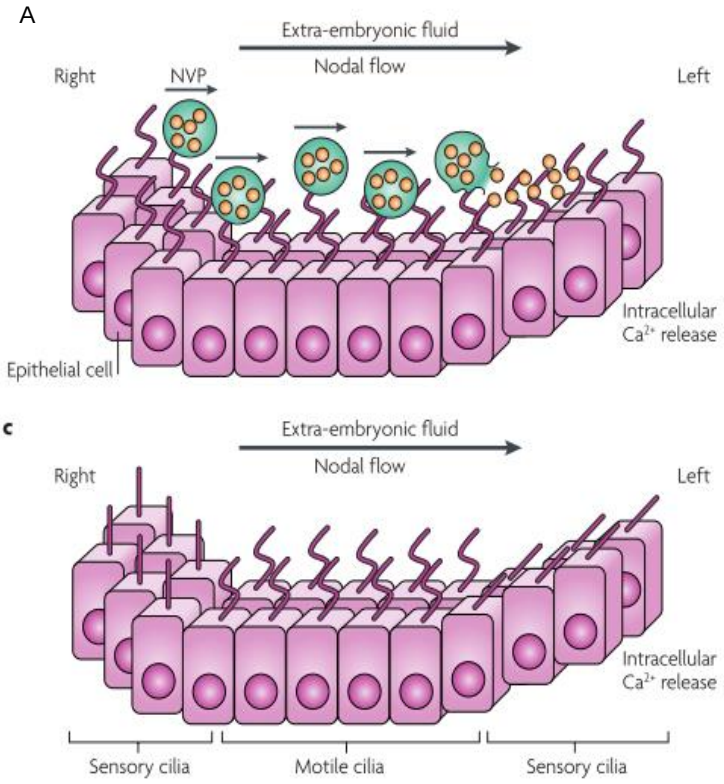

Figure 1.6: Current models for establishing LR asymmetry.

(A) The nodal vesicular parcel (NVP) model predicts that vesicles filled with morphogens are secreted into the fluid and are transported to the left side by nodal flow, where they are smashed releasing content. (B) In the two-cilia model argues that motile cilia in the node create a leftward nodal flow that is mechanically sensed through passive bending of non-motile sensory cilia at the periphery of the node. Bending of the cilia on the left side leads to a left-sided release of Ca2+ that initiates the establishment of body asymmetry (Fliegauf *et al*. 2007).

Both models can explain certain aspects of LR establishment, but a lot of questions remain unanswered, it is thus unclear which is the correct view of how nodal flow is interpreted by the embryo. It is plausible that both chemosensation and mechanosensation can be correct, acting together to form a robust process from which results the proper LR development.

1.5. Asymmetric Gene Cascade

Once the nodal flow is transduced by the node cells, it then triggers a left-sided genetic signaling cascade in the node, (that is not well explored) which is later transmitted to the lateral plate mesoderm (LPM). The requirement of Pkd2 calcium channel in LR axis formation strongly supports that calcium signaling plays a crucial role between sensing the flow and the activation of asymmetric gene pathway on the left side of the embryo.

In mouse, Pkd2 was found to be required only in the immotile ciliated crown cells, at the node periphery, regulating calcium signaling, which was increased in both sides of the node (Yoshiba *et al*. 2012). Dynamic calcium signals in the node were observed to become gradually biased to the left side, during development (Takao *et al*. 2013). Similar Pkd2-dependent calcium oscillations were observed within zebrafish cilia that were transduced to the cytosol and surrounding cells on the left side of the KV (Yuan *et al*. 2015). These data suggest that both calcium signal amplitude and frequency may regulate asymmetric patterning.

In mouse, two secreted proteins are expressed bilaterally in the node: the Nodal gene, which encodes a member of the transforming growth factor beta (TGFβ) (Collignon *et al*. 1996), and the Cerberus-like 2 (Cerl2) gene, Nodal antagonist. Upon the activation of the Nodal cascade signaling, Cerl2 levels become higher on the right side of the node and Nodal becomes restricted to the opposite side (Marques *et al*. 2004). Expression of Cerl2 appears to be the most direct outcome of the flow signal, hence it initiates Cerl2 mRNA degradation on the left side (Nakamura *et al*. 2012). Being a secreted protein, Nodal spreads out to the left side of the LPM, where exerts a positive feedback to induce its own expression and to activate its own negative regulators. Among these, the Lefty genes are crucial to prevent ectopic Nodal induction in the right side of LPM and to control the Nodal domain after initiation, where Lefty1 is expressed in the midline barrier and Lefty2 is expressed in the left lateral plate mesoderm. In addition, Nodal in the LPM regulates the expression of the downstream effector Pitx2, a key transcription factor responsible for the situs-specific organogenesis.

In zebrafish, the left-sided calcium increase through Pkd2 activates transiently CaMK-II, a Ca^{2+}/CaM-dependent protein kinase (Francescatto *et al*. 2010). CamK-II activation was observed only in cells lining the left sided functional KV, suggesting that CamK-II could enhance left sided Nodal-related protein, Southpaw (Spaw) in the node, or could influence the secretion of it into the LPM. Spaw and Dand5, a member of the Cerberus family, are the orthologues of Nodal and Cerl2 present in mouse node. Similarly to the genetic signaling cascade in the mouse, *dand5* is first expressed bilaterally in KV. At 8-10 somite stage, in response to the fluid flow the *dand5* expression pattern becomes stronger on the right side of KV (Lopes *et al*. 2010), where Dand5 antagonizes Spaw function and prevents *spaw* expression in the right LPM (Hashimoto *et al*. 2004). Despite in zebrafish *spaw* remains always bilateral in the KV, only on the left side of KV, Spaw can activate its own expression via an auto-regulation mechanism throughout the left LPM.

This process although presents some differences between species strengthens the evolutionary conserved feature of Cerl2/*dand5* expression as well as the Nodal cascade signaling during the LR axis formation.

1.6. Project goals

The main goal of this Master project was to investigate the molecular basis of biochemical and mechanical pathways activated by motile cilia in the zebrafish KV.

To test the chemosensory pathway, we studied several G protein couple receptors as well as the downstream effectors. This model is based on the presence of a morphogen flowing in the LR organizer, however there is yet no available technology sensitive enough to analyze the content of such small volume as is the fluid inside the KV. Therefore, we reasoned that the putative morphogen would trigger the chemosensory signaling through binding to a receptor expressed in motile KV cilia. We investigated the sweet taste receptors, *tas1r1*, *tas1r2.2* and *tas1r3*, because they were found to have chemosensory functions in spermatozoa (Meyer *et al*. 2012), the bitter taste receptors, *tas2r200.2* and *tas2r201.2*, as well as the downstream effector *plcb2*, and two other putative downstream effectors *gnaia* and *gna14* based on their capacity of sensing chemical signals within motile cilia, as reported by Shah and colleagues (Shah *et al*. 2009). These genes were expressed in an unpublished microarray from Lopes lab that analyzed the genes specifically expressed in the KV cells in WT embryos.

Regarding the mechanosensory model, we tested ten different genes potentially involved in LR signaling pathway, including wnt signaling (*wnt4a*, *csnk1g1*), bmp signaling (*fsta*, *bmp2b*, *smad4*), calcium binding signaling (*cacng2a*) and others (*foxi1*, *crb2a*, *azin1a*, *rragca, dlk1*). We wanted to find more asymmetric genes that could be intermediate players between flow, pkd2 pathway and *dand5* expression, a link not fully characterized. For this propose we used the previously mentioned microarray dataset for genes specifically expressed in the KV cells of WT embryos and Pkd2 morphants. The candidate genes were all expressed in both analyses and in order to test for asymmetries we did an *in situ* hybridization screen for their expression pattern in the KV. The two-cilia model gave rise to another interesting question: what determines the difference between the two cilia populations involved in LR axis formation. In the mouse node, the two types of cilia are proposed to be distinguished by the presence or absence of left-right dynein - Lrd. Where motile cilia are positive for Lrd and immotile cilia are negative for the Lrd (McGrath *et al*. 2003). However, in zebrafish KV cells we noticed that the percentage of motile and immotile cilia varied during the LR development. As the total number of cilia remains the same, we can observe that 80% of immotile cilia become motile. We hypothesized two possible explanations for this: (1) all cilia undergo the same ciliogenesis process, being structural equal to each other, and over time a specific molecule or signal switches the motility on in 80% of cilia. (2) 20% of cilia, the true immotile cilia, may have different ultra-structure, where plausibly the dynein motor proteins are absent. To test this, we evaluated the localization of Dnal1, an outer dynein arm component that links the motor proteins to the microtubules, within the KV cilia.

In summary, the main objectives of this project were: (1) Testing the Chemosensory Hypothesis; (2) Screening for asymmetric gene expression in the KV and (3) Looking for cilia motility vs. immotility markers.

2. MATERIALS AND EXPERIMENTAL PROCEDURES

In the best interest to answer our defined objectives, we performed different experimental procedures as described below.

2.1. Microarray Analysis

In order to identify genes which expression is regulated by Pkd2 function, before I joined Lopes' lab they decided to do a very strict tissue specific mRNA profiling analysis by microarray. They used non-injected embryos and pkd2 knockdown morphants at 14 hpf (10 somites stage) to extract KV-specific RNA. For that purpose they used one Foxj1a: GFP zebrafish reporter line, which expresses the minimum promoter region of a forkhead domain-containing transcription factor (*foxj1a*) driving the green fluorescent protein (GFP) tag. This line labels the KV cells and slighty the neural tube cells in green and it was used to purify this cell population by Fluorescence Activated Cell Sorter (FACS). Therefore, they ended up with two collection tubes, one with the KV cell population marked by GFP and another with the remaining cells without GFP fluorescence. After that, they extracted RNA from control embryos and pkd2 morphants KV cells and the transcripts were accurately detected as their expression were measured.

The aim of this transcriptomic study was to catalog and quantify the RNA content of KV cells, regardless of their structure or function, like a snapshot of all activated genes. By the time I came to the lab, a long gene list had already been compiled, thus we selected a shorter list based on literature of target genes that could have a role within left-right patterning.

We looked at genes whose expression was altered by the knockdown of *pkd*2 as possible targets of Pkd2 function. The rational was that by changing *pkd2* expression levels, the calcium signaling through cilia would be impaired and the corresponding downstream pathway would be affected. From this point of view, we selected the following genes: antizyme inhibitor 1a (*azin1a*, NCBI Gene ID: 550230); casein kinase 1, gamma 1 (*csnk1g1*, NCBI Gene ID: 494092); forkhead box i1 (*foxi1*, NCBI Gene ID: 353313); follistatin a (*fsta*, NCBI Gene ID: 100004116), bone morphogenetic protein 2b (*bmp2b*, NCBI Gene ID: 30632); crumbs homolog 2a (*crb2a*, NCBI Gene ID: 723994); wingless-type MMTV integration site family, member 4a (*wnt4a*, NCBI Gene ID: 30123), ras-related GTP binding Ca (*rragca,* NCBI Gene ID: 573492), SMAD family member 4 (*smad4*, NCBI Gene ID: 559111), calcium channel, voltage-dependent, gamma subunit 2a (*cacng2a*, NCBI Gene ID: 393614) and protein delta homolog 1 (*dlk1*, NCBI Gene ID: 101883341). We named them as Pkd2-dependent target genes.

Nevertheless, from the microarray analysis another list of genes came up as not significant nor differentially expressed between pkd2 morphant embryos and their siblings. Since experiments from our lab have suggested a Pkd2 independent pathway in left-right patterning, we decided to test this idea using these non-differentially expressed genes. We narrowed our research to genes related with taste sensing and perception in order to test the chemosensation hypothesis. The selected genes were: taste receptor,

type 1, member 1 (*tas1r1*, NCBI Gene ID: 654781); taste receptor, type 1, member 2, tandem duplicate 2 (*tas1r2.2*, NCBI Gene ID: 664686); taste receptor, type 1, member 3 (*tas1r3*, NCBI Gene ID: 562318); taste receptor, type 2, member 200, tandem duplicate 2 (*tas2r200.2*, NCBI Gene ID: 562318); taste receptor, type 2, member 201, tandem duplicate 2 (*tas2r201.2*, NCBI Gene ID: 100333330); guanine nucleotide binding (G protein), alpha inhibiting activity polypeptide a (*gnaia*, NCBI Gene ID: 323509); guanine nucleotide binding protein (G protein), alpha 14 (*gna14*, NCBI Gene ID: 445297) and phospholipase C, beta 2 (*plcb2*, NCBI Gene ID: 569376). These genes were considered as Pkd2-independent target genes.

A diagram with the main steps involved in this microarray dataset is presented below.

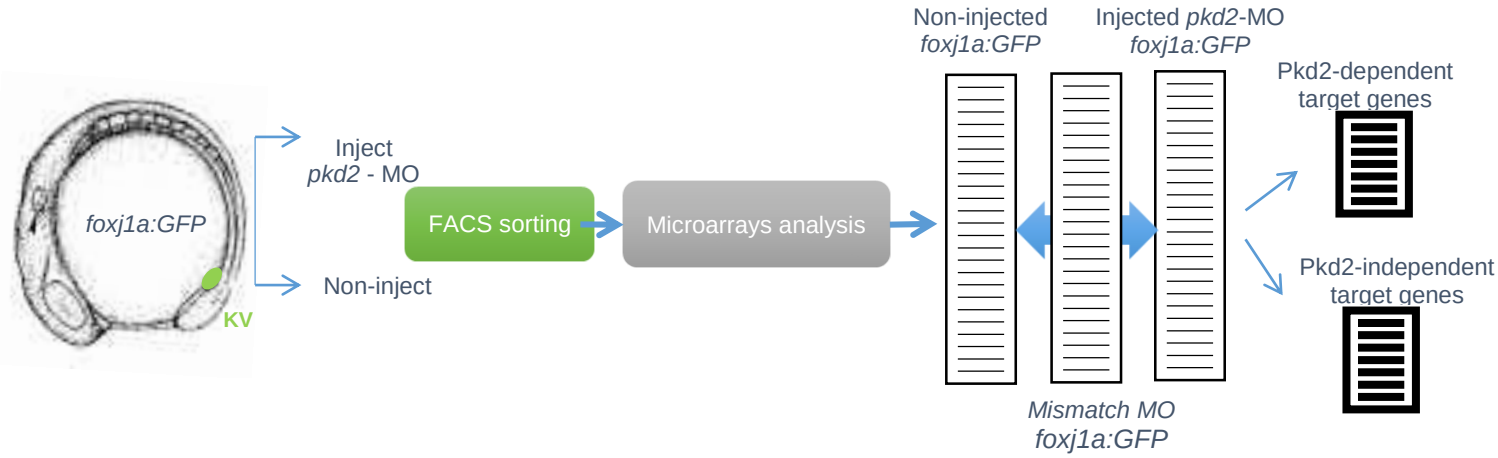

Figure 2.1: Diagram of microarray setup.
KV cells labeled with foxj1a:GFP from *pkd2* atgMO injected embryos, 5-mismatch MO injected embryos and their non-injected siblings were sorted by FACS. A 5-mismatch MO was used as a control of *pkd2* atgMO injection, specificity and toxicity. The expression levels of activated genes in KV cells were detected by the microarray analysis, and then we compared both transcriptomes. Genes that were found significant and differentially misregulated in Pkd2 injected embryos were grouped in a Pkd2-dependent targets list, while genes that were not differentially expressed were listed as Pkd2-independent targets.

2.2. Zebrafish breeding

Zebrafish general maintenance and breeding, and egg collection were performed at the CEDOC fish facility (Lisbon, Portugal), according to standard procedures described in the zebrafish book by Westerfield (1995).

For zebrafish breeding, we used mating tanks that have a removable insert with holes that allow eggs to fall through. This feature protects the eggs from being eaten by adult fish. Zebrafish adults are collected from the main tank system and are placed in a mating box during the afternoon or evening. Usually, in each mating tank we put one male and two females separated with a divider. This transparent partition avoids fishes from breeding before the desired time and allows the visual contact initiating the courtship behavior between the male and females. In the following morning, we remove the divider and reduce the water level, which favors the mating ritual behavior to continue. As the males chase the females around the tank, they stimulate spawning of eggs while releasing sperm into the water for external fertilization. After a few minutes, adults are removed from the tank by using a net and placed again into the main tank system. The eggs are collected and placed in one or more Petri dishes, in order to achieve an optimal density of 50 – 100 embryos per dish, with embryonic medium (5 mM NaCl, 0.2 mM KCl, 0.3 mM CaCl2, 0.3 mM MgSO4, ddH2O – pH 6.5). Embryos stayed in temperature-controlled incubators either at 25ºC or 28ºC until the desired developmental stage for our experiments.

Wild type AB line and transgenic line Arl13b: GFP zebrafish were used for this thesis purpose and embryos were staged according to Kimmel *et al* (Kimmel *et al.,* 1995). The period of embryogenesis is given in hours post-fertilization (hpf) and days post-fertilization (dpf) according to morphological features. For somite-staged embryos, we also took into account the number of somites to infer their developmental time.

2.3. Quantitative Real-Time Polymerase Chain Reaction (qPCR)

The qPCR analysis associates PCR amplification and detection into a single step, which allows to quantify gene expression even when we have minute amounts of nucleic acids. Amplicon recognition is achieved by monitoring the accumulation of fluorescent signal during each cycle.

For Pkd2-independent target genes, we wanted to evaluate the low transcription levels that we obtained with the microarray dataset. In order to do that and to confirm taste receptors and their downstream effectors expression, we used the qPCR technique in WT embryos. Regarding Pkd2-dependent target genes, the qPCR was also done, in order to compare and validate the gene expression levels from the microarray data between wt and Pkd2 knockdown embryos.

So first, for Pkd2-independent targets, we did both primer validation, to test primer specificity, and qPCR experimental assay for the ones that passed validation, in WT whole-embryos at 10 hpf (bud stage) and 13 hpf (8 somites stage). We also confirmed the expression levels of the most promising targets in samples of KV-specific cells (*tas2r201.2* and *gnaia*). Whereas for the possible downstream effectors of Pkd2, we used morphant embryos and their siblings at 13 hpf.

To design the primers for cDNA amplification, we used the Primer-BLAST bioinformatics tool from NCBI, which allow us to choose complementary sequences with exon-exon boundaries. This is an important feature because primers will bind specifically to messenger RNA and not to DNA sequence that may have been left in the sample. Primer sequences are described in Table 2.1. Regarding the reference genes, *rpl13a* (ribosomal protein L13a, NCBI Gene ID: 560828,) and *eef1a1a* (eukaryotic translation elongation factor 1 alpha 1a, NCBI Gene ID: 336334), the primers used had already been optimized in our lab.

Table 2.1: Nucleotide sequence of forward and reverse primers for each gene used in qPCR assays and respective probe length (bp).

Code	Primer Fw	Primer Rv	Probe length
rpl13a	TGACAAGAGAAAGCGCATGGTT	GCCTGGTACTTCCAGCCAACTT	117
eef1a1a	CCTTCAAGTACGCCTGGGTGTT	CACAGCACAGTCAGCCTGAGAA	182
tas1r1	GTGCGCTCTTTTCAGGTTGTTTGT	AGCATGCGGAGAACAGAGATGAA	146
tas1r2	CACTCTCTTGCCCTGGCATAAC	GGGGTCCCGAGTATAATCCACATA	154
tas1r3	TCTGTCCAGTTCCCTTCAGATTGT	TAGGCCATACCAGCCGCATAGT	148
tas2r200.2	GGAGTTGGGGTTGTCGGTGTTT	TGCCAACCACCATGCTGAGAATA	163
tas2r201.2	CCCACCTGTCTGGCTGTACATT	CAAGGCCATCGGACTGGAACAA	126
gnaia	GGCCGCCTGAGGATTGACTTT	CCCTCCAGAGCCGCTTGATTAC	133
gna14	CGCTGAGTGCCATGCAGTCTAT	GAATCCCGCTGTCGCTCCATAA	177
pbcβ2	AGCTCATCGGTTTGCCCAAAGA	GGGATGATGCGGTGACCAATGA	190
wnt4a	GACGCAAGTTTTGCGCTGAGAA	GCTTGGCCAGGTATAGCCAGTT	177
csnk1g1	CTCAGCACCAACCCTTGAGGAA	AAACAGCAGCACTTGGCCTCAT	145
bmp2b	AATCGGCAGTGGTCCCTCAGTA	GCCTCGAAAGCCTCTTCGTGAT	166
fsta	ACGCCTACTGTGTGACATGCAA	TCATCGCATGACTTGGCCTTGAT	184
rragca	GTCATCGACGCTCAGGATGACTA	AGCTTGCATCTGCCAGGTCAT	196
crb2a	GTTCCTGTTGGCCAGGTTTTGAA	TCCTGGTTGGCACTGACATACAT	179
foxi1	AGTTGCACGGGATGAGGATGAT	TAAGCGCGTCCTCGGATTTCA	152
azin1a	TCTCTTACATCGGTGCTCGTGTT	GTAGTTCAGGTACACACGGGAGAA	103

dlk1	TGTGAATCTCCCGGCGAGTGTA	GGCAGTGTGTAGCAGTGCAGAT	163
cacng2a	CCGTGCGAGCGTCTAGTATCTT	GTTACTGAGGCCTGCAGACACGAA	149
smad4	CCAGACCTCCACATACCACCACAA	CAGTATTCAGGAGCAGGGTGGTT	195

The qPCR reactions were performed in a LightCycler ® 96 Real-Time PCR system (Roche), using FastStart Essential DNA Green Master (Roche).

We performed a qPCR validation assay for each primer pair with a serial dilution of cDNA (1:10, 1:1, 1:0.1) with three replicates for each concentration. A negative control (water) reaction was also done for each primer in order to evaluate primer-dimers and possible contaminations. We used the following cycling parameters: pre incubation at 95ºC for 10min, three step amplification at 95ºC for 10s, 60ºC for 10s and 72ºC for 20s in 45 cycles, melting at 95ºC for 10s, 65ºC for 60s and 97ºC for 1s, and cooling at 37ºC for 30s.

Then we analyze the obtained melting peaks and standard curves to access primer annealing specificity and reaction efficiency, respectively. The melting curves represent melting peaks by plotting the first negative derivative of the fluorescence as a function of temperature (-dF/dT). Therefore, products of different lengths and sequences will melt at different temperatures and are observed as distinct peaks. If the chosen primers are specific, a single sharp peak appears. If we obtained more than one sharp peak that probably means that more than one amplicon was transcribed and means the designed primers are not suitable. Regarding the standard curve, it is constructed by plotting the log of the starting quantity of the template against the C_q values obtained (Taylor *et al.* 2010), to access qPCR efficiency. A 100% efficient reaction represents the maximum increase of amplicon which is 2-fold per cycle. Efficiencies lower than 90% or higher than 110% are indicative of reaction problems that can cause artifact results.

All data obtained were normalized with the reference genes. In these experiments, we used the *rpl13a* and *eef1a1a* genes that were validated as reference genes for developmental time course studies of zebrafish. They have not only a high transcript abundance but also a high expression stability during embryonic development (Tang *et al.,* 2007). Reference genes are important for proper normalization, in which they are responsible to compensate for the intra and inter-kinetic qPCR variations that result from basic difficulties during the method itself.

2.4. High Resolution Whole Mount *In Situ* Hybridization (WISH)

The *in situ* hybridization (ISH) method is a well-established technique which is used to detect and localize specific nucleic acid targets allowing to ensure the spatial and temporal expression patterns of particular genes, in preserved tissue sections or entire embryos. Using digoxigenin (DIG)-labeled RNA antisense probes that can bind to complementary sequences within the tissue, we are able to obtain valuable information in a specific way. Nevertheless, due to variable probe sensitivity in identifying targets that have low DNA or RNA copies and to tissue penetration, this technique is not so appropriated for transcript relative quantification as it is for transcript localization in tissues. The whole approach takes three days and, because ISH settings are the same for each probe tested, allows high throughput analysis of zebrafish gene expression for different targets in parallel.

We performed whole-mount *in situ* hybridization (WISH) experiments to evaluate the expression patterns of our selected target genes in zebrafish WT embryos and in pkd2 knockdown morphants.

2.4.1. ISH probes design

Since any RNA probe for our target genes had been developed in our lab and, instead of asking for each one of them to several groups, we decided to make new probes ourselves. We thought that by using the same parameters to select all probes we would have a more straightforward assay.

Therefore to perform the ISH experiments we started by doing primer design for amplification of probe templates. We designed primers with NCBI/Primer-BLAST bioinformatics tool. And probe sequences were aligned with zebrafish genome using BLAST: Basic Local Alignment Search tool, also from NCBI, to guarantee primer specificity (see an example in annex I). Thus, selected *in situ* probes bind specifically to the mRNA of each correspondent gene avoiding off targets. Primer sequences are described in Table 2.2.

Table 2.2: Nucleotide sequence of forward and reverse primers for each gene in study used in ISH assays and respective probe length (bp).

Code	Primer Fw	Primer Rv	Probe length
gnaia	TTGCAAGTCTGCCACCGTT	TGGGAAAGCCCATTTCTGCC	414
wnt4a	AGATGCACACGTGTCGGTGA	TCGTGCACAGAATCCACGGT	602
csnk1g1	ACAAGAGCCTTACCGGCACA	GAAACAGCAGCACTTGGCCT	605
bmp2b	AGTCTCCAAACAGCCACGGA	TGGGGTGGGTTTTCGCTTCA	545
fsta	AACCTCCCACCCCTCCAAAT	AGCGGTTTACGTCGTAGTGC	509
rragca	ACCCAGCGGGACATACATCA	ACTGGCTGGTTGCTTGTCCT	572
crb2a	AGGGTGCAACTGTTTGGGGT	TGCCCCAAAGCATCCCAAGT	878
foxi1	ACGGAAACGCGATGTCTGTG	AACTTCTGATCCGTCCCGGT	416
azin1a	AGCTAAACGCCTTCAACCGT	AGATGAGACGCCAAAGCCCT	671
dlk1	ACACACTGCACAGTCAACGG	GATGATGTTCACGGTGGCCT	543

Next, we amplified the respective fragments of each primer pair by PCR with Taq DNA Polymerase (Thermo Scientific). Cycling parameters used were as follows: initial denaturation at 95ºC for 10 min, denaturation at 95ºC for 1min, annealing at 54ºC (for azin1a, csnk1g1, foxi, bmp2b, cacng2a, wnt4a, rragca), 55ºC (for dlk) or 60ºC (for fsta) for 1min, extension at 72ºC for 1.5min in 35 cycles and final extension at 72ºC for 2min.

After, PCR products were purified using DNA clean and concentrator kit (Zymo Research) according to the instructions of the manufacture. Clean-up of reactions prior to ligation is recommended to remove primer dimers or other undesired reaction products and to improve ligation efficiency. Ligation reaction was performed using DNAligaseT4 (Promega) using a 1:3 molar ratio of the DNA insert to the pGem-Teasy vectors (Promega).

Then, competent E. Coli DH5α (NEB) were transformed with pGem-Teasy vector applying heat-shock transformation protocol. Cells with pGem-Teasy vector were selected based on bacterial resistance of the plasmid, growing on Luria Broth agar (Sigma) with 100µg/ml ampicillin as recommended concentration. To confirm that amplicillin resistant cells had the DNA insert and not just the circular vector, we performed a colony PCR using NZYTaq DNA polymerase (NZYTech) according to the manufacture instructions. We used the following cycling parameters: initial denaturation at 95ºC for 1min, denaturation at 95ºC for 1min,

annealing at 67ºC for 1min, extension at 72ºC for 1.5min in 30 cycles and final extension at 72ºC for 10min.

The positive bacteria for the DNA insert were inoculated to primary cultures. A liquid culture, that is capable of supporting a higher density of bacteria, was used to grow up sufficient numbers of bacteria necessary to isolate enough plasmid for DNA sequencing.

Plasmids were sequenced with T7 forward primer (5'-TAATACGACTCACTATAG-3') by STAB VIDA company through Sanger method. The sequencing results were analyzed allowing us to construct vector maps for each ISH probe and to select the suitable restriction enzymes for linearization.

The pGem-Teasy vector contains two opposable promoters - T7 and SP6 RNA polymerase promoters - flanking a multiple cloning region, which allowed us to do anti-sense and sense strands by using unique cutters restriction enzymes and then transcribing with T7 (Promega) and SP6 (Roche) RNA polymerases.

All restriction enzymes used were from NEB® Inc. and hydrolyze with CutSmart Buffer, at 37ºC. After we obtained the linear plasmids, we proceeded with DNA template transcription for synthesis of both probe (antisense strand) and negative control (sense strand) RNAs. RNA probes were labeled with digoxigenin (DIG) (Roche), which is one of the most sensitive non-radioactive based detection methods used in ISH.

TURBO DNase (ThermoFisher Scientific) was added during 15min, at 37ºC, to clear the sample from any remaining DNA.

At the end, RNA probes were diluted in hybridization mix solution supplemented with torular yeast RNA, which is added to reduce the non-specific binding that leads to the high background signal (see RNA probes dilutions in Table 2.3). After that, they were stored at -20ºC until the first day of ISH experiment.

2.4.2. Whole-mount *In Situ* Hybridization (WISH) protocol

The WISH was performed as described in Thisse's protocol (Thisse and Thisse 2008). The embryos, both Pkd2 morphants and their control siblings, developed until the pretended stages (see embryo stage used in Table 2.3) and then they were fixed in PFA-PBS 4% overnight. In the following day, PFA was replaced by methanol 100% and the embryos were stored at -20ºC until the beginning of the protocol.

In the first day, the embryos were rehydrated by going through a series of 75%, 50%, 25% MeOH-PBS for 5 min each at RT and then four washes for 5 min in PBT 100% (PBS/Tween20 0.1%). Next, we manually dechorinated the embryos and permeabilized them with Proteinase K (10µg/ml) at RT, during 1 min in case of 8ss embryos, 3 min to 16ss embryos, 15 min for 24 hpf embryos and 30 min for 48 hpf embryos. After that, all embryos were fixed in PFA-PBS 4% for 20 min, at RT, and then were washed 5 times for 5 min in PBT.

Embryos and RNA probes were incubated with pre hybridization mix solution (Formamide, 20x SSC, Tween20 10%, 1M Citric acid at pH 6 and Heparine (0.63mg/ml)) at 70ºC. Upon two hours of pre hybridization, probes were added to the embryos and incubated overnight.

In the following day, probes were recovered and stored at -20ºC and the embryos were put through 100%, 75%, 50% and 25% Hyb-Mix/2x SSC (NaCl 175.3g, Citric acid trisodium salt 88.2g dissolved in 1L of water) series of 15 min each at 70ºC, and then were washed with 2x SSC for 15 min. After the hot washes, embryos were submitted to room temperature (RT) washes in a series of 0.2x SSC two times for 30 min and 75%, 50%, 25% 0.2x SSC/PBT for 10 min each, and one last wash with PBT for 10 min. Embryos were blocked with blocking solution (50ml PBT, 100mg Bovin Serum Albumin and 1ml Goat Serum) in RT horizontal rotator for 5 hours. This step saturates nonspecific binding sites for the anti-DIG antibody conjugated to alkaline phosphatase (AP) (Roche), in which embryos were then incubated at a 1:5000 dilution in blocking solution, overnight at 4ºC.

In the third day, antibody staining was removed and embryos were washed with PBT, following an extensively set of 6 washes for 15 min in PBT. Next, the embryos were equilibrated in alkaline Tris staining buffer (1M Tris at ph 9.5, 1 MgCl2, 5M NaCl, Tween20 10%) changed 3 times at 5 min intervals. After that, staining buffer was replaced by color staining solution, a yellow stain made with NBT/BCIP (Roche). NBT/BCIP provides an intense and insoluble purple precipitate when reacted with AP. When the suitable level of purple staining was achieved, we stopped the revelation by adding PFA 4% for 20 min at RT, following a several washes with PBT. The clearance was done with 50% PBT 50% Glycerol and the embryos were stored at 4ºC until the photographic registration.

Table 2.3: WISH experiment. List of mRNA probes, dilution factors and developmental stages of the embryos used.

mRNA probes	Dilution factor	Developmental stages of the embryos used
gnaia	2.5:100	8-10 somites stage (~13 hpf) and 4 dpf
wnt4a	1:100	8-10 somites stage (~13 hpf) and 24 hpf
csnk1g1	1:100	8-10 somites stage (~13hpf)
bmp2b	1:100	8-10 somites stage (~13 hpf) and 24 hpf

fsta	2.5:100	8-10 somites stage (~13 hpf) and 48 hpf
rragca	1:100	8-10 somites stage (~13 hpf)
crb2a	2:100	8-10 somites stage (~13 hpf) and 30 hpf
foxi1	5:100	8-10 somites stage (~13 hpf) and 30 hpf
azin1a	1:100	8-10 somites stage (~13 hpf) and 24 hpf
dlk1	1:100	8-10 somites stage (~13 hpf)

2.4.3. Mounting zebrafish embryos for photographic register

After the WISH assay, the embryos were mounted in glass slides in order to register the expression patterns of each target gene among the embryo and also to specifically observe the Kupffer's vesicle, our organ of interest. For the whole mounted embryos, two small lamellas were fixed with silicone to the two edges of a glass slide, in this way when we had to cover the embryos we would not smash them down. In the center, the embryo was placed in 50% PBT 50% Glycerol. A larger lamella was used to cover the sample and by moving it gently the embryo was re-orientated until it reached the right position. Regarding the flat mounted embryos, the process was similar but firstly the yolk sac had to be removed using two forceps. Then, the embryo was placed in a glass slide within a circle made with silicone. Embryos were positioned with the dorsal side facing the objective lens, in order to get dorsal views, and a lamella was used to cover the sample. A little pressure was applied to seal the preparation and remove air bubbles.

All samples were observed and photographed in Olympus IX51 Inverted Microscope (4x/0.1NA and 10x/0.25NA objective lens) using the High Resolution Color Camera (Olympus DP72, Japan). The images acquired were treated with the free software "imageJ".

2.5. Morpholino Injection

Morpholino (MO) oligonucleotides are a well-established anti-sense knockdown tool that has been widely used among the zebrafish society. MOs are short synthetic chains of about twenty-five subunits, with a similar structure to the natural nucleic acids. Each subunit contains a nucleic acid base and a morpholine ring that are linked by a non-ionic phosphorodiamidate intersubunit. MOs bind specifically through complementary base pairing to the target RNA with high affinity, avoiding the off-target expression modulation. MOs can either block their mRNA target translation initiation in the cytoplasm or modify pre-mRNA splicing in the nucleus, instead of sending them to degradation. In this way, we are able to knockdown gene expression without inducing immune responses nor major toxic effects.

2.5.1. Morpholino design

We wanted to evaluate the expression pattern of our target genes by in situ in both wt and *pkd*2 knockdown situations. For that, we injected a MO against *pkd*2 in half of the embryos obtained in each laying to compare with their siblings. We had already a morpholino for knockdown of *pkd*2 in the lab and it had been designed according to Schottenfeld (Schottenfeld *et al*. 2007b). Therefore, its sequence was: 5' AGGACGAACGCGACTGGAGCTCATC 3'. This MO is a *pkd*2 augMO, meaning that begins at the start AUG and extends into the first exon, preventing the mRNA from being translated into a protein.

We also wanted to block *gnaia* translation to analyze if it would cause LR defects in zebrafish embryos. The sequence of the morpholino used as a tool for knocking down g*naia* was: 5' AGAATTATCATACACAGGCGGGTGA 3'. This *gnaia* augMO binds to the mRNA sequence within the initial coding region (AUG) (Annex II) inhibiting the ribosome assembly. As a consequence, the translation is blocked and the protein is not produced. This morpholino was designed and supplied by Gene Tools LLC (Philomath, OR) and was sent as lyophilized stock. So then, according to the manufacturer's instructions, we resuspended it with Milli-Q water in order to get a final concentration of 1mM stock.

2.5.2. Microinjection of morpholinos

The MOs delivery into the cells was done through microinjection, using a Nikon injector. These injections were done in embryos at one cell stage to ensure the uptake of the MO by every cell. So for that, after zebrafish breeding, the eggs were collected immediately and lined up against a microscope slide in a Petri dish, forming a single column of embryos. The embryonic medium was nearly all removed to provide surface tension, as it prevents the embryo from getting stuck to the needle when the needle is removed after injection. The MO was loaded into a fine-tipped needle, which was connected to a micro-injector and an air source. Injection volume can be adjusted by the micro-injector pressure and through the needle tip width, in order to inject always the same desirable amount of MO. Needles were broken in the air by

gently scraping the tip with clean forceps. To calibrate and calculate the volume of solution injected, a S1 stage micrometer (10mm/0.1mm Graticule Ltd., Tonbridge, Kent) was used and the injected time of the micro-injector was adjusted so that 1.4 nL of solution was delivered with each pulse. Then, the needle was plunged through the chorion and into the embryo's yolk and the MO was expelled by pressing a foot pedal device. As MOs are small oligo sequences, they can easily diffuse into the embryonic cell. This method allows the injection of many embryos in an effective way. Afterwards the embryos were placed into a new Petri dish at 28ºC for the following days. To check for MO effects, we looked into the final visceral organ laterality position and took into consideration organ situs percentage.

Beyond the phenotypes, we also calculated the mortality rates, in order to optimize our MOs working concentrations. The ideal MO working concentration should lead to specific defects but without having a mortality percentage above 15%. We injected: 4.2ng, 3ng, 2.7ng, 2.4ng and 1.2ng for *gnaia* augMO at 0.5mM, 0.35mM, 0.30mM, 0.25mM and 0.2mM. For *pkd*2 augMO, we injected 1.8ng at 0.5mM as previously optimized in lab.

2.6. Evaluation of organ position

In order to understand the function of *gnaia* in left-right asymmetry patterning, we used MO technonology and evaluated the impact of *gnaia* lower levels on heart and gut positioning. Organ *situs* was observed under the Stereoscope Zoom Microscope (SMZ745, Nikon Corporation) and afterwards by *in situ* hybridization using specific riboprobes for these organs.

As previously described, after the *gnaia* augMO injection, embryos were incubated at 28ºC. At 30 hpf, in wt embryos, the heart is already pumping and it can be easily seen positioned on the left side below the left eye. However, when LR signaling pathway is impaired, the heart can appear displaced either on the right side below the right eye or in middle between the two eyes, which is denominated as central heart. We scored *gnaia* morphants for heart jogging in vivo using a Zoom Stereomicroscope (SMZ745, Nikon Corporation) and observing the embryos from the ventral side. Embryos were then separated according to their phenotype. At this step, the embryo medium was usually replaced by new one, to which was added 100µM of 1-phenyl 2-thiourea (PTU, Sigma) to avoid the formation of pigment. PTU inhibits tyrosinase activity, which is essential for melanogenesis initiation, and abolishes pigmentation so that it would be easier to visualize internal organs. As PTU does not have a permanent effect, the embryos will remain transparent as long as they are in this solution. Later, the embryos were fixed at 48hpf and we analyzed abdominal organ position by performing an *in situ* hybridization for *foxA3*.. *foxA3* is a visceral organ marker expressed early in the endoderm, as well as later in the liver, pancreas and intestine. At the 48 - 50 hpf stage, we could observe the liver on the left side and the pancreas on the opposite site when looking from the dorsal side. In case of embryos with laterally defects, these two organs position can be

reversed or centralized. Liver and pancreas position were scored also under the stereoscopic Zoom Microscope.

2.7. Cloning *dnal1* and mRNA injection

KV cilia can be motile or immotile, nevertheless the difference either structural or functional between them is not known. To address this issue we decided to clone a dynein axonemal light chain (*dnal1,* NCBI Gene ID: 445048), a component of the outer dynein arms, in order to see if all cilia from the KV have the machinery that allows them to move. By molecular cloning, we could overexpress the mRNA of our gene of interest fused to a fluorescent tag, which allowed us to localize the expression of the translated protein within the embryonic tissue.

Primers for PCR based cloning have to have specific features in order to to amplify the gene and then insert it on a cloning plasmid. Therefore, they consist of a hybridization sequence, which it will bind to the sequence to be amplified, a restriction site for the cloning-selected enzyme and a named leader sequence. This last sequence comprises an extra base pair on the 5' end of the primer where the restriction enzyme will sit before starting the digestion, improving cutting efficiency. Also restriction enzymes were selected so they would only hydrolize in the desired location in the plasmid Multiple Cloning Site (MCS), but would not cut anywhere else on the plasmid or within the insert (see in annex II the cloning-primer pair used).

To amplify *dnal1*, we run a PCR using iProof™ High-Fidelity DNA Polymerase (Bio-Rad), a proofreading enzyme to minimize potential mutations. Cycling parameters used were as follows: initial denaturation at 98ºC for 5min, denaturation at 98ºC for 1min, annealing at 59ºC for 1min, extension at 72ºC for 2min in 30 cycles and final extension at 72ºC for 10min. The PCR product was isolated from the rest of PCR reaction using a DNA clean and concentrator kit (Zymo Research) according to the instructions of manufacture. Once we got the insert cleaned, both PCR product and recipient plasmid were digested overnight, first at 37ºC with BamHI (NEB® Inc.) and then at 65ºC with BstBI (NEB® Inc.). We used the pCS2+mCherry plasmid for this purpose. pCS2+ vector is a high copy number plasmid that contains a strong enhancer/promoter simian CMV IE94 followed by a mCherry tag and the SV40 late polyadenlyation site. mCherry was the fluorescent protein used as a marker to tag Dnal1, so that we could later trace it by confocal microscopy. The SV40 signal leads to the addition of a poly(A) tail to the 3' end of the messenger RNA, improving RNA translation and stability. A good control for digestion is to cut the plasmid with the two enzymes separately, and then run all samples on an agarose gel, to guarantee that both enzymes worked. These enzymes, BamHI and BstBI, were also chosen because they produce sticky ends, which avoid self-ligating.

After purification, the concentration of the insert and plasmid was determined. This is important because for ligation processes the ideal is to have a plasmid to insert ratio of approximately 1:3. Ligation reaction

was done over weekend at 4ºC and the resulting product was transformed into DH5α bacteria. Bacterial transformation and colony PCR to select positive colonies were done as previously described for ISH probes (see section 2.4.1.). Positive colonies were sequenced using a pCS2+ reverse primer (5'-CTGCATTCTAGTTGTGGTTT -3') by STAB Vida company. The sequencing results were aligned with *dnal1* sequence to confirm the presence of insert as well as to check the sequence itself as for overexpression effects, RNA sequence should not have any base-pair substitutions to prevent subsequent protein misfolding. Using SnapGene software, we constructed a plasmid map with the insert and all vector features. By choosing "Unique Cutters" set, we easily identified a suitable restriction enzyme for linearization. Sac II enzyme from NEB® Inc. was used at 37ºC, overnight. We used the Ambicon mMESSAGE mMACHINE Kit Kit (ThermoFisher Scientific) to synthesize *in vitro* capped mRNA. To remove the template DNA, samples were treated with TURBO DNase (ThermoFisher Scientific) during 15min, at 37ºC. The RNA was purified, quantified, aliquoted and stored at -80ºC.

Zebrafish mating and egg collection was done as previous described above in section 2.2 and the microinjection procedure of mCherry-dnal1 RNA was very similar to the morpholino injection (see section 2.5.2.). Nevertheless, RNA delivery is more effective when directly injected into the embryonic cell at one cell stage, instead of the yolk. To inject at one cell stage, embryos were collected more or less twenty minutes after spawning, giving them time to form the first cell towards the animal pole. When lined up against a microscope slide in a Petri dish, embryos were re-orientated carefully using a pipette tip such that the cell would face the needle. The injection process, starting in needle calibration and ending up with pressing the foot pedal to expel the content of the needle, is equal for both MOs and RNAs. In the end, injected embryos were incubated at an optimized temperature of 25ºC for allowing the live imaging of 8-10 somite stage embryos in the following morning.

2.8. Live imaging

Imaging of living cells and tissue has became a powerful approach to investigate cellular dynamics and function. Fluorescent imaging depends on illumination of fluorescently tagged proteins with a defined short wavelength of light and detection of emitted light at a longer wavelength. Therefore, using confocal microscopy we can 3D scan zebrafish embryos at different depths and localize the labeled proteins within the living tissues.

2.8.1. Mounting zebrafish live embryos for KV imaging

We did live imaging in order to try to understand if all KV cilia are structurally equal or not. So for that we injected 300pg of RNA construct *mCherry-dnal1*, as previous described above, into a transgenic zebrafish line tg(Arl13b:GFP), which presents all KV cilia labeled with GFP. The embryos developed until 8-10 somite stage and then they were gently dechorionated with sharped forceps. In a small Petri dish with a thin glass at the bottom, the embryos were placed in the center surrounded by a ring made of glass. We filled the ring with low-melting agarose at 1% and turned the embryos using a micro-loader pipette tip. The agarose is essential to maintain the embryos in the right position without affecting their survival and development. As an inverted microscope with the camera recording from the bottom was used, the embryos were mounted with the dorsal side of the KV fronting the objective lens.

2.8.2. Confocal microscope Setup

Mounted embryos were observed under the inverted bright-field confocal light microscope LSM710 (ZEISS) at room temperature. With a 40x/1.2NA water objective lens, KV cells were focused and images were obtained using a High Resolution Camera and the Zen Blue 2010b SP1 software.

2.9. Statistical analysis

The software *GraphPah – Prism*® version 5.0 (GraphPad Prism Software Inc. San Diego, CA) was used to analyze our data. Regarding qPCR experiments, differences in the expression levels during developmental time were evaluated using a Student's t-test with Wech's correction, meaning it is assumed that two samples have unequal variances. For statistically significance, we considered confidence intervals of 95%.

3. RESULTS

As different subjects were addressed throughout this thesis, the discussion as well as the results were divided in three sections. According to the proposed objectives, the first chapter is about testing the chemosensation hypothesis, the second chapter is related with the screening for asymmetric genes in the KV and the last but not least is focused on cilia motility marker *dnal1.*

3.1. Testing the Chemosensation Hypothesis

As we were analyzing the microarray dataset, we found a surprising number of taste sense related genes expressed in the KV ciliated cells. Moreover, taste receptors have been reported to be expressed in motile cilia from human airway epithelial cells associated with sensory functions (see Shah *et al*. 2009, also reviewed in Kinnamon 2012). Given that cells are highly efficient machines, we hypothesized that cells would not waste the energy required to target taste receptors to the cilium if they were not serving a specific function within it. So we decided to test if these genes had some role within KV cilia, in regard to sensing the flow and enhancing the asymmetric left-right gene cascade.

3.1.1. Analysis of taste receptors and downstream effectors levels of expression

Since taste receptors had a quite low expression in the microarray, we first wanted to confirm its transcription levels at 10hpf and 13hpf by qPCR. For this qPCR experiment, we used three replicate samples of each experimental condition that were normalized with the reference genes, *rpl13a* and *eef1a1,* and the average was calculated (Figure 3.1). A summary of qPCR validation is presented below in Table 3.1.

Table 3.1: Pkd2-independent target gene list and qPCR validation.

Microarray list	Cluster	Gene	qPCR validation
Pkd2-independent target genes	Sweet taste receptors	*tas1r1*	no
		tas1r2.2	yes
		tas1r3	no
	Bitter taste receptors	*tas2r200.2*	yes
		tas2r201.2	yes
	Downstream effectors of taste signaling	*gnaia*	yes
		gna14	no
		plcβ2	yes

Our results showed that primers for *tas1r1*, *tas1r3* and *gna14* genes were not validated by qPCR.

The qPCR results for the remaining genes were in agreement with the microarray dataset, showing very low transcriptional levels for the taste receptors *tas1r2, tas2r200.2* and *tas2r201.2*, and for *plcβ2* and higher levels for *gnaia* (Figure 3.1). *gnaia* codes for a *guanine nucleotide binding protein (G protein), alpha inhibiting activity polypeptide a* that is usually coupled to a receptor and has been described as the first step in the gustatory transduction pathway (as explained in the introduction).

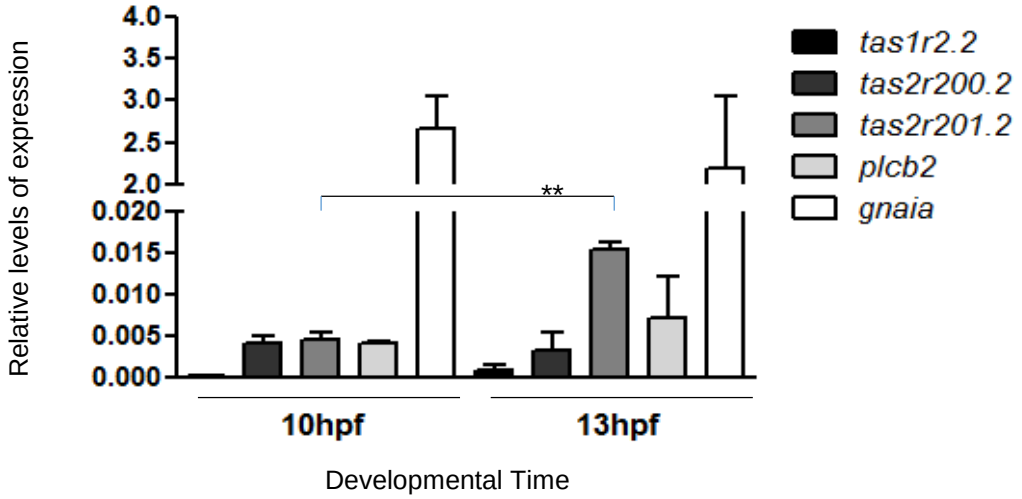

Figure 3.1: Taste sense related genes are expressed in WT embryos.
Transcription levels obtained by qPCR from whole-embryos at 10hpf and 13hpf. A Student's t-test was used for statistical analysis (** represent a p value below 0.001). The color code for each gene bar is represented on the right side.

Comparing both stages, almost every taste receptors had a slight increase over time, but these differences were not significant ($p>0.05$). Only *tas2r201.1* had a significant increment at 13hpf ($p<0.01$). As for *gnaia*, although during this time window, between 10 hpf and 13 hpf, its expression did not vary much, it seems to be highly expressed with a transcription level of 2.5% relative to controls. Taking this analysis in consideration, we decided to confirm the expression levels of *tas2r201.2* and *gnaia* at 13 hpf, where both genes had a high expression, but this time specifically within KV cells (Figure 3.2) that were previously sorted by FACS using the GFP reporter line foxj1a:GFP at 13 hpf.

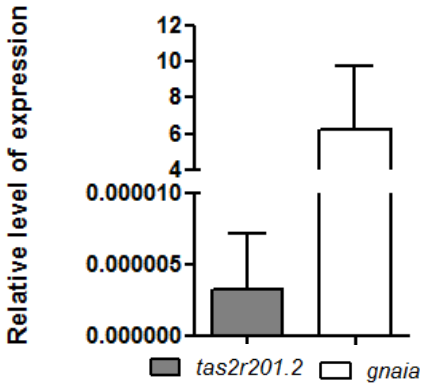

Figure 3.2: *tas2r201.2* and *gnaia* expression in the KV.
Transcription levels obtained by qPCR from KV cells at 13hpf.

Using only cells from our organ of interest, we confirmed that *gnaia* was more expressed than *tas2r201.2*. From this data, the gene *gnaia* was our best candidate to be involved in signaling transduction of a chemosensory pathway through the KV ciliated cells, which prompted us to further study the spatial expression of this gene, by whole-mount *in situ* hybridization, and its molecular function by knocking it down.

3.1.2. Expression pattern of *gnaia*

In order to know if *gnaia* was expressed specifically in the KV, we evaluated its expression pattern by WISH. For this purpose we produced a new ISH probe that we had to test first. For a positive control, we used 4dpf embryos, since it has already been reported *gnaia* expression in taste bud cells at this stage (Ohmoto *et al*. 2011). Taste buds are chemosensory cells that occur in the mouth region epithelia without any obvious pattern of distribution (Ohkubo *et al*. 2005). They can be detected within the lips and gill arches, at 3-4dpf, in the mouth cavity and oropharyngeal area, at 4-5dpf, and later on taste cells are formed in the skin of barbels and on the head (Hansen *et al*. 2002).

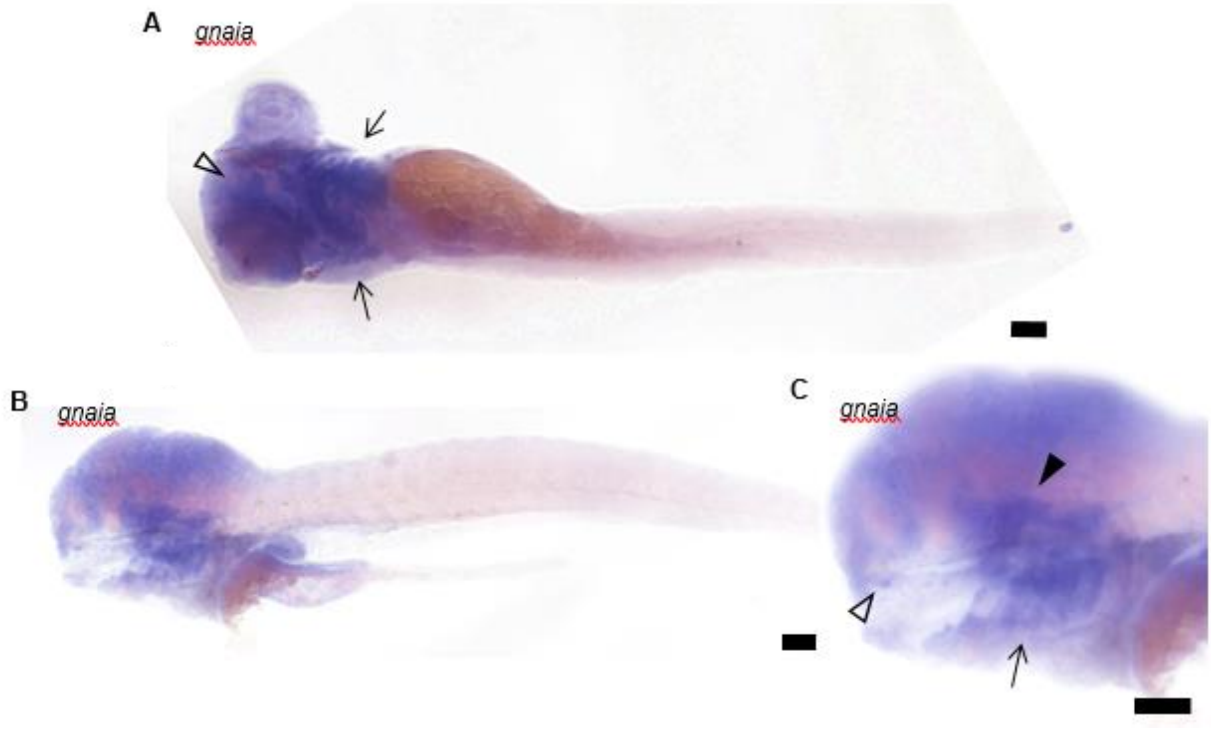

Figure 3.3: Whole-mount *in situ* hybridization showing expression pattern of *gnaia* in WT zebrafish larvae at 4dpf.
Embryos are oriented in ventral (A) and lateral (B and C) view. Embryo was dissected and the eyes were cut off to facilitate focusing the stained areas (B, C). C is a head higher magnification of B. Arrows indicate gill arches. Black arrowhead points to the pharyngo-branchial region. Unfilled arrowhead indicates the mouth cavity. Scale bars = 1µm.

In summary, we observed the predicted expression pattern for *gnaia* in zebrafish larvae with 4dpf (Figure 3.3). As reported, *gnaia* was expressed in taste bud cells, which were spread through the mouth cavity, the pharynx region and gill arches. This data confirmed that our probe was working, so then we used it to analyze the expression pattern at 8 somite stages (~13hpf), when the KV is present in the early embryo.

Although the negative control (Figure 3.4.A) presented a little bit of background, we knew that our anti-sense RNA probe was working and was specific for *gnaia* based on the previous experiments (Figure 3.3.). Taking this in consideration, we observed a slight basal expression through the whole embryo (Figure 3.4.C), and a very subtle horseshoe shaped expression in the KV region (Figure 3.4.D)**.**

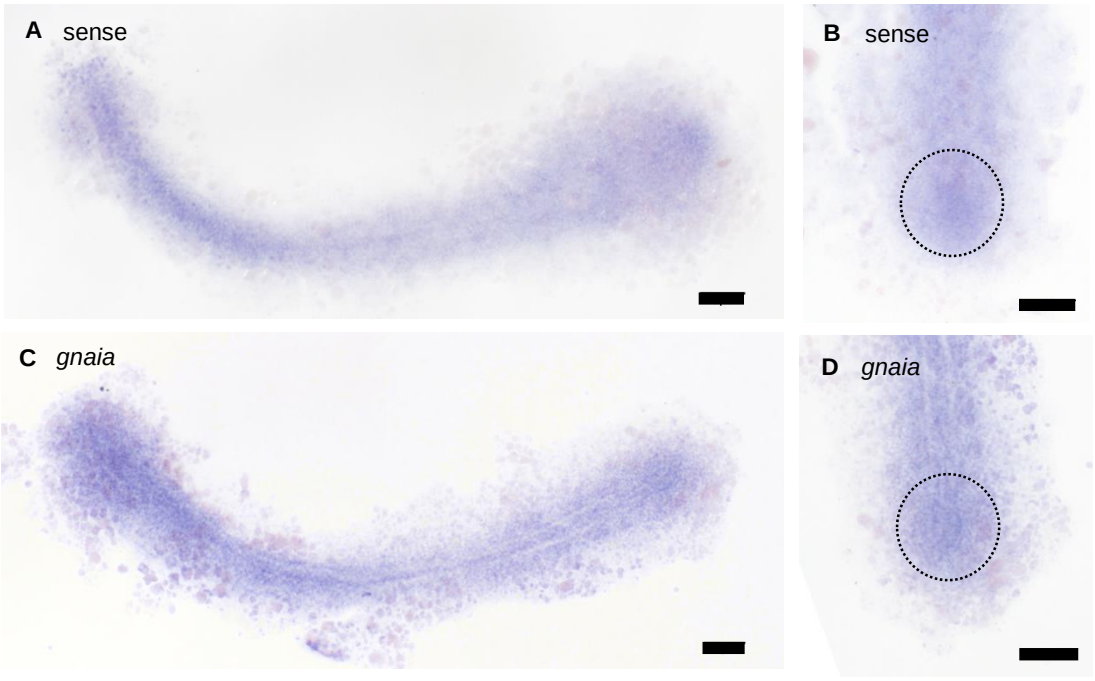

Figure 3.4.: Whole-mount *in situ* hybridization showing expression of *gnaia* in WT zebrafish embryos at 13hpf. Embryos are oriented in dorsal view. Negative control using a sense RNA probe for *gnaia* (A and B). *gnaia* expression pattern using the anti-sense RNA probe (C and D). B and D are tail region higher magnifications of A and C, respectively. Dashed circle delimitates the KV area. Scale bars = 1µm.

Even though, *gnaia* seemed to have an ubiquitous basal expression at 8 somite stage, we decided to proceed with the morpholino injection owing to the high levels of expression obtain by qPCR, previously described in Figure 3.2.

3.1.3. Molecular study of *gnaia* function by morpholino knockdown

We injected a wide range of morpholino concentrations to test its toxicity and to infer our working concentration. To study if the reduction of *gnaia* had an impact on LR establishment, we looked for the heart and gut LR positioning, which are the main organs affected in this process.

After *gnaia* atgMO injection, morphant embryos and their WT siblings developed for 30 hours, by this time we scored them *in vivo* for heart asymmetry and then they were fixed at 48hpf for a whole-mount *in situ* hybridization with *foxA3,* which allowed us to score the liver and pancreas position (see section 2.6.).

3.1.3.1. Evaluation of organ position

We tested several morpholino concentrations from 1.2 ng up to 4.2 ng, though we did not obtain major heart positioning defects comparing to WT non-injected embryos. Our results showed that 100% of a total number of 294 WT embryos had normal heart asymmetry (Figure 3.5.A). For embryos injected with *gnaia* atgMO, in the worst scenario 10% showed LR heart defects that were mainly inverted hearts and appeared on the right of the body axis (Figure 3.5.B).

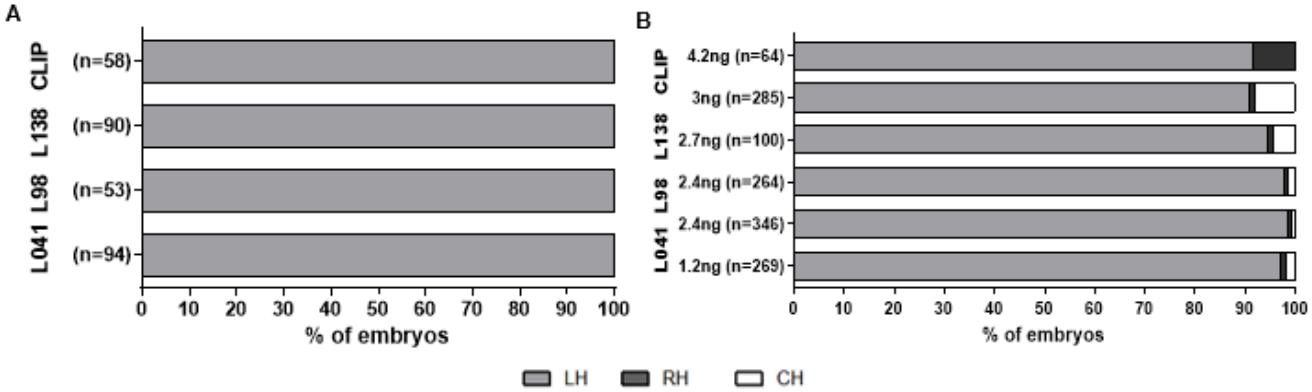

Figure 3.5: Heart laterality of *gnaia* atgMO injected embryos.
Scoring for heart situs at 30hpf of WT non-injected embryos (A) and of *gnaia* atgMO-injected embryos (B). L041, L98, L138 and CLIP are the designations for different AB lines tested. n correspond to the number of embryos used in each condition. Soft grey bars represent the percentage of embryos with left heart (LH). Dark grey bars denote the percentage of embryos with right heart (RH). White bars label the percentage of embryos with central hearts (CH).

As we were injecting the different concentrations of *gnaia* atgMO, we noticed that high amounts of *gnaia* atgMO were causing severe defects in development and embryos were not surviving. To continue further studies, we determined a suitable working concentration for *gnaia* morpholino in order to avoid such toxicity. For that we analyzed percentage of dead and abnormal embryos for every amount of *gnaia* atgMO injected and for WT embryos in a calibration curve (Figure 3.6). Abnormal embryos appear from the off-target effects of the MO mediated by activation of p53 apoptosis pathway, which can lead to death.

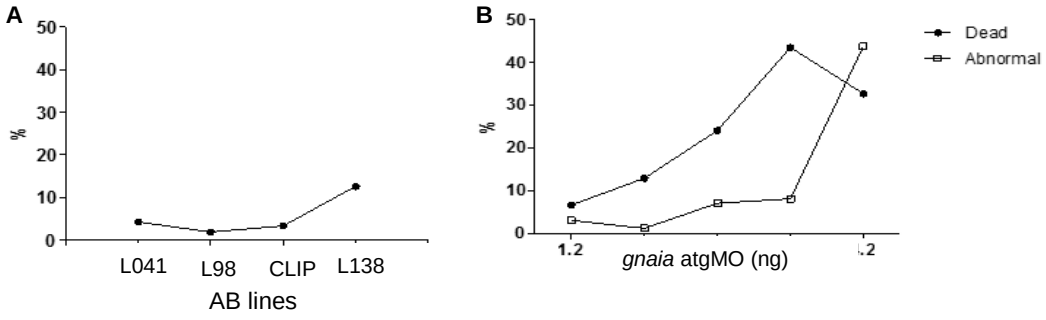

Figure 3.6: Toxicity of *gnaia* atgMO.
Calibration curves with percentage of dead and abnormal embryos for WT embryos (A) and for each amount of *gnaia* atgMO injected embryos (B) were used to determine the better working concentration.

Based on the ratio between the percentage of dead and abnormal embryos, we could use 2.7 ng of gnaia atgMO per each injection, where 124 embryos were analyzed without major toxicity effects. Nevertheless, we decided to use 2.4 ng as a precaution measure and because we had more robust values for this amount of *gnaia* atgMO as more embryos were analyzed (665 embryos).

Then, we analyzed the spatial localization of the liver and the pancreas, for both WT non-injected embyos and 2.4 ng injected embryos, by foxA3 WISH (Figure 3.7). In normal situations, in zebrafish larvae the liver is positioned on the left side by opposition to the pancreas, located on the right side.

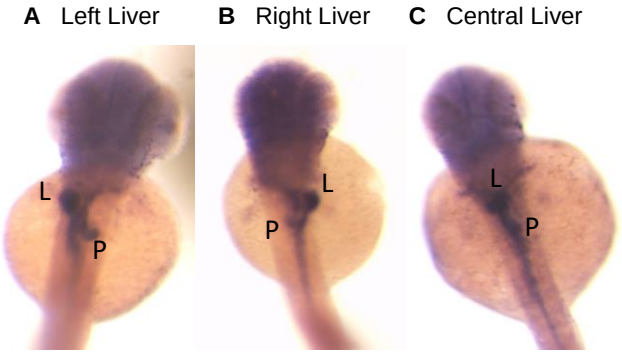

Figure 3.7: Gut laterality of *gnaia* atgMO injected embryos.
Scoring for gut situs at 50 hpf of WT non-injected embryos and of *gnaia* atgMO-injected embryos. In a normal situation (A) the liver (L) is positioned on the left side and the pancreas (P) is located on the right side. Laterality defects can lead to a right liver and a left pancreas (B) or to central liver and pancreas (C).

Given that we accessed both organs position for the same embryos, we classified them according to their phenotype, where the normal situation is denominated as *situs solitus* (in zebrafish both heart and liver on the left side), and LR defects were divided in *situs inversus* (both heart and liver on the right side) and *heterotaxia* (when heart or liver are mis-located or when both are in the middle of the body axis).

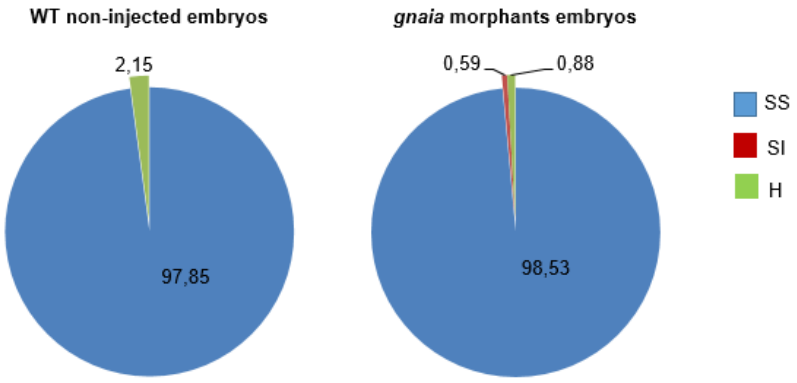

Figure 3.8: Scoring of heart and liver positioning in WT non-injected and *gnaia* morphants embryos.
Blue slice represents the percentage of embryos with *situs solitus* (SS). Red slice denotes the percentage of embyos with *situs inversus* (SI). Green slice represents the percentage of embryos with *heterotaxia* (H). Total number of embryos used: 93 embryos WT non-injected and 340 embryos *gnaia* atgMO injected.

In summary, we observed that only a minor percentage of *gnaia* atgMO injected embryos was not *situs solitus* (Figure 3.8). This amount of LR defects is not relevant when compared with control embryos. These results showed us that even though *gnaia* was highly expressed at 8 somite stage within the KV cells, it does not have an important role in LR patterning. However further studies with an anti-Gnaia antibody that recognizes the zebrafish protein (currently not available) should be performed in order to insure that the morpholino was indeed working and the amount of protein was reduced.

In Zebrafish International Resource Center (ZIRC), two *gnaia* transgenic lines (la023212Tg and la028689Tg) through viral insertion (Burgess, S., and Lin, S. (2011) Viral Insertion Mutants. ZFIN Direct Data Submission (http://zfin.org)) are available. Burgess and colleagues initially predicted that these insertions would be mutagenic, however they revealed us that integrations in the first intron are good candidates only if the intron is smaller than 5000 bp and gnaia has a first intron with about 6000 bp. So Burgess recommended us to targeting *gnaia* gene with CRISPR and such mutant could be done in the future.

3.2. Screening for asymmetric gene expression in the KV

The main objective of the microarray between pkd2 morphants embryos and their siblings was to discover mis-regulated genes that work downstream of Pkd2 within the context of LR patterning. So, our lab teamed up to cover as much information as we could and explore different angles of the Pkd2 dysfunction:

One lab member colleague was interested in sphingolipids and CFTR, the cystic fibrosis transmembrane conductance regulator, and polycystins mis-regulation from the point of view of autosomal dominant polycystic kidney disease (ADPKD), since she had reported the zebrafish KV as a good model system to study this disease (Roxo-Rosa *et al*. 2015). Another colleague was focused on wnt signaling and how wnt-ligands could regulate the early steps of LR asymmetry establishment downstream of Pkd2 signalling pathway. My goal was to find new asymmetric genes that could be intermediate players between flow, Pkd2 pathway and asymmetric *dand5* expression. So far *dand5* is the only gene expressed in the KV that becomes asymmetric after the flow is established (Sampaio *et al*. 2014; Hojo *et al*. 2007; Nakamura *et al*. 2012; Schweickert *et al*. 2010).

In order to do that, I selected a short list of eleven genes to analyze by whole-mount *in situ* hybridization, which were organized in four main clusters: wnt signaling, bmp signaling, calcium binding signaling and others. The main criteria to select these eleven genes were: potential relevance in the LR pathway for which we used extensive literature search; coverage and quality of the zebrafish sequencing project and number of paralogous genes. I should notice that, as we observed for *dand5*, these genes did not need to be differentially expressed between wt and *pkd2* knockdown embryos. We were simply looking for

asymmetric expression patterns that changed with *pkd2* knockdown but that did not require a change in the total levels of expression.

The Wnt pathway has been widely studied and associated with many different biological processes either through the canonical or the non-canonical pathway, based on the involvement of b-catenin as the primary effector on the signal transduction cascades. During early vertebrate development, wnt proteins are expressed in a tightly and conserved way in order to generate the body plan of an embryo (van Amerongen and Nusse 2009). Regarding the left-right axis, KV-specific and global wnt gain of function lead to a randomized side-specific gene expression (Schneider *et al.,* 2008; Carl *et al.,* 2007; Lin and Xu 2009), which ultimately results in organ laterality defects. In addition to this, wnt loss of function studies using both mutants and morphants also show a randomized side-specific gene expression and a failure in organ placement (Nakaya *et al.,* 2005; Lin and Xu 2009; Zhang *et al.,* 2012). Moreover, at zebrafish KV, wnt signaling controls cilia formation and function (Lin and Xu 2009; Caron *et al.,* 2012; Zhu *et al.,* 2015). Based on this evidence, we selected two wnt proteins, *wnt4a* – a ligand of the non-canonical wnt signaling (Matsui *et al*. 2005) – and *csnk1g1* – a subunit of casein kinase, casein kinase 1 gamma 1, that phosphorylates canonical-wnt components (Cruciat, 2014) – as possible asymmetric gene candidates..

The bone morphogenetic proteins (BMPs) cover the largest group of the transforming growth factor beta (TGF-β) family of signaling molecules (Mulloy and Rider 2015). Functionally, BMP activation leads diverse biological processes as cell proliferation and differentiation in order to establish the early vertebrate body plan and to regulate the formation of organs and tissues (Kingsley 1994; Hogan 1996). For the dorsoventral axis development, BMPs usually are expressed in the ventral side of the embryo acting as ventralizing factors in opposition to dorsal-specific BMP antagonists such as Chordin, Noggin, Follistatin and the DAN family (differential screening-selected gene in neuroblastoma) (Sasai *et al.,* 1995; Fainsod *et al.,* 1997; Kishimoto *et al.,* 1997; Hsu *et al.,* 1998). Furthermore, BMPs are secreted proteins acting as short-range morphogens (Jones *et al*. 1996), meaning that they alter the developmental fate of target cells in a concentration-dependent manner, to coordinate LR asymmetry (Fujiwara *et al*. 2002). Also downstream molecules of BMP pathway had been reported to be involved in LR patterning, such as *smad2* (Nakamura *et al*. 2012) and *smad5* (Chang *et al*. 2000). Indeed, loss of function studies of BMP signaling result in LR-specific gene expression defects and compromised heart and gut position either through morpholino injection at one cell stage and at 512-cell stage embryos (Chocron *et al*. 2007), which result in the uptake of MO by the dorsal forerunner cells that will form KV (Amack and Yost 2014), or through mouse Bmp4 mutant (Fujiwara *et al*. 2002). So, to study the involvement of BMPs as asymmetric expressed genes in the KV during early LR patterning, we selected *bmp2b* – a dorsoventral organizer-specific BMP ligand (Xue *et al*. 2016) –, *fsta* – a BMP antagonist, follistanin a (Iemura *et al*. 1998) – and *smad4* – a downstream nuclear effector of BMP signaling (Shi and Massagué 2003).

For the cluster of calcium binding proteins, neither *cacng2a*, a calcium channel, voltage-dependent gamma subunit 2a, nor *rragca*, a ras-related GTP binding Ca, had been associated with LR

establishment. Nevertheless, at the time of the experimental design of my project Pkd2 channel was thought to be the main sensor of LR flow, leading to an increase of intracellular calcium within the cells of the KV left side and consequently to the LR gene cascade signaling (Yuan *et al*. 2015). So, analyzing the expression pattern of calcium binding proteins was experimentally valid.

We also embraced genes from pathways that have not been associated with LR asymmetry yet. At this point, we decided that our small screening for asymmetries should be independent, meaning we would not excluded targets only because at the time they were not LR-related genes. In fact, genome duplication events that zebrafish had over time, lead to subfunctionalization (partition of different functions of the ancestral gene), nonfunctionalization (loss of function) and also to neofunctionalization, as the origin of new functions, so genes can have other functions besides the ones already reported. From this point of view, we selected the following 4 targets:

(1) Crumbs 2a (*crb2a*), which is an essential component of apico-basal polarity and adherens junctions, known to be both necessary and sufficient to confer apical properties to embryonic epithelia (Wodarz *et al*. 1995); (2) Foxi1, a transcriptional factor involved in proper organization of zebrafish otic vesicle, required for neuronal fate and subtype visceral sensory identity of placodal progenitor cells (Lee *et al*. 2003), by inhibiting FGF and BMP signaling (Yao *et al*. 2014); (3) Antizyme inhibitor 1a, *azin1a,* a regulatory protein of the tight controlled polyamines homeostasis (Hascilowicz *et al*. 2002). Polyamines are small polycations essential for proper cell growth and differentiation, namely by modulation of DNA structure (Iacomino *et al*. 2012) and inhibition of a transient receptor potential canonical calcium-permeable channel (TRPC4) (J. Kim *et al*. 2016); (4) Delta-like 1 homolog, *dlk1,* an epidermal growth factor-like protein which operates inhibiting Notch signaling pathway (Rodríguez *et al*. 2012).

After we had selected all our targets, I made specific primers for each one and validated them, so my colleague could do the qPCR experiments to confirm their levels of expression, given by the microarray. We analyzed those results as a ratio between the expression levels in pkd2 morphants embryos and WT embryos, in order to infer the present mis-regulation, in other words to understand if they were up-regulated or down-regulated. A summary of the target genes info and the ratios obtain by microarray and qPCR analysis can be consulted in Table 3.2.

Table 3.2: Target gene list and ratios of expression levels obtain by microarray and qPCR analysis.

Microarray list	Cluster	Gene	Ratio by microarray	Ratio by qPCR
Differential expressed in pkd2 morphants	wnt signaling	*wnt4a*	Up	equal
		csnk1g1	Up	equal
	bmp signaling	*bmp2b*	Up	up
		fsta	Up	up
		smad4	Up	equal

	calcium binding signaling	*cacng2a*	Up	not amplified
		rragca	Down	down
	others	*crb2a*	Up	up
		foxi1	Up	up
		azin1a	Up	up
		dlk1	Up	equal

Since qPCR has a higher detection sensitivity, precision and reproducible quantfication than microarray technique, it is usually used to validate microarray results in a more accurate way. As described in Table 3.2. some genes did not pass qPCR validation, referred to as equal, hence the levels of expression between pkd2 morphants and WT embryos were not significantly different. Still more than half of the genes were validated by qPCR. We agreed on pursuing with both significantly and not significantly differentially expressed genes, because of the levels of expression of our reference gene *dand5*. Although it is asymmetrically expressed in WT embryos and it becomes symmetric in pkd2 morphants, when we compare the amount of transcripts in both situations, the levels are the same (unpublished data).

Furthermore, no expression was detected for *cacng2a,* mostly likely due to unsuitable primers and the expression of *smad4* was not specific for our target, since zebrafish has two very similar smad4 transcripts (smad4a and sma4b). For these reasons, we decided to not proceed further studies with these two genes.

3.2.1. Expression pattern of target genes in wildtype embryos

In order to accomplish our goals in identifying new asymmetric distributed genes, we did whole-mount *in situ* hybridization for our targets, as described in section 2.4.2. Probes made from *de novo* have to be optimized. For that we made a couple of WISH to clean the probes of any remaining reverse transcription products that may have been left and could contribute to background staining. Then we made a few more tests to check different probe concentrations to obtain the best signal-to-background ratio.

Since our probes were made from scratch we had to test them first. We used specific developmental times where our targets had already been reported as positive controls for our experiments (see Table 2.3.) and then we used 8 somite stage as the developmental stage of interest to check for KV asymmetric expression patterns.

For *wnt4a*, our developmental time of interest, 8 somite stage where KV is present, luckily corresponded to the stage used as positive control. So at 8 somite stage (~13hpf), *wnt4a* gene expression was detected in the neural ectoderm near the forebrain-midbrain boundary, the neural tube and in the anterior lateral plate mesoendoderm (Figure 3.9.C) as expected (Ungar *et al*. 1995).

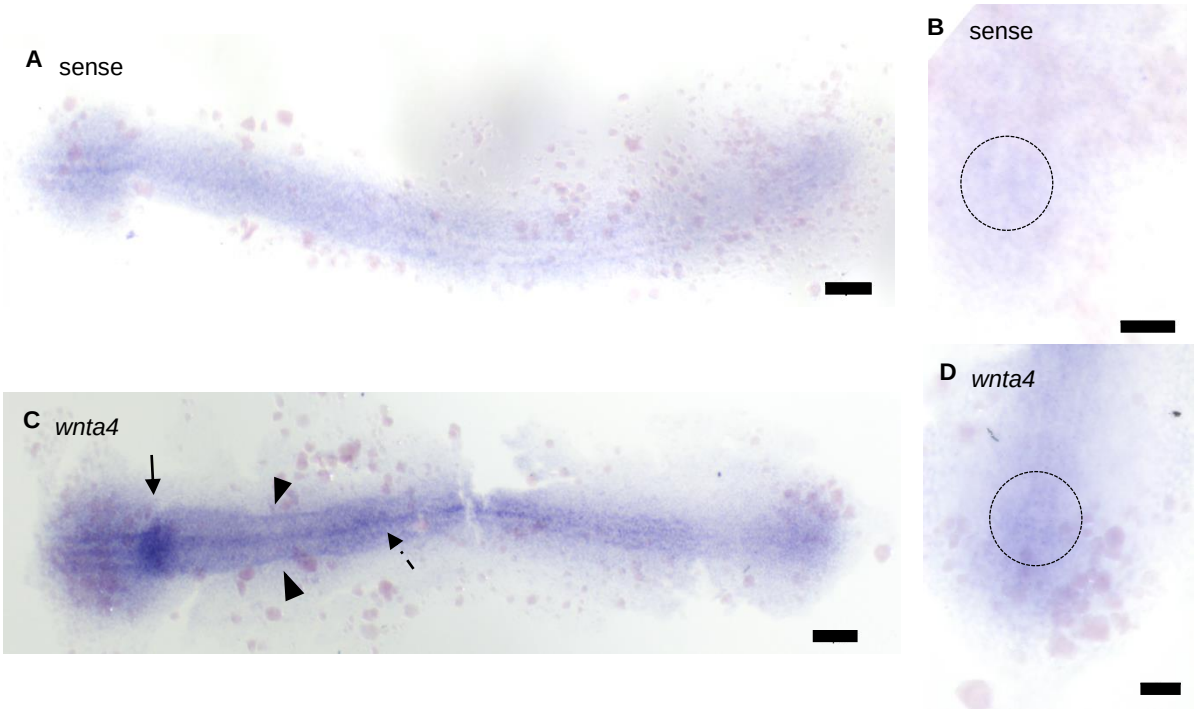

Figure 3.9: Whole-mount *in situ* hybridization showing expression of *wnt4a* in WT zebrafish embryos at 13hpf. Embryos are oriented in dorsal view. Negative control using a sense RNA probe for *wnt4a* (A and B). *wnt4a* expression pattern using the anti-sense RNA probe (C and D). B and D are tail region higher magnifications of A and C, respectively. Arrow points to forebrain-midbrain boundary. Black triangles indicate lateral edges of mesoendoderm. Dashed arrow points to neural tube. Dashed circle delimitates the KV area. Scale bars = 1µm.

Since our probe was working, we looked in more detail to the Kupffer's Vesicle located in the zebrafish tail region. In Figure 3.9.D, we observed a slight expression of wnt4a in the KV region, hardly detectable. We could see, however that it was not asymmetrically expressed in WT embryos, and that it was not specific for the KV cells, but more broadly expressed in that area despite the very weak expression level.

Regarding *fsta* gene, we did the WISH for 48hpf embryos, as a positive control. At 48hpf, expression of *fsta* was detected throughout the central nervous system, in the diencephalon, the hindbrain, the midbrain, the optic nerve, as well as in the dorsal tectum, the pharyngeal arch skeleton and the posterior otic vesicle (Omata *et al*. 2007; Thisse *et al*. 2001: ZFIN direct data submission), which we were able to reproduce as observed in Figure 3.10.

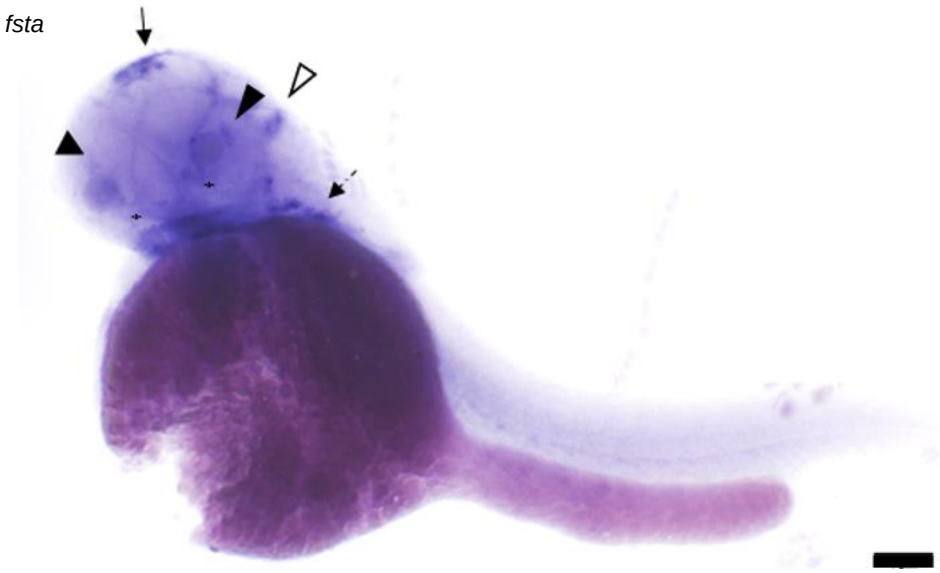

Figure 3.10: Whole-mount *in situ* hybridization showing expression of *fsta* in WT zebrafish embryos at 48hpf. Embryo is oriented in an oblique ventral view. *fsta* expression pattern was detected in the dorsal tectum (arrow), optic nerve (asterisks), posterior otic vesicle (black triangles), hindbrain (white triangle) and branchial arches (dashed arrow). Scale bar = 1µm.

At 8 somite stage (13 hpf), *fsta* was observed to be expressed in the eye, the diencephalon, the hindbrain and in the first pairs of somites (Figure 3.11.C and D).

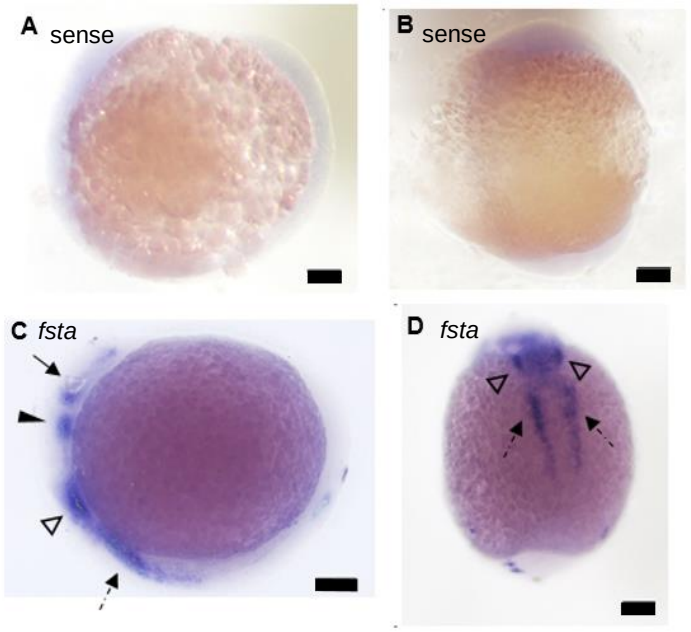

Figure 3.11: Whole-mount *in situ* hybridization showing expression of *fsta* in WT zebrafish embryos at 13hpf. Embryos are oriented in lateral (A and C) and dorsal (B and C) view. Negative control using a sense RNA probe for *fsta* (A and B). *fsta* expression pattern (C and D) in the eye (arrow), ventral diencephalon (black triangle), ventral hindbrain (white triangle) and somites (dashed arrow). Scale bars = 1µm.

At this point, no expression was detected in the tail region, so we kept the embryos in a longer labelling incubation time to extend the staining reaction. Since the labelling reaction occurs through formation and accumulation of the substrate NBT/BCIP products by the enzyme, alkaline phosphatase conjugated with the anti-digoxigenin antibody that recognizes the RNA probes, tissues with lower amounts of transcripts will take more time to precipitate visible NBT/BCIP products.

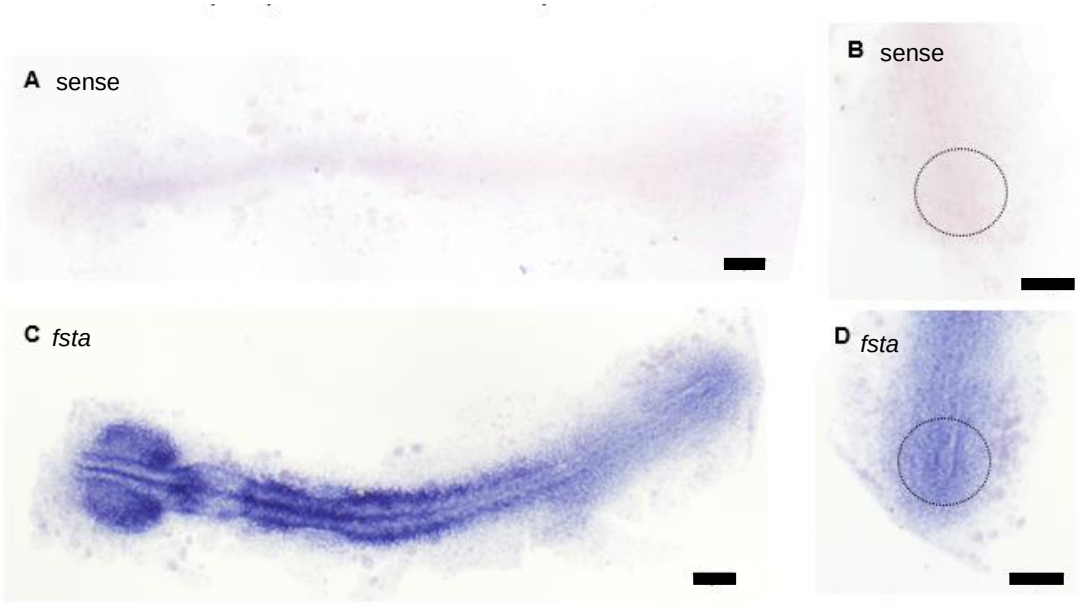

Figure 3.12: Whole-mount *in situ* hybridization showing expression of *fsta* after a longer labelling incubation time.
Embryos are oriented in dorsal view. Negative control using a sense RNA probe for *fsta* (A and B). *fsta* expression pattern using the anti-sense RNA probe (C and D). B and D are tail region higher magnifications of A and C, respectively. Dashed circle delimitates the KV region. Scale bars = 1µm.

After a longer staining reaction, the previous sites of expression had more pronounced signal (Figure 3.12.C) and in the tail region a slender signal appeared (Figure 3.12.D). As in the negative control no signal was detected (Figure 3.11.A and B) we knew that the expression was specific for *fsta* and it was not just background. Nevertheless, *fsta* was expressed all around the KV area on both left and right sides in a symmetric pattern.

As for *crb2a*, 30hpf embryos were used as positive controls. *crb2a* was expressed in the brain, eyes and nose (Figure 3.13), in agreement with previous data published by Hsu *et al* (Hsu *et al*. 2006).

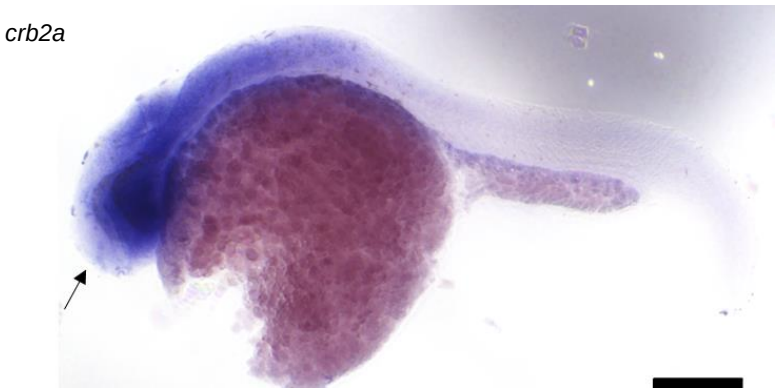

Figure 3.13: Whole-mount *in situ* hybridization showing expression of *crb2a* in WT zebrafish embryos at 30hpf.
Embryo is oriented in lateral view. *crb2a* expression pattern in the brain, eye and nose (arrow) . Scale bar = 1µm.

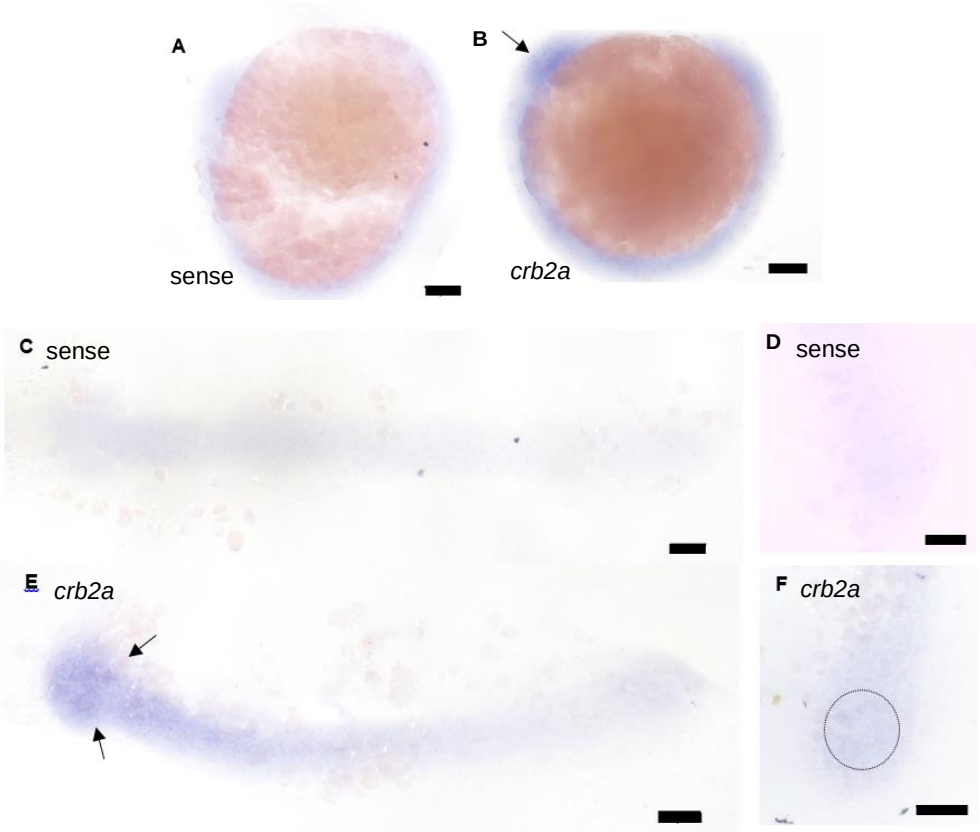

Figure 3.14.: Whole-mount *in situ* hybridization showing expression of *crb2a* in WT zebrafish embryos at 13hpf.
Embryos are oriented in lateral (A and B) and dorsal (C, D, E and F) view. Negative control using a sense RNA probe for *crb2a* (A, C and D). *crb2a* expression pattern (B, E and F) in the eye (arrow). D and F are tail region higher magnifications of C and E, respectively. Dashed circle delimitates the KV site. Scale bars = 1µm.

At 8 somite stage, *crb2a* expression was also detected in the eye region (Figure 3.14.B), but no signal was noticed within the KV region (Figure 3.14.F), even when we left the embryos to incubate with the staining reaction for a longer period. So we went back to qPCR data and we noticed that transcriptions levels in WT embryos were very low, probably under the *in situ* hybridization detection limits. And this was valid for all of our targets, being *fsta* the only one with high expression levels.

Unfortunately we were not able to reproduce the specific expression patterns for the other targets, as they had been reported in ZFIN (The Zebrafish Model Organism Database, https://zfin.org/). We double checked all the probe synthesis process, looking for off targets or any kind of error that we could had missed. Still RNA probes can be very difficult to work with as they are very sensitive to RNases.

In order to make sure that those probes are properly labelled and to infer about the DIG-labeling efficiency we should do a dot blot. If the probes were fine a TEA, triethanolamine, treatment could be added to protocol, since it can help reduce background staining, by acetylating the positively charged amino groups in the tissues that may bind probe nonspecifically. If they were not good indeed, we should check probes size, although longer probes can show poor tissue penetration, they exhibit the highest sensitivity and specificity.

3.2.2. Expression pattern of target genes in *pkd2* atgMO injected embryos

At this point we had three probes working well, although we could not observe them clearly in the KV region. Looking at the transcription levels of these three genes, *wnt4a*, *fsta* and *crb2a*, they were very low expressed. On the other hand, *fsta* and *crb2a* were up-regulated in the pkd2 morphants embryos, so we decided to check their expression pattern in those embryos. Since *wnt4a* was barely detectable in WT embryos and as qPCR results had shown no significant difference of transcription levels in pkd2 morphants embryos, (in opposition to *fsta* and *crb2a*) decided not to proceed further studies with this gene. Even if wnt4a expression pattern changed in pkd2 morphants, we would not be able to detect it.

In pkd2 morphants, *fsta* expression was stronger through the whole embryo, confirming qPCR results (Figure 3.15.A, B and C). However in the tail region, no significant signal difference was detected (Figure 3.15.D) when compared with WT embryos. Since the purpose of this screening was to evaluate the existence of asymmetries in gene expression, we concluded that *fsta* was not asymmetrically expressed in the KV cells.

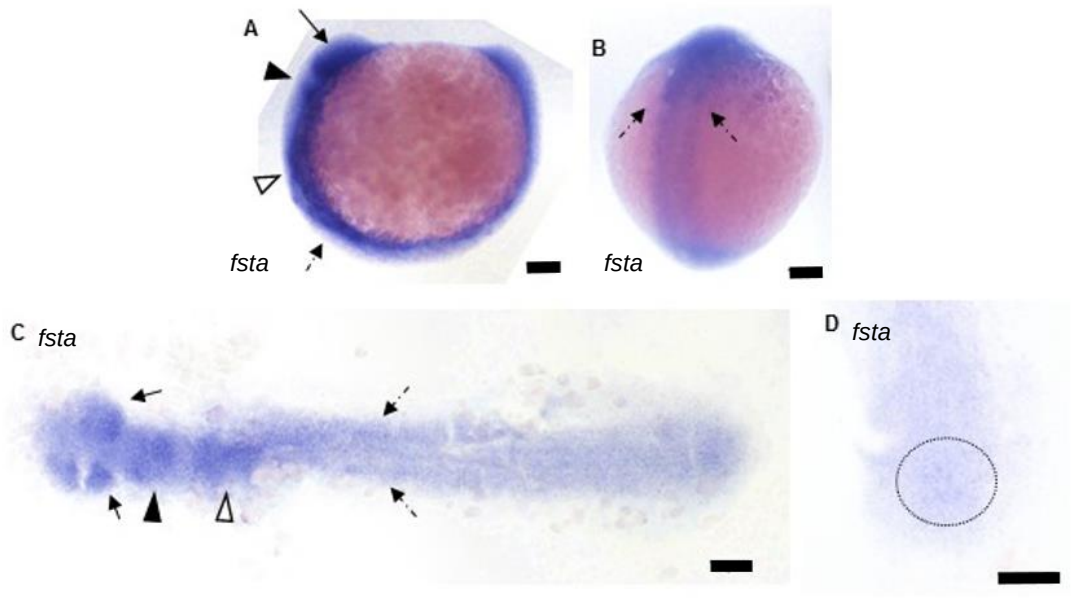

Figure 3.15: Whole-mount *in situ* hybridization showing expression of *fsta* in pkd2 morphants embryos.
Embryos are oriented in lateral (A) and dorsal (B, C and D) view. D is a tail region higher magnification of C. *fsta* expressed in the eye (arrow), ventral diencephalon (black triangle), ventral hindbrain (white triangle) and somites (dashed arrow). Dashed circle delimitates the KV site. Scale bars = 1µm.

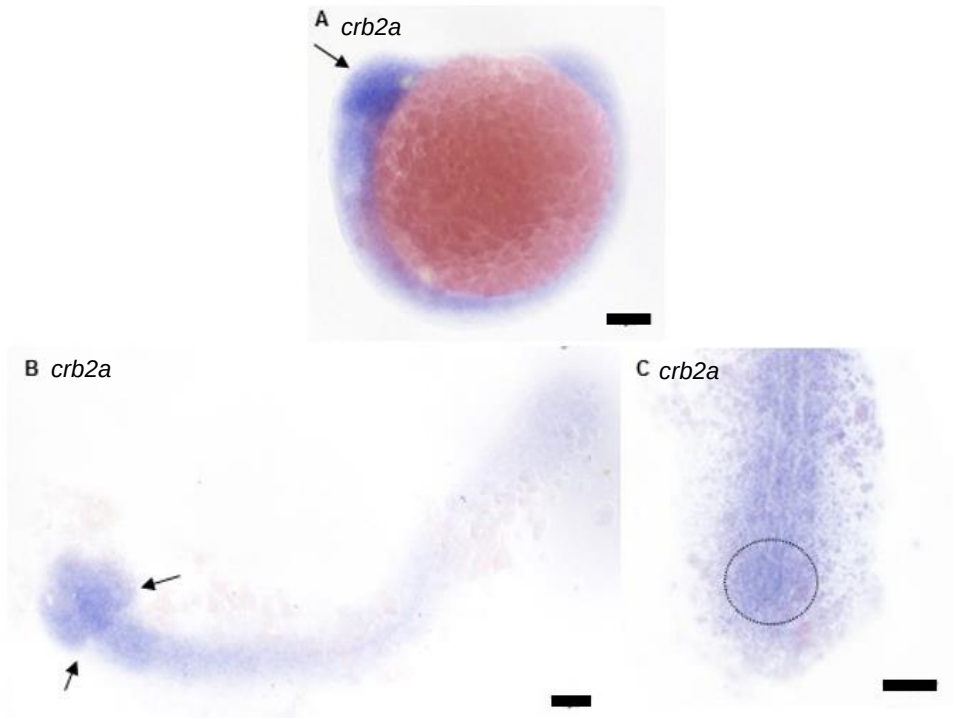

Figure 3.16: Whole-mount *in situ* hybridization showing expression of *crb2a* in pkd2 morphants embryos.
Embryos are oriented in lateral (A) and dorsal (B and C) view. C is a tail region higher magnification of B. *crb2a* expressed in the eye (arrow). Dashed circle delimitates the KV site. Scale bars = 1µm.

We observed also a stronger signal for *crb2a,* confirming its up regulation in pkd2 morphants (Figure 3.16). In these embryos we could see *crb2a* expression in the KV (Figure 3.16.C), however it seemed to be expressed around the whole KV meaning it is not an asymmetric gene either.

In summary, although we could not find any asymmetric gene pattern, it does not mean that these genes have not a role in LR patterning.

3.3. Kupffer's Vesicle Cilia Motility

Another main interest of our lab is to understand cilia motility and how it can generate a directional flow in order to initiate the proper LR establishment. Within the KV, we reported the presence of immotile and motile cilia (Sampaio *et al*. 2014). This observation raised the question if the difference between these two populations of cilia is just functional or if it is structural. Since motility is provided by dynein arms, the molecular motors for the beating of these organelles, we decided to study the localization of one dynein arm chain.

3.3.1. Analysis of the cilia motility marker Dnal1

dnal1 gene encodes the outer dynein arm (ODA) light chain 1, an ODA component that comprises the molecular motors for ATP-dependent cilia movement. We produced a mCherry-dnal1 construct in order to investigate the localization of this protein in KV ciliated cells by RNA injection at one cell stage.

To do this experiment, we cloned the dnal1 sequence into a pCS2+ plasmid that a colleague, Bárbara Tavares had cloned previously with a mCherry tag. Using BstBI and BamHI restriction enzymes, dnal1 was inserted in frame with the mCherry tag (Figure 3.17).

cDNA clone was checked by sequencing analysis and matched to Reference Sequence gene accession number NM_001003442.1 (dnal1) (see annex IV). After transcribing mCherry-dnal1, embryos were injected with the mRNA. Dnal1 was expressed within KV cilia, in opposition to the primary cilia that protrude from the surrounding tissues, as expected. This indicates that the construct was working, where the Dnal1 protein was correctly folded and was sent to a specific localization, most likely to its endogenous location.

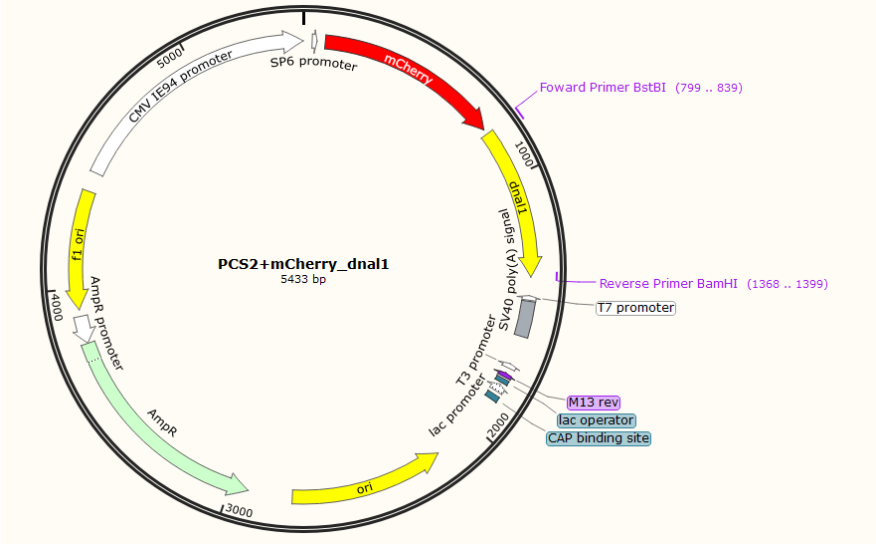

Figure 3.17: pCS2+mCherry-dnal1 map.
Vector pCS2+ contains a strong enhancer/promoter (simian CMV IE94) followed by a polylinker and the SV40 late polyadenylation site. An SP6 promoter is present in the 5' untranslated region of the mRNA from the sCMV promoter. A T7 promoter is in reverse orientation between the polylinker and the SV40 polyA site. The vector includes the ampicillin resistance (AmpR), an origin (ori) and a f1 origin (f1 ori) of replication, lac operator, CAP binding site and T3 promoter. First mcherry tag and then dnal1 sequence were cloned in frame within the polylinker of the vector. The pCS2+mCherry-dnal1 map was done using the SnapGene® Viewer 2.8.2. Software (GSL Biotech LLC, Chicago).

Furthermore, we used a transgenic zebrafish line tg(Arl13b-GFP), which labels the membrane of all KV cilia, and filmed the entire volume of the KV of live embryos via confocal microscopy. Through this technique, we were able to distinguish the two cilia populations, whereas immotile cilia were bright and sharp, motile cilia appeared as cones with a blurred GFP label caused by the ciliary movement, as represented below (Figure 3.18.).

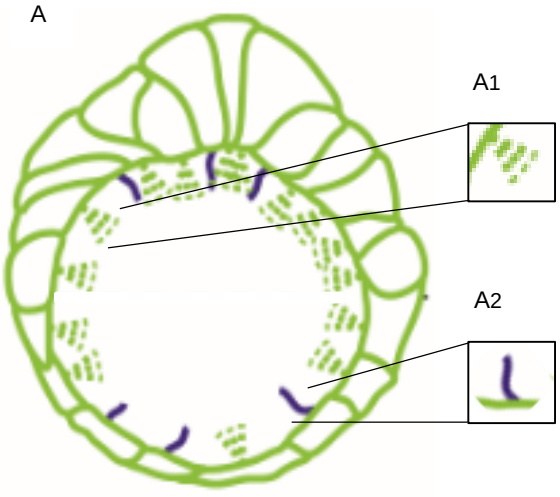

Figure 3.18: Kupffer's Vesicle cilia representation.
Schematic representation of a confocal image from the KV (A) lined by motile cilia (A1) that appear as cones and by sharp immotile cilia (A2).

Using these tg(Arl13b-GFP) embryos, we observed that mCherry-Dnal1 was present in both cilia populations (Figure 3.19). Nevertheless, mCherry-Dnal1 was not expressed in all KV cilia perhaps due to mRNA injection mosaicism.

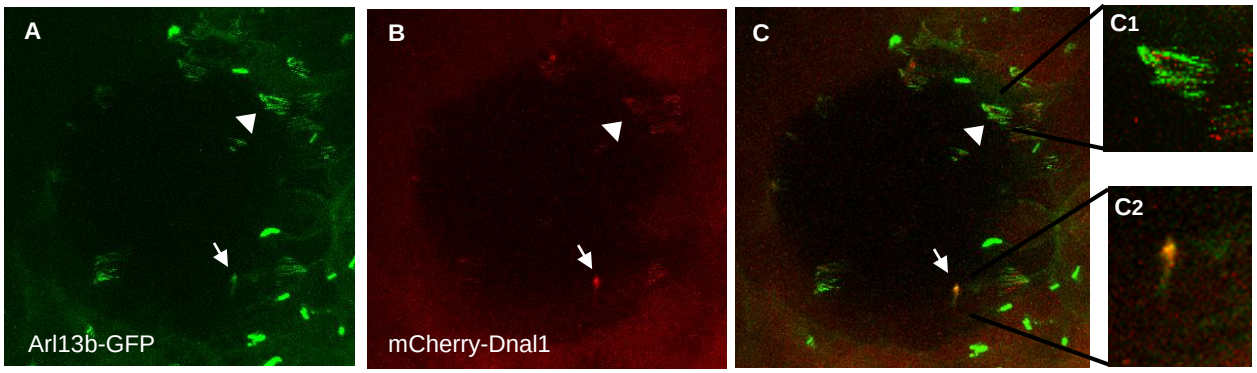

Figure 3.19: Dnal1 localization in transgenic Arl13b-GFP embryos.
Kupffer's Vesicle is shown by fluorescent confocal microscopy. (A) The cilia membrane is labeled with Arl13b-GFP and (B) mCherry-Dnal1 labels cilia that have this protein. (C) Co-localization between Dnal1 and Arl13b proteins. Higher magnifications of motile cilia (C1) and immotile cilia (C2). Arrow indicates immotile cilia. Arrow head points to motile cilia. Total number of embryos: 1.

Dnal1 was reported to be distributed only in motile cilia, wherein it assembles multiple proteins to promote cilia beating. Dnal1 links the motor heavy chains to the microtubules, which binding is likely to lead to the modulation of motor activity (King and Patel-King 2012). The observation that ODA components are also present in immotile cilia indicates that they may have the machinery necessary to produce movement.

Another construct had already been done by a colleague in the lab for *ccdc151* gene, which encodes a coiled coil domain containing 151 assembly factor. The Ccdc151 protein is important for assembly of the ODA-docking complex and for the ODA itself (Hjeij *et al*. 2014). Using the same transgenic line tg(Arl13b-GFP) embryos, we injected the mCherry-Ccdc151 and again we observed that Ccdc151 was found in either motile and immotile cilia within the KV (Figure 3.20).

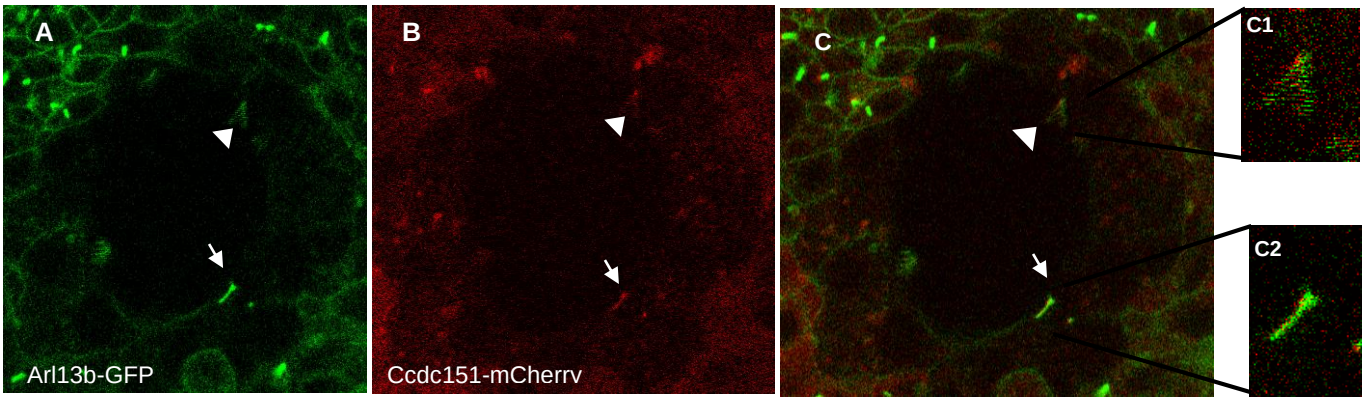

Figure 3.20: Ccdc151 localization in transgenic Arl13b-GFP embryos.
Kupffer's Vesicle is shown by fluorescent confocal microscopy. (A) The cilia membrane is labeled with Arl13b-GFP and (B) ccdc151-mCherry labels cilia that have this protein. (C) Co-localization between Ccdc151 and Arl13b proteins. Higher magnifications of motile cilia (C1) and immotile cilia (C2). Arrow indicates immotile cilia. Arrow head points to motile cilia. Total number of embryos: 6.

These preliminary results, using the constructs mCherry-Dnal1 and Ccdc151-mCherry suggests that cilia within the KV may have the same structure, meaning they all may have the capacity to move.

4. DISCUSSION

This study integrated a FCT project, named the “Quantitative analysis of asymmetric gene expression in the left-right organizer in response to flow forces: what comes downstream of cilia driven flow?”. The ultimately goal of this project was to understand how mechanical and biochemical forces can modulate intracellular signaling, during LR axis specification in the course of embryogenesis, focusing on the zebrafish LR organizer (Kupffer’s Vesicle).

4.1. Testing the Chemosensation Hypothesis

The first step of LR symmetry breaking is mediated by a biological fluid flow mechanism (Nonaka *et al*. 1998). This directional counterclockwise swirl is generated by individual beating cilia. In the mouse, the motile monocilia of the node produce a leftward flow of extraembryonic fluid, whereas immotile cilia peripherally located are thought to have the ability to sense it (McGrath *et al*. 2003). Zebrafish also has both motile and immotile cilia in the KV (Sampaio *et al*. 2014). Although no special arrangement of spatial distribution has been reported for these two populations. It is plausible that immotile cilia in the zebrafish KV may function as flow sensors, as described for crown cell cilia of the mouse node (Yoshiba *et al*. 2012). Nevertheless, in the medaka KV, no distinct subset of immotile cilia was detected, even peripheral cilia were found to be motile (Kamura *et al*. 2011). Suggesting that all cilia, regardless of their motile capabilities, might carry out sensory functions, as to be competent to respond to hydrodynamic forces.

This leads to the second step of LR asymmetry establishment, which is sensing the flow. In vertebrates, cilia are commonly thought to act as antennae that receive chemical and/or mechanical signals, raising the question whether LR organizer cilia exhibit chemosensitive or mechanosensitive properties. The chemosensation hypothesis proposes that some molecules, morphogen(s) or lipid-bounded microvesicles are directly released to the extraembryonic fluid and then carried by the flow towards the left side (Nonaka *et al*. 1998; Okada *et al*. 1999 and Tanaka *et al*. 2005). Then, chemoreceptores around the organizer detect the differential accumulation of these morphogens, transmitting sided information into surrounding cells. On the other hand, the two-cilia hypothesis is based on mechanosensation rather than chemosensation. This model predicts that the mechanical stress of the directional flow produced by autonomously rotating motile cilia is sensed by the immotile cilia population (McGrath *et al*. 2003; Tabin and Vogan 2003), translating the transmitted information from the extracellular flow into intracellular signals, such as the left-sided intracellular calcium signaling (Yoshiba *et al*. 2012). In support to this model, *pkd2,* a gene encoding a Ca^{2+} permeable cation channel, is involved in mechanosensory responses in the kidney, leading to the influx of calcium across the plasma membrane (Nauli *et al*. 2003). Pkd2 was also observed in mouse node monocilia and thought to be part of a mechanosensor complex that would serve as a mechanotransducer (McGrath *et al*. 2003).

However, recently the Clapham lab reported evidence that may disprove the two-cilia hypothesis (Delling *et al*. 2016). They showed that nodal primary cilia do not respond to physiological flow velocity and shear

stress through cilia originated calcium transients. Delling *et al*. propose that previous studies may have taken the wrong imaging approach leading to artefacts that arose when flow relocated the cilium out of the focus plane, instigating changes in fluorescence. Furthermore, they alert that a second source of error is the insufficient time resolution, because the cilium can become quickly infused with calcium from the cytoplasm that flows in from the cell body, which can be mistaken as originating in the cilium. Such evidence prompted us to test the chemosensation hypothesis.

Sensory cilia are involved in detecting light in retina, sound waves in the ear and chemical signals in airway epithelial cells and also in taste bud cells (reviewed in Prasad *et al*. 2014). Although there are some discrepancies in the field, the idea of immotile cilia as sensory organelles seems to be generally accepted (Singla and Reiter 2006). On the other hand, the evidence for sensory functions of motile cilia is more recent (Shah *et al*. 2009). So we searched for sensory-related genes in our microarray expression data. We assumed that this mechanism of sensing flow would be independent of the mechanosensor complex Pkd1l1-Pkd2, so we focused on the non-differential expressed gene list between pkd2 morphants and their siblings. We found several genes involved in taste sensing and olfactory perception. From here, we decided to continue further studies only with taste related genes because they were adopted widely as a chemodetection system in a variety of organ systems throughout the body, rather than expressed only in the gustatory cells. Hence, taste receptors mediated responses do not seem to be limited to tissues with direct access to the environmental compounds, since such receptors and taste signaling molecules have been observed not only in gastrointestinal tract and respiratory system, but also in the nervous system, testis and immune system (Voigt *et al*. 2015). More importantly, taste receptors and downstream effectors have been observed in motile cilia eliciting different effects, totally unrelated to taste buds (Shah *et al*. 2009).

In vertebrates, two families of G-protein-coupled receptors (GPCRs), named Tas1Rs and Tas2Rs, are expressed in taste bud cells, in order to detect sweet, bitter and umami compounds (Hoon *et al*. 1999; Adler *et al*. 2000; Ishimaru *et al*. 2005). This low affinity GPCRs all couple to the same downstream signaling effectors that include a G-protein alpha (α) subunit gustducin (McLaughlin *et al*. 1992) and its partners beta and gamma (βγ) subunits (Huang *et al*. 1999) to activate phospholipase Cβ2 (Rössler *et al*. 1998) and increase intracellular calcium. In the airways, Tas2Rs, G protein α-gustducin and PLCβ2 were also found to be expressed from the upper airways to the lungs. Shah and co-workers (2009) observed Tas2Rs and G protein alpha α-gustducin specifically in motile cilia of the epithelial airway cells, and PLCβ2 appeared to sit below the cilia in the apical portion of the cell. Taste stimuli elicited increase of intracellular calcium concentration, which the authors speculated to increase cilia beat frequency in order to rush elimination of noxious and harmful substances (Shah *et al*. 2009). Moreover, Tas1R and G protein α-gustducin have been found in mammalian spermatozoa, where they were thought to function as chemosensors during the sperm's passage through the female genital tract (Meyer *et al*. 2012).

These findings encouraged us to investigate the chemosensory hypothesis in the ciliated cells of KV using Tas1Rs, Tas2Rs and PLCβ2. Orthologous genes have already been discovered in zebrafish taste bud cells showing a high degree of identity to the respective mammalian genes and suggesting that there are common mechanisms of taste reception and intracellular signaling among vertebrates (Ishimaru *et al*. 2005). The exception seems to be the G protein α-gustducin because it is absent from the zebrafish genome, probably due to independent gene losses in the teleost lineage. Nevertheless, in zebrafish taste bud cells two other G alpha genes – *gnaia* and *gnai14* – were found, whereas Tas1Rs and Tas2Rs are restricted to a subset of *gnaia*-expressing taste bud cells (Oka and Korsching 2011; Ohmoto *et al*. 2011). Since *gnaia* and *gna14* were expressed in our microarray dataset, we decided to investigate both these genes.

According to our results, the taste receptors tested, both Tas1Rs and Tas2Rs, as well as PLCβ2, were very low expressed at 8 somite stage embryos (Figure 3.1.). This could indicate that zebrafish express others GPCRs as chemosensor receptors, as it has been suggested before in taste bud cells. Although Tas1Rs and Tas2Rs are generally considered to be the primary taste receptors other GPCRs have been identified in mammalian taste buds. Moreover, in zebrafish two subsets of gustatory epithelial cells were observed to express *gna14* or *gnaia* without expressing any Tas1R or Tas2R genes, suggesting the existence of other mechanisms or at least unidentified Tas2R genes (Ohmoto *et al*. 2011).

The qPCR results (Figure 3.2) prompted us to analyze *gnaia,* the guanine nucleotide binding G protein alpha inhibiting activity polypeptide a, in more detail. Gnaia is an alpha subunit of a heterotrimeric G protein complex, member of Gi family genes, which are known to mediate receptor-dependent inhibition of several adenylyl cyclases. Although Gnaia and G protein α-gustducin are not orthologous, both act in order to decrease intracellular levels of cyclic AMP (adenosine monophosphate), through different mechanisms, probably to control upstream effectors through their phosphorylation state.

In order to infer about the expression pattern of *gnaia* along the zebrafish body we performed a WISH. We confirmed that our probe was working in 4dpf zebrafish larvae (Figure 3.3.), where *gnaia* have been reported to be expressed in the lips, the pharyngeal region including gill arches and the esophagus (Ohmoto *et al*. 2011). The WISH experiment at 8 somite stage, let us observe a basal level of expression throughout the whole embryo (Figure 3.4.), also seen in ZFIN. With a higher magnification, we were able to notice that *gnaia* was expressed in KV-lining cells (Figure 3.4.), though not very strongly. This was probably due to the probe concentration, which was optimized for the larvae stage (4dpf), and may not be the same for younger embryos because of the differences in the amount of transcripts.

At this stage, we were expecting that by knocking down gnaia, the gnaia-mediated signaling, as well as the activation Gi-dependent release of βγ complexes would be impaired, so PLCβ2 would remain inactive and consequently calcium from intracellular stores would not be released. In the end, this signaling cascade failure would lead to LR defects, supporting Delling and co-workers data about the calcium wave being initiated in the cytoplasmic (Delling *et al*. 2016). However, molecular studies using our *gnaia* atgMO

indicated that Gnaia had no impact in LR establishment. Both heart and gut were found in the correct places (98% of the embryos were *situs solitus*). Since *gnaia* is well expressed in KV, which is the organ responsible for LR establishment without other known functions, these knockdown results seem to be contradictory. In order to validate them and to insure that the morpholino was indeed blocking Gnaia translation, a splice-site targeting MO could have been used and transcript levels evaluated via quantitative real-time PCR to analyze knockdown efficiency. An anti-Gnaia antibody could also have been used to test the levels of protein.

We should also take into consideration that two G proteins alpha subunits were associated to the chemosensation pathway in zebrafish taste bud cells, Gnaia and Gna14, as previously mentioned above. These are both expressed in our microarray. This led us to think that these two proteins could have redundant functions within the KV cells, which would explain the lack of results with the single Gnaia knockdown.

Unfortunately, we were not able to infer about the expression levels of *gna14*, as well as other two Tas1R, *tas1r1* and *tas1r3.* During *gna14* qPCR validation assay, we observed a jagged signal throughout the amplification plot and no amplification was detected, which could be due to a mechanical error, buffer instability, non-optimized thermal cycling conditions, degraded template or unsuitable primers. New assays should be done in order to understand the actual problem and if necessary order a new set of primers. For *tas1r1*, we detected two melting peaks during the validation assay, meaning that the primers were not specific and either amplified other amplicon or formed and accumulated primer-dimers. New primers should be purchased. Whereas, primers for *tas1r3*, only amplified at the highest concentration of cDNA, showing very high Ct values. This suggests that we were working beyond the limits of our assay, as our transcript was very low expressed.

Nevertheless, at this stage we cannot exclude the possibility that there are other genes expressed in KV ciliated cells with the ability to sense chemical inputs important for correct LR asymmetry establishment.

4.2. Screening for asymmetric gene expression in the KV

Independently from the mechanism used to sense the flow (or what it contains), a gene signaling cascade is initiated and propagated throughout the lateral plate mesoderm to give rise the correct organ LR position. Our lab found out that in zebrafish *dand5* is the first asymmetric gene to be expressed within KV cells (Lopes *et al*. 2010), which aroused our interested in discovering new asymmetric genes with a role in LR signaling pathway. Since Dand5 has been suggested to be the major target of Pkd2-mediated signaling (Yoshiba *et al*. 2012), we compared the transcriptome of pkd2 morphants, missmatchMO control embryos and WT embryos to try to find new targets of Pkd2 mediated signaling. Among these we independently screened for other asymmetric targets of Pkd2 signaling by WISH.

We screened nine target genes that were misregulated in pkd2 morphants by generating new eighteen *in situ* probes, a sense and an anti-sense probe. However some did not work as expected, meaning they overstained without showing any specific signal, which forced us to re-analyze all probe synthesis steps and look carefully for problems during the WISH protocol. All probe synthesis steps seemed well performed. As for the WISH protocol, our lab had already optimized a suitable protocol for whole zebrafish embryos.

RNA probes may vary between 250 and 1.500 base pairs in length, hence probes of approximately 800 bases long exhibit the highest sensitivity and specificity. Although longer probes can show poor tissue penetration, they decrease the likelihood of non-selective binding to non-targeted gene sequences. So it is also possible that our probes (around 600 bp) were too small for this assay.

In addition, we re-analyzed the values obtained by microarray and qPCR as we had begun to suspect that our targets were very low expressed in the KV cells. We used *dand5* as a reference gene, to address the correlation between the level of expression and the visible amount of transcripts by *in situ* assays. *dand5* expression pattern throughout its transcriptional period had been well characterized (Lopes *et al*. 2010), therefore we can easily see *dand5* expressed in the KV cells. Regarding its transcriptional levels, a qPCR assay was performed with cDNA specific from the KV cells of 8-10 somite stage WT embryos, the same template that was used on qPCR validation assay for our target genes, as well as the same housekeeping genes so we could compare both experiments. *dand5* showed a value of relative expression of 6-fold change higher than the house-keeping genes, whereas *fsta* and *crb2a*, the two genes with the highest levels of transcription of our list, showed a fold change of -2 and -5, respectively. All the other targets had even lower levels. These relative expressions were calculated based on the Ct values for each sample, and normalized with the housekeeping genes. Although it is not the absolute concentration of transcripts, the discrepancies were there, supporting our idea that our targets were very low expressed.

This happens because changes in expression levels do not necessarily reflect the mean itself. For instance, imagining that a certain gene X expressed 10 mRNA copies, while gene Y was transcribed 100 times, an increase of 10 copies would be easier to detect for the X gene, as it would correspond to a 2 fold increase, than for the Y gene. Even though the X gene is transcribing now 20 mRNA copies, the levels of expression remain very low when compared with the Y gene.

We concluded that genes with relative expression levels below 0.2 are not reliable to consider in gene expression studies by WISH, or at least special thoughts should be given, mainly in the choice of probe avoiding short repeated sequences, in order to increase sensitivity.

By the time we were performing our *in situ* procedures, Kim and colleagues showed that secreted wnt ligands activate PKD1/PKD2 channel complex, regardless of their ability to signal through β-catenin, to induce a calcium influx on target cells (Kim *et al*. 2016). This lead us to think that wnt4a, as a member of wnt noncanonical signaling, could be the ligand present in the KV, responsible for the left-sided increase

in intracellular calcium through Pkd2 activation (Yuan *et al*. 2015). Our qPCR results showed that *wnt4a* was not differentially expressed between Pkd2 morphants and their siblings, supporting the idea that Wnt4a functions upstream of Pkd2. However, the very low levels of *wnt4a* expression in KV cells obtained by microarray and confirmed by qPCR, and the *in situ* pattern, indicated that this gene was likely not active in the LR establishment process.

As for *fsta* and *crb2a* expression patterns, our results showed that they were expressed in KV-lining cells, but without any LR side-biased expression.

Regarding *crb2a* gene, no asymmetry was detected within the KV cells. Nevertheless, this gene proved to be very interesting in the Pkd2 context, hence we observed that zebrafish mutants for *pkd2* showed differences in KV-cell morphology when compared with WT KV cells. During KV formation in early segmentation, cells undergo different processes in order to accomplish a specific cilia density in anterior-dorsal regions and consequently to generate an efficient leftward flow (Okabe *et al*. 2008). Initially, KV cells show no regional differences in cell density along the anterior-posterior and dorsal-ventral axes. After the 4th somite stage, as KV volume increase, cell shape changes and cells accumulate in the anterior and dorsal sides and consequently cells in the posterior side become more wide (Compagnon *et al*. 2014), meaning that they show a larger apical surface facing the lumen. In our lab, two colleagues had characterized KV cell shape and fluid flow in *pkd2* mutants, and they observed that mutants still retained the anterior normal cell shape, but the posterior cells showed different length and width compared to their siblings. Since Crb2a is necessary and sufficient to confer apical character on a membrane domain (Wodarz *et al*. 1995), we hypothesized that *crb2a* may be involved in regional cell shape changes in order to control the development of the anterio-posterior asymmetry of the KV. However further studies are needed to test this hypothesis.

Fsta*,* follistatin, is a specific binding protein that functions as a TGFβ inhibitor, antagonizing the effect of BMPs and Activins. As it is widely distributed in a range of tissues, it is considered to have an important role in embryogenesis, development and adult life (Phillips and de Kretser 1998). In zebrafish, *fsta* has been studied in the context of axis formation and early dorsoventral (DV) patterning, showing a capacity to lead to a general dorsalization of WT embryos (Bauer *et al*. 1998). In this DV organizer, Fsta has been shown to block the ventralizing effect of Bmp4 (Fainsod *et al*. 1997), which was also expressed in our microarray dataset. Bauer and colleagues studied the temporal expression pattern of *fsta*, reveling that it begins at 80% epiboly and continues throughout the following 5 days, with a maximum at the 8-15 somite stages, suggesting that *fsta* has an imperative role during this period, which matches the KV lifetime.

On the other hand, at 8 somite stage *bmp4* is expressed in the two poles of the embryo, the anterior in cells surrounding the tip of the neural keel and the posterior pole in the tip of the tail (Martinez-Barbera *et al*. 1997). In the posterior expression domain, *bmp4* transcription is detected both at the periphery of Kupffer's Vesicle without any difference in levels of expression between left and right side, as well as in the LPM, with a transient left-sided up-regulation. Bmp4 is a secreted protein of the BMP family that acts

in two distinct phases during LR axis establishment. First, Bmp4 is required to inhibit nodal-like *spaw* expression in the right LPM and thereby regulates both visceral ad cardiac LR laterality. And then, Bmp4 is necessary to regulate left-sided gene expression of *cyclops, lefty1* and *lefty2*, in the left cardiac field, as a second wave of BMP signaling to ensure the correct position of the heart (Chocron *et al*. 2007; Chen *et al*. 1997).

In mouse, Bmp4 is expressed symmetrically in the LPM (Fujiwara *et al*. 2002) however higher levels of BMP signaling were detected in the right LPM, suggesting that asymmetric regulation of BMP signaling does not depend on gene expression pattern (Mine *et al*. 2008). Mine and colleagues showed that BMP antagonists follistatin-like, Noggin and Chordin, redundantly repress Bmp4 in the left-sided LPM, promoting a permissive environment for Nodal expression. Therefore their data suggests that Bmp4 activity inhibits Nodal expression like in zebrafish, and that BMP signaling is regulated by its antagonists in LPM. On the other hand, in the mouse node region, Nodal is inhibited by Cerl2. Additionally, Mine and co-workers observed that Noggin expression is induced by Nodal signaling arguing that BMP antagonists function together at two major aspects in LR patterning: they are required in the node for normal node morphology and for perinodal expression of Nodal and subsequently they are necessary in the left LPM to antagonize BMP signaling activity and to promote Nodal expression.

Based on these reports, we theorize that two distinct mechanisms, one through Dand5/Cerl2 and other via Bmp4-mediated inhibition regulate *spaw/nodal* expression, both in zebrafish as in mouse, and that fsta may be the BMP antagonist responsible for repressing the BMP signaling in zebrafish, similarly to Noggin and Chordin in the mouse. Therefore, Fsta and Bmp4 proteins would function as a buffer in the node to control *nodal* expression levels, for the correct propagation to the left LPM, as suggested by Lenhart (Lenhart *et al*. 2011). In Pkd2 morphants, *fsta* is up regulated but no significant difference was detected for *bmp4*, which indicates that this BMP signaling regulation occurs at the protein level. Two observations support this view: (1) Fsta directly binds to Bmp4 and its receptor, forming a trimeric complex and blocking the intracellular BMP signaling (Iemura *et al*. 1998) and symmetric bmp4 expression is translated in higher levels of BMP signaling in the right side of LPM (Mine *et al*. 2008). This evidence reinforces the idea that *fsta* even being symmetrically expressed in the Kupffer's Vesicle can have a role in LR axis patterning.

In order to better understand the impact of *fsta* during the early steps of LR axis patterning, we think it is worth to study this gene function using approaches, such as CRSPR technology, either to activate or repress *fsta*.

In conclusion, as no asymmetric genes were found within the KV cells, we started to think that perhaps *dand5* is the only gene with a LR bias transcription, via Pkd2 activation. Nevertheless, asymmetries could appear at the protein level, hence not always the expression of RNA corroborates the distribution of the protein. These discrepancies can be due to post-translational modifications which can influence protein subcellular location and activity. As an example, Francescatto and colleagues have shown that CaMK-II, a Ca^{2+}/CaM-dependent protein kinase, being homogeneously expressed around the KV, it is only activated

in cells on the left side, in response to the left-sided calcium increase (Francescatto *et al*. 2010). They also proved that CaMK-II functions downstream of Pkd2 for the correct LR organ positioning. This means that the main gap of this process continues to be the regulation of *dand5* expression, raising the question if CaMK-II is capable to promote *dand5* degradation.

4.3. Kupffer's Vesicle Cilia Motility

The Lopes' lab discovered that KV cilia are a mixed population of motile and immotile cilia (Sampaio *et al*. 2014), since then a lot of effort has been made in order to understand the differences between these two cilia populations. Such differences can be molecular or structural. In zebrafish KV, cilia have either the classical 9+2 organization of microtubules (Kramer-Zucker *et al*. 2005) or the 9+0 structure (Ferrante *et al*. 2009; Gao *et al*. 2010). However, we cannot associate each structure to one motility pattern, hence the presence or absence of the central pair of singlet microtubules is not exclusive for motile or immotile cilia (reviewed in Choksi *et al*. 2014).

To address this question, one lab member has counted the number of motile and immotile cilia populations throughout the 3th to 8th somite stage and she found that although the total number remained the same, at the beginning the majority of cilia was immotile and then the number of motile cilia was increasing until 80% (unpublished data). Also Foxj1a is the major forkhead domain-containing transcription factor that directly activates the genes responsible for motile cilia synthesis, including dynein arms, central pair and radial spokes (Yu *et al*. 2008). However we previous observed that Foxj1a was expressed in cells harbouring both motile and immotile cilia within the KV. These observations suggested cilia could be structurally equal and along KV expansion there might be a molecular switch that controls motility.

Both inner arm dyneins and outer arm dyneins are essential for efficient cilia motility. Multiproteins comprising heavy, intermediate and light chains assemblies into outer dynein arms, which have ATPase activity that provides the energy to drive rhythmic movement of the axonemes and to govern beat frequency. In addition, accessory structures provide a rigid structure and regulate dynein-mediated motility, as radial spokes and central pair apparatus. In case of total or partial absence of dynein arms, defects in accessory structures or anomalies in peripheral microtubules, the coordinated ciliary wave is impaired leading to primary ciliary dyskinesia (PCD). PCD patients present recurrent respiratory tract infections, sinusitis, male infertility, and 50% of them also have *situs inversus* due to the defects in cilia motility within the LR organizer.

Previous studies have shown that in the gastrulation stage Dnal1 was confined to the embryonic node cilia and interacted with the Dnah5 (Horváth *et al*. 2005) as well as a point mutation had been reported to cause PCD (Mazor *et al*. 2011), supporting the importance of Dnal1 in cilia-beat generation. Our results based on overexpression of a construct with mCherry-*dnal1* showed that both motile and immotile cilia express this Dnal1 protein, supporting our hypothesis that all KV cilia may have the machinery necessary for motility. In

addition, we observed that *ccdc151*, a coiled-coil domain containing 151 gene, was also localized in motile and immotile cilia using the tg(Arl13b:GFP) zebrafish line. Ccdc151 plays an essential role for targeting of outer arm dyneins for assembling and docking it to the axoneme, furthermore loss of function studies leaded randomization of visceral organ positioning, showing that Ccdc151 is necessary for the correct LR establishment (Hjeij *et al*. 2014).

Therefore, Ccdc151 is an important assembly factor in motile cilia. However, we must be cautious because when overexpressed, Ccdc151 could theoretically assemble the motility machinery in every ciliated cell. In opposition, Dnal1, being a component of ODAs, even when overexpressed could not be assembled by itself into the cilium without the remaining dyneins nor the other interconnecting multiprotein complexes. Which lead us to reason that Dnal1 presence in immotile cilia might be true. Fortunately, like the Dnal1, Ccdc151 was not detected in primary cilia. Meaning that their presence in both KV types of cilia may be correct. These preliminary results reinforce the idea that both cilia populations may have the same structure.

In summary, in this work we combined different genetic techniques as well as live imaging in order to try to enlighten this important but poorly understood phenomenon, which is the early patterning of the LR axis.

Our results of gene expression studies helped us to establish a threshold in the microarray where values below 5 in a scale up to 12 are not trustworthy to study by *in situ* hybridization. This will be useful to take into consideration in further analyzes of microarray dataset genes.

With the localization study of Dnal1, we discovered that Dnal1 is present in motile and immotile cilia, suggesting that both cilia populations have the machinery and consequently the capacity to move. In light of these results it would be important to create a new knock-in transgenic zebrafish line, reporting dnal1 endogenously, to avoid the overexpression-associated problems. And it is our future goal to identify the molecules responsible for the switching on cilia beating, which can be activators that will turn on the cilia motility program or inhibitors that will block the *foxj1a* downstream effector thus maintaining the motility program down.

REFERENCES

Adler, E. et al., 2000. A novel family of mammalian taste receptors. *Cell*, 100(6), pp.693–702.

Afzelius, B. a, 1976. A human syndrome caused by immotile cilia. *Science*, 193(4250), pp.317–319.

Amack, J.D. & Yost, H.J., 2014. The T Box Transcription Factor No Tail in Ciliated Cells Controls Zebrafish Left-Right Asymmetry. *Curr Biol*, 14(8), pp.685–690.

van Amerongen, R. & Nusse, R., 2009. Towards an integrated view of Wnt signaling in development. *Development*, 136(19), pp.3205–3214.

Avasthi, P. & Marshall, W., 2012. Stages of ciliogenesis and regulation of ciliary length. *Differentiation*, 83(2), pp.S30–42.

Badano, J.L. et al., 2006. The ciliopathies: an emerging class of human genetic disorders. *Annu Rev Genomics Hum Genet*, 7, pp.125–148.

Bauer, H. et al., 1998. Follistatin and noggin are excluded from the zebrafish organizer. *Dev Biol*, 204(2), pp.488–507.

Bellomo, D. et al., 1996. Cell proliferation in mammalian gastrulation: The ventral node and notochord are relatively quiescent. *Dev Dyn.*, 205(4), pp.471–485.

Bisgrove, B.W. et al., 2005. Polaris and Polycystin-2 in dorsal forerunner cells and Kupffer's vesicle are required for specification of the zebrafish left-right axis. *Dev Biol.*, 287(2), pp.274–288.

Bloodgood, R. a, 2010. Sensory reception is an attribute of both primary cilia and motile cilia. *J Cell Sci*, 123(Pt 4), pp.505–509.

Brokaw, C.J. & Kamiya, R., 1987. Bending patterns of Chlamydomonas flagella: IV. Mutants with defects in inner and outer dynein arms indicate differences in dynein arm function. *Cell Motil Cytoskeleton*, 8(1), pp.68–75.

Carl, M. et al., 2007. Wnt/Axin1/beta-Catenin Signaling Regulates Asymmetric Nodal Activation, Elaboration, and Concordance of CNS Asymmetries. *Neuron*, 55(3), pp.393–405.

Caron, A., Xu, X. & Lin, X., 2012. Wnt/Beta-catenin signaling directly regulates Foxj1 expression and ciliogenesis in zebrafish Kupffer's vesicle. *Development*, 139(3), pp.514–524.

Cartwright, J.H.E. et al., 2007. Embryonic nodal flow and the dynamics of nodal vesicular parcels. *J R Soc Interface*, 4(12), pp.49–55.

Chang, H. et al., 2000. Smad5 is essential for left-right asymmetry in mice. *Dev Biol.*, 219(1), pp.71–8.

Chen, J.N. et al., 1997. Left-right pattern of cardiac BMP4 may drive asymmetry of the heart in zebrafish. *Development*, 124(21), pp.4373–4382.

Chilvers, M.A., Rutman, A. & O'Callaghan, C., 2003. Ciliary beat pattern is associated with specific ultrastructural defects in primary ciliary dyskinesia. *J Allergy Clin Immunol*, 112(3), pp.518–524.

Chocron, S. et al., 2007. Zebrafish Bmp4 regulates left-right asymmetry at two distinct developmental time points. *Dev Biol*, 305(2), pp.577–588.

Choksi, S.P. et al., 2014. Switching on cilia: transcriptional networks regulating ciliogenesis. *Development*, 141(7), pp.1427–1441.

Clapp, T.R. et al., 2008. Tonic activity of Gα-gustducin regulates taste cell responsivity. *FEBS Lett*, 582(27), pp.3783–3787.

Collignon, J., Varlet, I. & Robertson, E.J., 1996. Relationship between asymmetric nodal expression and the direction of embryonic turning. *Nature*, 381(6578), pp.155–158.

Compagnon, J. et al., 2014. The Notochord Breaks Bilateral Symmetry by Controlling Cell Shapes in the Zebrafish Laterality Organ. *Dev Cell*, 31(6), pp.774–783.

Cruciat, C.-M., 2014. Casein kinase 1 and Wnt/β-catenin signaling. *Curr Opin Cell Biol.*, 31, pp.46–55.

Davidson, B.P. et al., 1999. Impact of node ablation on the morphogenesis of the body axis and the lateral asymmetry of the mouse embryo during early organogenesis. *Dev Biol.*, 211(1), pp.11–26.

Delling, M. et al., 2016. Primary cilia are not calcium-responsive mechanosensors. *Nature*, 531(7596), pp.656–660.

Essner, J.J. et al., 2005. Kupffer's vesicle is a ciliated organ of asymmetry in the zebrafish embryo that initiates left-right development of the brain, heart and gut. *Development*, 132(6), pp.1247–1260.

Fainsod, A. et al., 1997. The dorsalizing and neural inducing gene follistatin is an antagonist of BMP-4. *Mech Dev*, 63(1), pp.39–50.

Ferrante, M.I. et al., 2009. Convergent extension movements and ciliary function are mediated by ofd1, a zebrafish orthologue of the human oral-facial-digital type 1 syndrome gene. *Hum Mol Genet*, 18(2), pp.289–303.

Field, S. et al., 2011. Pkd1l1 establishes left-right asymmetry and physically interacts with Pkd2. *Development*, 138(6), pp.1131–1142.

Fisch, C. & Dupuis-Williams, P., 2011. Ultrastructure of cilia and flagella - back to the future! *Biol Cell*, 103(6), pp.249–270.

Fliegauf, M., Benzing, T. & Omran, H., 2007. When cilia go bad: cilia defects and ciliopathies. *Nat Rev Mol*

Cell Biol, 8(11), pp.880–893.

Francescatto, L. et al., 2010. The activation of membrane targeted CaMK-II in the zebrafish Kupffer's vesicle is required for left-right asymmetry. *Development*, 137(16), pp.2753–2762.

Fujiwara, T. et al., 2002. Distinct requirements for extra-embryonic and embryonic bone morphogenetic protein 4 in the formation of the node and primitive streak and coordination of left-right asymmetry in the mouse. *Development*, 129(20), pp.4685–4696.

Gao, C. et al., 2010. Oda16/Wdr69 is essential for axonemal dynein assembly and ciliary motility during zebrafish embryogenesis. *Dev Dyn.*, 239(8), pp.2190–2197.

Goodenough, U.W. & Heuser, J.E., 1985. Outer and inner dynein arms of cilia and flagella. *Cell*, 41(2), pp.341–342.

Hansen, A., Reutter, K. & Zeiske, E., 2002. Taste bud development in the zebrafish, Danio rerio. *Dev Dyn.*, 223(4), pp.483–496.

Hascilowicz, T. et al., 2002. Regulation of ornithine decarboxylase by antizymes and antizyme inhibitor in zebrafish (Danio rerio). *Biochim Biophys Acta.*, 1578(1-3), pp.21–28.

Hashimoto, H. et al., 2004. The Cerberus/Dan-family protein Charon is a negative regulator of Nodal signaling during left-right patterning in zebrafish. *Development*, 131(8), pp.1741–1753.

Hildebrandt, F., Benzing, T. & Katsanis, N., 2011. Ciliopathies. *N Engl J Med*, 364(16), pp.1533–1543. Available at: http://www.nejm.org/doi/full/10.1056/nejmra1010172.

Hilgendorf, K.I., Johnson, C.T. & Jackson, P.K., 2016. The primary cilium as a cellular receiver: organizing ciliary GPCR signaling. *Curr Opin Cell Biol.*, 39, pp.84–92.

Hjeij, R. et al., 2014. CCDC151 mutations cause primary ciliary dyskinesia by disruption of the outer dynein arm docking complex formation. *Am J Hum Genet.*, 95(3), pp.257–274.

Hogan, B.L.M., 1996. Bone morphogenetic proteins: multifunctinal regulators of vertebrate development. *Genes Dev*, 10(13), pp.1580–1594.

Hojo, M. et al., 2007. Right-elevated expression of charon is regulated by fluid flow in medaka Kupffer's vesicle. *Dev Growth Differ.*, 49(5), pp.395–405.

Hoon, M.A. et al., 1999. Putative Mammalian Taste Receptors. *Cell*, 96(4), pp.541–551.

Horani, A. et al., 2016. Genetics and biology of primary ciliary dyskinesia. *Paediatr Respir Rev*, 18, pp.13–24.

Horváth, J. et al., 2005. Identification and analysis of axonemal dynein light chain 1 in primary ciliary dyskinesia patients. *American Journal of Respiratory Cell and Molecular Biology*, 33(1), pp.41–47.

Hsu, D.R. et al., 1998. The Xenopus dorsalizing factor Gremlin identifies a novel family of secreted proteins that antagonize BMP activities. *Mol Cell*, 1(5), pp.673–683.

Hsu, Y.-C. et al., 2006. Mosaic Eyes is a novel component of the Crumbs complex and negatively regulates photoreceptor apical size. *Development*, 133(24), pp.4849–4859.

Iacomino, G., Picariello, G. & D'Agostino, L., 2012. DNA and nuclear aggregates of polyamines. *Biochim Biophys Acta*, 1823(10), pp.1745–1755.

Ibañez-Tallon, I., Heintz, N. & Omran, H., 2003. To beat or not to beat: roles of cilia in development and disease. *Hum Mol Genet*, 12(1), pp.R27–R35.

Iemura, S. et al., 1998. Direct binding of follistatin to a complex of bone-morphogenetic protein and its receptor inhibits ventral and epidermal cell fates in early Xenopus embryo. *Proc Natl Acad Sci USA*, 95(16), pp.9337–9342.

Ishikawa, H. & Marshall, W.F., 2011. Ciliogenesis: building the cell's antenna. *Nat Rev Mol Cell Biol*, 12(4), pp.222–234.

Ishimaru, Y. et al., 2005. Two families of candidate taste receptors in fishes. *Mech Dev*, 122(12), pp.1310–1321.

Jain, R. et al., 2012. Sensory functions of motile cilia and implication for bronchiectasis. *Front Biosci (Schol Ed)*, 4, pp.1088–1098.

Jerber, J. et al., 2014. The coiled-coil domain containing protein CCDC151 is required for the function of IFT-dependent motile cilia in animals. *Hum Mol Genet*, 23(3), pp.563–577.

Jones, C.M., Armes, N. & Smith, J.C., 1996. Signalling by TGF-beta family members: short-range effects of Xnr-2 and BMP-4 contrast with the long-range effects of activin. *Curr Biol*, 6(11), pp.1468–1475.

Kamiya, R., 2002. Functional diversity of axonemal dynein as studied in chlamydomonas mutants. *Int Rev Cytol*, 219, pp.115–155.

Kamiya, R., Kurimoto, E. & Muto, E., 1991. Two types of Chlamydomonas flagellar mutants missing different components of inner-arm dynein. *J Cell Biol.*, 112(3), pp.441–447.

Kamura, K. et al., 2011. Pkd1l1 complexes with Pkd2 on motile cilia and functions to establish the left-right axis. *Development*, 138(6), pp.1121–1129.

Kim, J. et al., 2016. Intracellular spermine blocks TRPC4 channel via electrostatic interaction with C-terminal negative amino acids. *Pflugers Arch*, 468(4), pp.551–561.

Kim, S. et al., 2016. The polycystin complex mediates Wnt/Ca2+ signalling. *Nat Cell Biol*, 18(7), pp.752–764.

Kimmel, C.B. et al., 1995. Stages of embryonic development of the zebrafish. *Dev Dyn*, 203(3), pp.253–310.

King, S.M., 2016. Axonemal Dynein Arms. *Cold Spring Harb Perspect Biol.*, p.doi: 10.1101/cshperspect.a028100.

King, S.M. & Patel-King, R.S., 2012. Functional architecture of the outer arm dynein conformational switch. *J Biol Chem.*, 287(5), pp.3108–3122.

Kingsley, D.M., 1994. The TGF-beta superfamily: new members, new receptors, and new genetic tests of function in different organisms. *Genes Dev*, 8(2), pp.133–146.

Kinnamon, S.C., 2012. Taste Receptor Signaling-- From Tongues to Lungs. , 204(2), pp.158–168.

Kishimoto, Y. et al., 1997. The molecular nature of zebrafish swirl: BMP2 function is essential during early dorsoventral patterning. *Development*, 124(22), pp.4457–4466.

Kobayashi, D. & Takeda, H., 2012. Ciliary motility: The components and cytoplasmic preassembly mechanisms of the axonemal dyneins. *Differentiation*, 83(2), pp.S23–S29.

Kramer-Zucker, A.G. et al., 2005. Cilia-driven fluid flow in the zebrafish pronephros, brain and Kupffer's vesicle is required for normal organogenesis. *Development*, 132(8), pp.1907–1921.

Lamver, T. et al., 2016. Abnormalities of Fetal Situs: An Overview and Literature Review. *Obstet Gynecol Surv*, 71(1), pp.33–38.

Lee, S.A. et al., 2003. The zebrafish forkhead transcription factor Foxi1 specifies epibranchial placode-derived sensory neurons. *Development*, 130(12), pp.2669–2679.

Lenhart, K.F. et al., 2011. Two additional midline barriers function with midline lefty1 expression to maintain asymmetric Nodal signaling during left-right axis specification in zebrafish. *Development*, 138(20), pp.4405–4410.

Lin, A.E. et al., 2014. Laterality defects in the national birth defects prevention study (1998-2007): Birth prevalence and descriptive epidemiology. *Am J Hum Genet.*, 164(10), pp.2581–2591.

Lin, X. & Xu, X., 2009. Distinct functions of Wnt/beta-catenin signaling in KV development and cardiac asymmetry. *Development*, 136(2), pp.207–217.

Lindemann, C.B. & Lesich, K.A., 2010. Flagellar and ciliary beating: the proven and the possible. *J Cell Sci*, 123(Pt 4), pp.519–528.

Liu, Z. et al., 2008. Partially functional outer-arm dynein in a novel Chlamydomonas mutant expressing a truncated gamma heavy chain. *Eukaryot Cell*, 7(7), pp.1136–1145.

Lopes, S.S. et al., 2010. Notch signalling regulates left-right asymmetry through ciliary length control.

Development, 137(21), pp.3625–3632.

Marques, S. et al., 2004. The activity of the Nodal antagonist Cerl-2 in the mouse node is required for correct L/R body axis. *Genes Dev*, 18(19), pp.2342–2347.

Martinez-Barbera, J.P. et al., 1997. Cloning and expression of three members of the zebrafish Bmp family: Bmp2a, Bmp2b and Bmp4. *Gene*, 198(1-2), pp.53–59.

Matsui, T. et al., 2005. Noncanonical Wnt signaling regulates midline convergence of organ primordia during zebrafish development. *Genes Dev*, 19(1), pp.164–175.

Matsui, T. & Bessho, Y., 2012. Left–right asymmetry in zebrafish. *Cell Mol Life Sci*, 69(18), pp.3069–3077. Available at: http://link.springer.com/10.1007/s00018-012-0985-6.

Matsumoto, I., Ohmoto, M. & Abe, K., 2013. Functional diversification of taste cells in vertebrates. *Semin Cell Dev Biol.*, 24(3), pp.210–214.

Mazor, M. et al., 2011. Primary ciliary dyskinesia caused by homozygous mutation in DNAL1, encoding dynein light chain 1. *Am J Hum Genet.*, 88(5), pp.599–607.

McGrath, J. et al., 2003. Two populations of node monocilia initiate left-right asymmetry in the mouse. *Cell*, 114(1), pp.61–73.

McGrath, J. & Brueckner, M., 2003. Cilia are at the heart of vertebrate left-right asymmetry. *Current Opinion in Genetics and Development*, 13(4), pp.385–392.

Meyer, D. et al., 2012. Expression of tas1 taste receptors in mammalian spermatozoa: Functional role of tas1r1 in regulating basal ca 2+ and camp concentrations in spermatozoa. *PloS One*, 7(2), p.e332354.

Mine, N., Anderson, R.M. & Klingensmith, J., 2008. BMP antagonism is required in both the node and lateral plate mesoderm for mammalian left-right axis establishment. *Development*, 135, pp.2425–2434.

Mitchell, D.R., 2007. The evolution of eukaryotic cilia and flagella as motile and sensory organelles. *Adv Exp Med Biol*, 607, pp.130–140.

Mulloy, B. & Rider, C.C., 2015. The Bone Morphogenetic Proteins and Their Antagonists. In *Vitamins and Hormones*. Elsevier Inc., pp. 63–90.

Nakamura, T. et al., 2012. Fluid flow and interlinked feedback loops establish left-right asymmetric decay of Cerl2 mRNA. *Nature Commun*, 3, p.1322.

Nakaya, M. et al., 2005. Wnt3a links left-right determination with segmentation and anteroposterior axis elongation. *Development*, 132(24), pp.5425–5436.

Nauli, S.M. et al., 2003. Polycystins 1 and 2 mediate mechanosensation in the primary cilium of kidney cells. *Nat Genet*, 33(2), pp.129–137.

Niehrs, C., 2004. Regionally specific induction by the Spemann-Mangold organizer. *Nature reviews. Genetics*, 5(6), pp.425–434.

Nonaka, S. et al., 2002. Determination of left-right patterning of the mouse embryo by artificial nodal flow. *Nature*, 418(6893), pp.96–99.

Nonaka, S. et al., 1998. Randomization of left-right asymmetry due to loss of nodal cilia generating leftward flow of extraembryonic fluid in mice lacking KIF3B motor protein. *Cell*, 95(6), pp.829–837.

Ohkubo, Y. et al., 2005. Distribution and Morphological Features of Taste Buds in the Zebrafish, Danio rerio. *Journal of Oral Biosciences*, 47(1), pp.77–82.

Ohmoto, M. et al., 2011. Mutually exclusive expression of Gαia and Gα14 reveals diversification of taste receptor cells in zebrafish. *J Comp Neurol*, 519(8), pp.1616–1629.

Oka, Y. & Korsching, S.I., 2011. Shared and unique G alpha proteins in the zebrafish versus mammalian senses of taste and smell. *Chem Senses*, 36(4), pp.357–365.

Okabe, N., Xu, B. & Burdine, R.D., 2008. Fluid dynamics in zebrafish Kuppfer's vesicle. *Dev Dyn*, 237(12), pp.3602–3612.

Okada, Y. et al., 1999. Abnormal nodal flow precedes situs inversus in iv and inv mice. *Mol Cell*, 4(4), pp.459–468.

Okada, Y. et al., 2005. Mechanism of nodal flow: A conserved symmetry breaking event in left-right axis determination. *Cell*, 121(4), pp.633–644.

Oldham, W.M. & Hamm, H.E., 2008. Heterotrimeric G protein activation by G-protein-coupled receptors. *Nat Rev Mol Cell Biol*, 9(1), pp.60–71.

Omata, Y. et al., 2007. Role of Bone morphogenetic protein 4 in zebrafish semicircular canal development. *Dev Growth Differ*, 49(9), pp.711–719.

Papon, J.F. et al., 2010. A 20-year experience of electron microscopy in the diagnosis of primary ciliary dyskinesia. *Euro Respir J*, 35(5), pp.1057–1063.

Pennekamp, P. et al., 2002. The ion channel polycystin-2 is required for left-right axis determination in mice. *Current Biology*, 12(11), pp.938–943.

Phillips, D.J. & de Kretser, D.M., 1998. Follistatin: a multifunctional regulatory protein. *Front. Neuroendocrinol*, 19(4), pp.287–322.

Qian, F. et al., 1997. PKD1 interacts with PKD2 through a probable coiled-coil domain. *Nat Genet*, 16(2), pp.179–183.

Rodríguez, P. et al., 2012. The non-canonical NOTCH ligand DLK1 exhibits a novel vascular role as a strong inhibitor of angiogenesis. *Cardiovas Res*, 93(2), pp.232–241.

Roxo-Rosa, M. et al., 2015. The zebrafish Kupffer's vesicle as a model system for the molecular mechanisms by which the lack of Polycystin-2 leads to stimulation of CFTR. *Biol Open*, 4(11), pp.1356–1366.

Sampaio, P. et al., 2014. Left-Right Organizer Flow Dynamics: How Much Cilia Activity Reliably Yields Laterality? *Dev Cell*, 29(6), pp.716–728.

Sasai, Y. et al., 1995. Regulation of neural induction by the Chd and Bmp-4 antagonistic patterning signals in Xenopus. *Nature*, 376(6538), pp.333–336.

Schneider, I. et al., 2008. Calcium fluxes in dorsal forerunner cells antagonize beta-catenin and alter left-right patterning. *Development*, 135(1), pp.75–84.

Schottenfeld, J., Sullivan-Brown, J. & Burdine, R.D., 2007a. Zebrafish curly up encodes a Pkd2 ortholog that restricts left-side-specific expression of southpaw. *Development*, 134(8), pp.1605–1615.

Schottenfeld, J., Sullivan-Brown, J. & Burdine, R.D., 2007b. Zebrafish curly up encodes a Pkd2 ortholog that restricts left-side-specific expression of southpaw. *Development (Cambridge, England)*, 134(8), pp.1605–1615.

Schweickert, A. et al., 2010. The Nodal Inhibitor Coco Is a Critical Target of Leftward Flow in Xenopus. *Current Biology*, 20(8), pp.738–743.

Shah, A.S. et al., 2009. Motile Cilia of Human Airway Epithelia Are Chemosensory. *Science*, 325(5944), pp.1131–1134.

Shapiro, A.J. et al., 2015. The prevalence of clinical features associated with primary ciliary dyskinesia in a heterotaxy population: results of a web-based survey. *Cardiol Young*, 25(4), pp.752–759.

Shi, Y. & Massagué, J., 2003. Mechanisms of TGF-β signaling from cell membrane to the nucleus. *Cell*, 113(6), pp.685–700.

Singla, V. & Reiter, J.F., 2006. The primary cilium as the cell's antenna: signaling at a sensory organelle. *Science*, 313(5787), pp.629–633.

Smith, E.F. & Yang, P., 2004. The Radial Spokes and Central Apparatus: Mechano-Chemical Transducers That Regulate Flagellar Motility. *Cell MOtil Cytoskeleton*, 57(1), pp.8–17.

Sobkowicz, H.M., Slapnick, S.M. & August, B.K., 1995. The kinocilium of auditory hair cells and evidence for its morphogenetic role during the regeneration of stereocilia and cuticular plates. *J Neurocytol*, 24(9), pp.633–653.

Sukharev, S. & Corey, D.P., 2004. Mechanosensitive channels: multiplicity of families and gating paradigms. *Science's STKE*, 2004(219), p.re4.

Sulik, K. et al., 1994. Morphogenesis of the murine node and notochordal plate. *Dev Dyn.*, 201(3), pp.260–278.

Supp, D.M. et al., 1997. Mutation of an axonemal dynein affects left–right asymmetry in inversus viscerum mice. *Nature*, 389(6654), pp.963–966.

Supp, D.M. et al., 1999. Targeted deletion of the ATP binding domain of left-right dynein confirms its role in specifying development of left-right asymmetries. *Development*, 126(23), pp.5495–5504.

Tabin, C.J. & Vogan, K.J., 2003. A two-cilia model for vertebrate left-right axis specification. *Genes Dev*, 17(1), pp.1–6.

Takao, D. et al., 2013. Asymmetric distribution of dynamic calcium signals in the node of mouse embryo during left-right axis formation. *Dev Biol.*, 376(1), pp.23–30.

Takeda, S. et al., 1999. Left-right asymmetry and kinesin superfamily protein KIF3a: New insights in determination of laterality and mesoderm induction by KIF3A(-/-) mice analysis. *J Cell Biol.*, 145(4), pp.825–836.

Tanaka, Y., Okada, Y. & Hirokawa, N., 2005. FGF-induced vesicular release of Sonic hedgehog and retinoic acid in leftward nodal flow is critical for left-right determination. *Nature*, 435(7039), pp.172–177.

Tang, R. et al., 2007. Validation of zebrafish (Danio rerio) reference genes for quantitative real-time RT-PCR normalization. *Acta Biochimica et Biophysica Sinica*, 39(5), pp.384–390.

Taylor, S. et al., 2010. A practical approach to RT-qPCR-Publishing data that conform to the MIQE guidelines. *Methods*, 50(4), pp.S1–S5.

Thisse, C. & Thisse, B., 2008. High-resolution in situ hybridization to whole-mount zebrafish embryos. *Nature Protocols*, 3(1), pp.59–69.

Ungar, A.R., Kelly, G.M. & Moon, R.T., 1995. Wnt4 affects morphogenesis when n- & expressed in the zebrafish embryo. *Mech Dev*, 52(2-3), pp.153–164.

Vermot, J. et al., 2005. Retinoic Acid Controls the Bilateral Symmetry of Somite Formation in the Mouse Embryo. *Science*, 308(5721), pp.563–566.

Vincensini, L., Blisnick, T. & Bastin, P., 2011. 1001 model organisms to study cilia and flagella. *Biol Cell*, 103(3), pp.109–130.

Wettschureck, N. & Offermanns, S., 2005. Mammalian G Proteins and Their Cell Type Specific Functions. *Physilological Review*, pp.1159–1204.

Westerfield, M., 1995. The Zebrafish Book. Eugene: University of Oregon Press.

Wodarz, A. et al., 1995. Expression of crumbs confers apical character on plasma membrane domains of ectodermal epithelia of drosophila. *Cell*, 82(1), pp.67–76.

Wong, G.T., Gannon, K.S. & Margolskee, R.F., 1996. Transduction of bitter and sweet taste by gustducin. *Nature*, 381(6585), pp.796–800.

Xue, Y. et al., 2016. Coordinate involvement of Nodal-dependent inhibition and Wnt-dependent activation in the maintenance of organizer-specific bmp2b in zebrafish. *The International Journal of Developmental Biology*, 60(1-2-3), pp.13–19.

Yao, D. et al., 2014. Dissecting the differentiation process of the preplacodal ectoderm in zebrafish. *Developmental Dynamics*, 243(10), pp.1338–1351.

Yoshiba, S. et al., 2012. Cilia at the node of mouse embryos sense fluid flow for left-right determination via Pkd2. *Science*, 338(6104), pp.226–231.

Yu, X. et al., 2008. Foxj1 transcription factors are master regulators of the motile ciliogenic program. *Nature genetics*, 40(12), pp.1445–1453.

Yuan, S. et al., 2015. Intraciliary Calcium Oscillations Initiate Vertebrate Left-Right Asymmetry. *Current biology : CB*, pp.1–12.

Zhang, M. et al., 2012. β-Catenin 1 and β-catenin 2 play similar and distinct roles in left-right asymmetric development of zebrafish embryos. *Development*, 139(11), pp.2009–2019.

Zhang, X.M., Ramalho-Santos, M. & McMahon, A.P., 2001. Smoothened mutants reveal redundant roles for Shh and Ihh signaling including regulation of L/R asymmetry by the mouse node. *Cell*, 106(2), pp.781–792.

Zhang, Z. et al., 2007. The transduction channel TRPM5 is gated by intracellular calcium in taste cells. *J Neurosci*, 27(21), pp.5777–5786.

Zhu, P., Xu, X. & Lin, X., 2015. Both ciliary and non-ciliary functions of Foxj1a confer Wnt/ -catenin signaling in zebrafish left-right patterning. *Biology Open*, pp.1–11.

ANNEXES

Annex I: Sequencing result of crumb2a (*crb2a*) ISH probe sequence

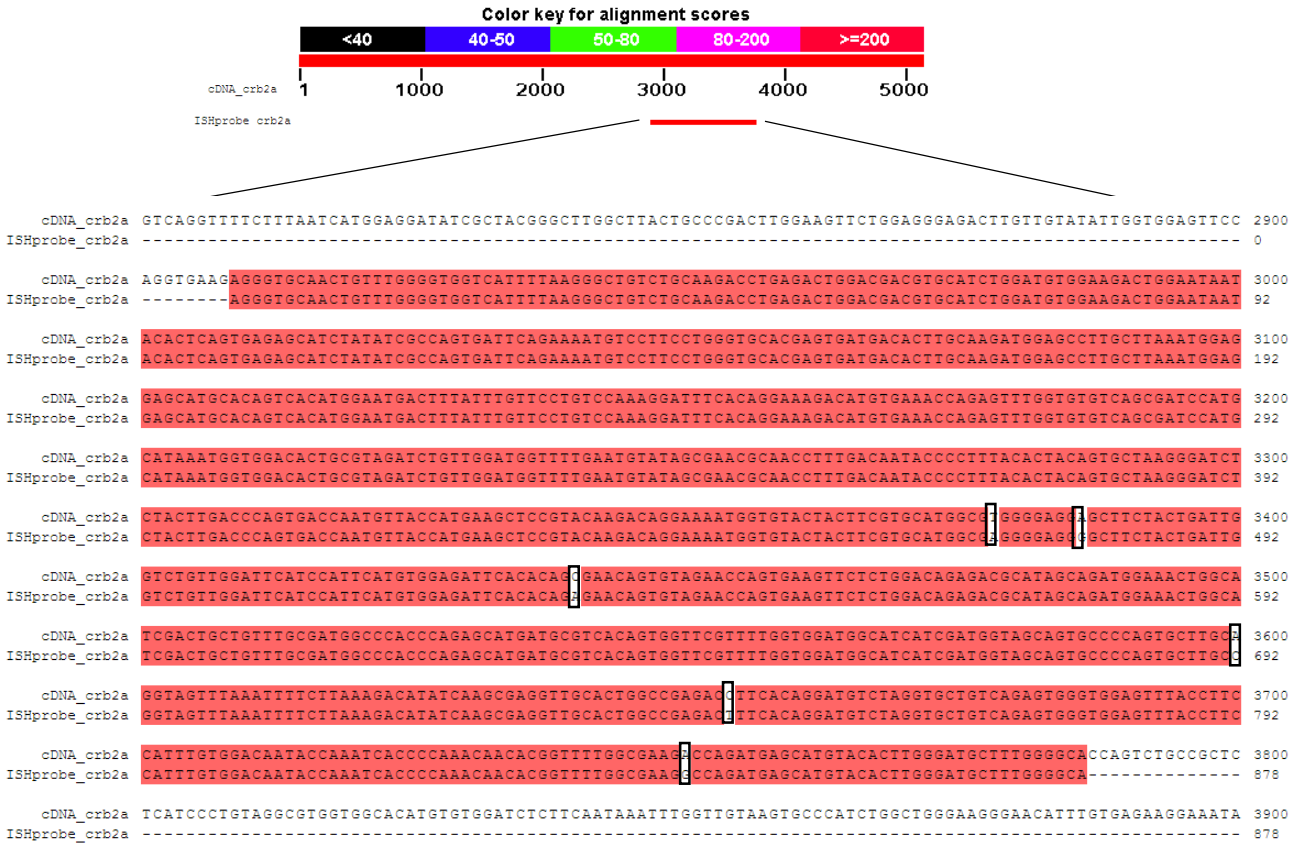

Figure S1.: Alignment of cDNA *crb2a* and ISH probe *crb2a* sequences.
Sequence of ISH probe for *crb2a* (878bp) sequenced by StabVida was aligned with cDNA *crb2a* sequence (NCBI, 5153bp), using BLAST: Basic Local Alignment Search tool (NCBI) and Multiple Align Show Software. Matching sequence is highlighted in red. White boxes indicates different bases between cDNA *crb2a* and ISH probe *crb2a* sequences.

Annex II: *gnaia* atgMO sequence

```
 cDNA_gnaia CTATGTATGAAAAGAAACAGGAAACTCCTCCGATCTGATCTGTTCGACACTTTAACAGCAGTGGAAGAATCGGAGGCAAAGGCTGGCAGTTAATGACTTC 100
gnaia atgMO ---------------------------------------------------------------------------------------------------- 0

 cDNA_gnaia ATTTCACTCTCTTTTTAATCAACGATGGCCGTAAAGGCACTCGATTGATTATCGACGCCGTCTCTTTTATACTTTTAACTTTAGAAGCTCCGGAAATTTA 200
gnaia atgMO ---------------------------------------------------------------------------------------------------- 0

 cDNA_gnaia AAAAACTCCAGTTTAAAGCGGCGGTGCGCGTGTGTGAAAGAGTTGGGCGTGAGTCGTCGGGTGGCTCCATATTTCACCCGCCTGTGTATGATAATTCTTT 300
gnaia atgMO ----------------------------------------------------------------------TCACCCGCCTGTGTATGATAATTCT-- 25

 cDNA_gnaia ACTTTTTGACACTTCGACTTCTTAAATCATTTAGAAGCCTTTTAAACTTCGAAAAGATGGGGTGCACCCTGAGCTCGGACGACAAGAGCGCCCAGGAGAG 400
gnaia atgMO ---------------------------------------------------------------------------------------------------- 25

 cDNA_gnaia AAGTAAAATGATTGACAGAAACCTGCGGGATGATGGAGAGAAAGCGTCGCGAGAGGTCAAGCTGCTGCTGCTGGGCGCTGGTGAATCCGGGAAAAGCACA 500
gnaia atgMO ---------------------------------------------------------------------------------------------------- 25

 cDNA_gnaia ATTGTCAAACAAATGAAAATCATCCATGAAGCGGGGTACTCAGAGGAAGAGTGCAAACAATACAGAGTCGTGGTTTACAGCAACACAATCCAGTCCATCA 600
gnaia atgMO ---------------------------------------------------------------------------------------------------- 25

 cDNA_gnaia TTGCCATCATAAGAGCCATGGGCCGCCTGAGGATTGACTTTGCGGATCCTGAACGAGCTGATGACGCAAGACAGCTGTTTGTGATGGCCGGCTCCGTAGA 700
gnaia atgMO ---------------------------------------------------------------------------------------------------- 25

 cDNA_gnaia TGAGGGTTTCATGACGAGTGAGCTTGCCGGAGTAATCAAGCGGCTCTGGAGGGATGAAGGCGTACGGCTTTGTTTCCATCGCTCCAGAGAGTACCAGCTC 800
gnaia atgMO ---------------------------------------------------------------------------------------------------- 25

 cDNA_gnaia AATGACTCTGCCTCATACTACCTGAATGATCTGGACAGAATATCCAATAGTTCATATGTCCCAACACAGCAAGATGTTCTGAGGACCAGAGTGAAGACTA 900
gnaia atgMO ---------------------------------------------------------------------------------------------------- 25

 cDNA_gnaia CTGGTATTGTGGAAACCCACTTCACATTCAAGGATCTTCACTTCAAGATGTTTGACGTAGGTGGCCAAAGATCTGAGAGGAAGAAATGGATTCACTGCTT 1000
gnaia atgMO ---------------------------------------------------------------------------------------------------- 25

 cDNA_gnaia TGAAGGAGTGACCTCCATCATCTTCTGCGTGTCCCTCAGTGATTATGACCTGGTCCTGGCTGAGGATGAGGAGATGAACCGAATGCATGAGAGCATGAAG 1100
gnaia atgMO ---------------------------------------------------------------------------------------------------- 25

 cDNA_gnaia CTGTTTGACAGCATCTGCAATAACAAGTGGTTTACGGACACCTCCATCATCCTGTTTCTCAACAAGAAGGATCTGTTTGAAGAGAAGATCAGGATGAGCC 1200
gnaia atgMO ---------------------------------------------------------------------------------------------------- 25

 cDNA_gnaia CGCTTAGTATTTGTTTCCCAGAATATCCAGGATCTGACGTATATGAAGAGGCGGCTGCTTACATCCAGTGTCAGTTTGAGGACCTGAATAAGAGGAAGGA 1300
gnaia atgMO ---------------------------------------------------------------------------------------------------- 25

 cDNA_gnaia CACCAAAGAGATTTACTCTCACTTCACCTGTGCCACTGACACCAAGAACGTGCAGTTCGTCTTTGATGCCGTCACTGATGTCATCATCAAAAACAACCTA 1400
gnaia atgMO ---------------------------------------------------------------------------------------------------- 25

 cDNA_gnaia AAGGACTGCGGCCTCTTCTAAAGCCAGCTCATTGTGTTGACAGCGAGTGGCCTGATGTTAAATCTTTGGGAGAACCAAAACAGGAAGAAGGTCAACCATG 1500
gnaia atgMO ---------------------------------------------------------------------------------------------------- 25

 cDNA_gnaia AACCTGAATGTTGAATGCATTACTTAACTTCATATTTATGTTCTCTGAACATTTTAGATTTTTTTAGGGTGTTTTAGGGAAGAAAAAAAAGAGCATTTTG 1600
gnaia atgMO ---------------------------------------------------------------------------------------------------- 25

 cDNA_gnaia TGTAAAATATTTGTACAACTGTAATTGTTCCTGGAATTTTTCACCATTTTTAGACATTGTCTTTAAAGGTCCTTTTTAAAGGCTATTTTTCATTCAAAGG 1700
gnaia atgMO ---------------------------------------------------------------------------------------------------- 25

 cDNA_gnaia GTTTCTGGGAACAATTTTTTTTCCAGTTTTTACTCCGAATACTAAGGTCATGTGCCTTCAGTTAATGTTGCAGTGCTTTTCTTTGCCACTTCAACTGAGT 1800
gnaia atgMO ---------------------------------------------------------------------------------------------------- 25

 cDNA_gnaia TTAATAAGAGACAGTTGATATTTATCCACACAACTCTCATCTGCTCAACTGTAGTATAAAAAGCCTGATATTTTTAAGACCAAACAACTGTGAGTGACTG 1900
gnaia atgMO ---------------------------------------------------------------------------------------------------- 25

 cDNA_gnaia TTTAAATGTATAGTAGCTTATTTCTGTCACAGGATTAACTTACGTTTTTGGTTTTGACATATAATCTTGGAATAAAAGTAGCAAAAACAAAATTAAATAA 2000
gnaia atgMO ---------------------------------------------------------------------------------------------------- 25

 cDNA_gnaia ATGTTACACAGTGTTTCAAGAAGGTCTCAAATCTGGGATACAAATTGCAAGCTAAAACTTTTCATTCTGAGCTTGTCGCATTTCTACATATATTGCATTC 2100
gnaia atgMO ---------------------------------------------------------------------------------------------------- 25

 cDNA_gnaia TTGTTTTTTTTATGTGGCAGTACTTGGTTCATCTTGAATTCAGATTTTTAGAATTGTTAATTTAAGTTTTTGGTAACTTTATTTTGATGGTCCCATTACA 2200
gnaia atgMO ---------------------------------------------------------------------------------------------------- 25

 cDNA_gnaia CATTTTGTTGACAAAGTTGCAGTGCAACTACATTCCAATTACTTCTAATTTGAGTATTAGTAGAGGGTCTGCTCCTTCAACATATTTAACTGCCTAAGAG 2300
gnaia atgMO ---------------------------------------------------------------------------------------------------- 25
```

Figure S2: Alignment of cDNA *gnaia* and *gnaia* atgMO sequences.
Sequence of *gnaia* atgMO (25 bp) given by Gene Tools was aligned with cDNA *gnaia* sequence (NCBI, 3781bp), using BioEdit Sequence Alignment Editor and Multiple Align Show Software. Matching sequence is highlighted in red.

Annex III: *dnal1* primers sequence

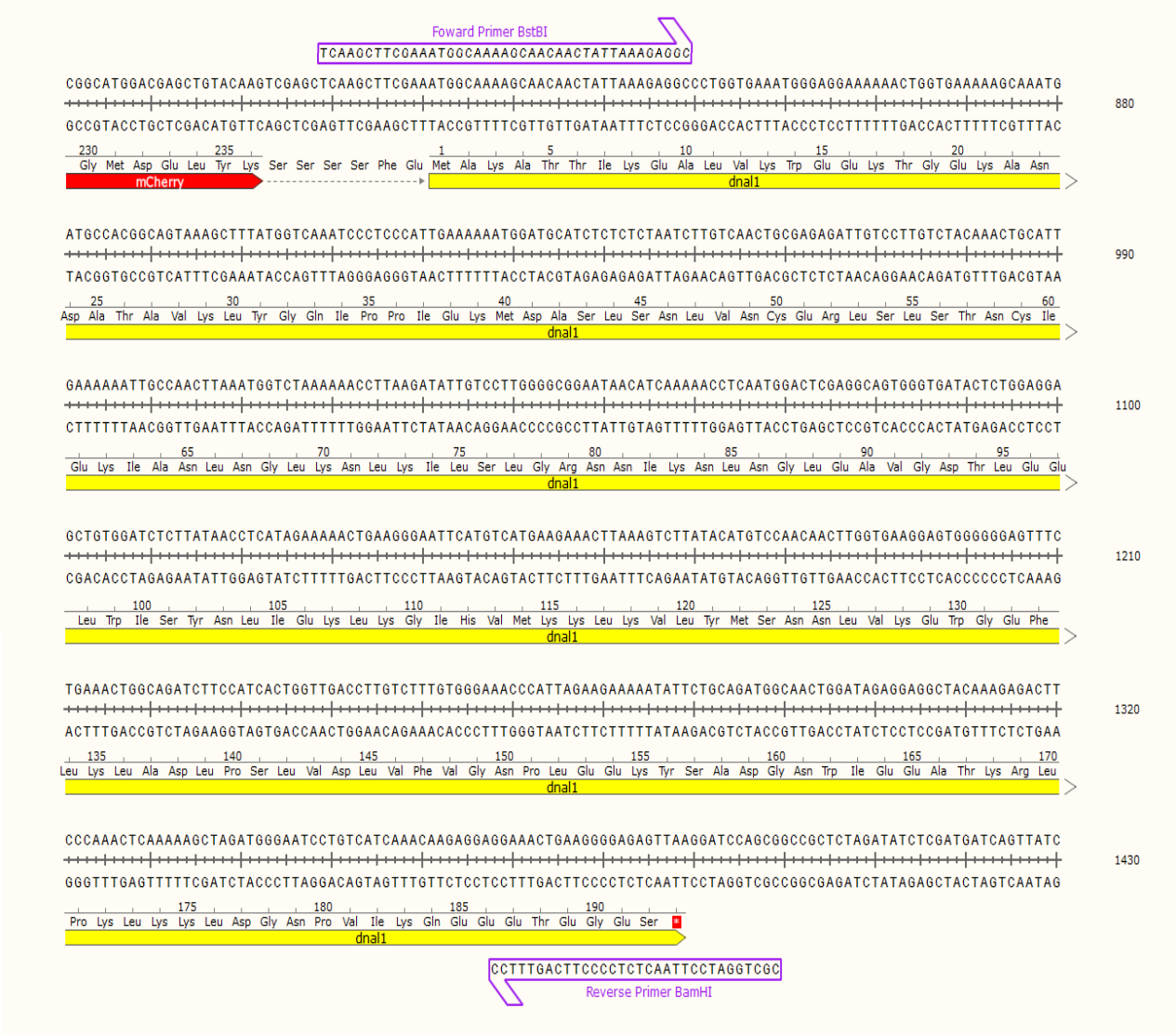

Figure S3: Forward and reverse primers used to clone dnal1
To clone dnal1 gene from cDNA into the PCS2+mCherry vector, specific primers were designed according to the restriction enzymes used. Forward primer containing the restriction site for BstBI enzyme (5' TTCGAA 3'). Reverse primer containing the restriction site for BamHI (5' GGATCC 3').

Annex IV: Sequencing result of dnal1 cloned sequence

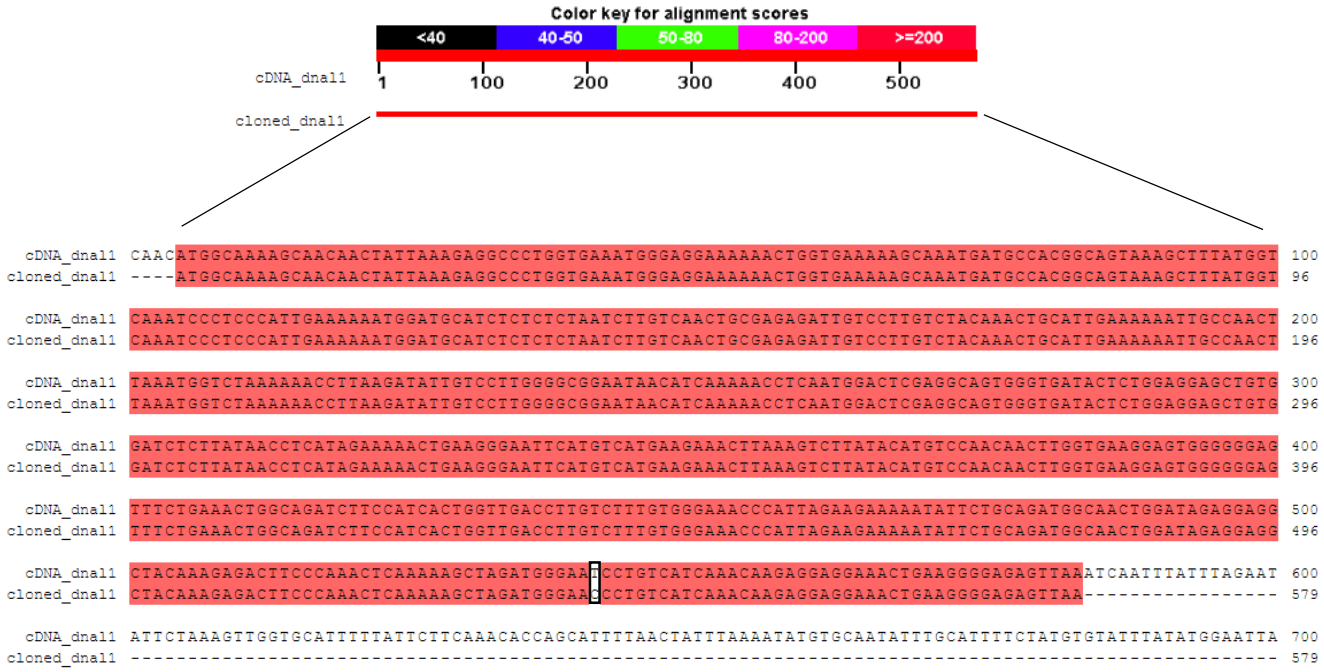

Figure S4: Alignment of cDNA *dnal1* and cloned *dnal1* sequences.
Sequence of dnal1 cloned into the PCS2+mCherry vector sequenced by StabVida was aligned with cDNA *dnal1* sequence (NCBI, 579bp), using BLAST: Basic Local Alignment Search tool (NCBI) and Multiple Align Show Software. Matching sequence is highlighted in red. White boxes indicates different bases between cDNA *dnal1* and cloned *dnal1* sequences.